Nano Materials Science 1 (2019) 2–30

Contents lists available at ScienceDirect

Nano Materials Science

journal homepage: www.keaipublishing.com/cn/journals/nano-materials-science/

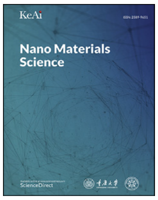

Some basic aspects of polymer nanocomposites: A critical review

Shaoyun Fu [*], Zheng Sun, Pei Huang, Yuanqing Li [**], Ning Hu

College of Aerospace Engineering, Chongqing University, Chongqing, 400044, China

ARTICLE INFO

Keywords:
Polymer nanocomposite
Nanofiller
Processing
Characterization
Mechanical and physical properties

ABSTRACT

Polymer nanocomposites have been investigated for about three decades. To get deep insights into the modifying effects of various nanofillers on mechanical and physical properties of polymer nanocomposites, the three basic aspects of processing, characterization and properties are critically reviewed in this paper. Nanofillers can be classified into three major types of two-dimensional (2D) layered, one-dimensional (1D) fibrous and zero-dimensional (0D) spherical ones and this review thus discusses in detail the processing, characterization and properties of the three types of polymer nanocomposites. It starts with an introduction of various nanoscale fillers such as two-dimensional (2D) nano-clay, graphene and MXene, one dimensional (1D) carbon nanofibers and nanotubes, zero dimensional (0D) silica nanoparticles and ZnO quantum dots as well as nanofiller-polymer interfaces. The processing of these polymer nanocomposites using different methods and the characterization of nanofillers and polymer nanocomposites using various techniques are described. Finally, the mechanical and physical properties of these polymer nanocomposites are discussed by considering the effects of nanofiller type, dispersion and contents; also, interface properties show significant effects on the mechanical properties of polymer nanocomposites and are discussed in some details.

1. Introduction

Polymers are commonly reinforced by various sized fillers to alleviate some of the limitations of polymers and hence to broaden their applications. The usage of nanoscale fillers to improve mechanical and physical properties of polymers has led to a radical alternative to conventional polymer composites [1,2]. The nanoscale fillers have at least one characteristic length scale of the order of nanometers and vary essentially from isotropic to highly anisotropic sheet-like or needle-like morphologies. Nanoscience and nanotechnology afford unique opportunities to create revolutionary combinations of nanoscale fillers and polymer materials to get polymer nanocomposites with interesting properties.

Polymer nanocomposites can be generally categorized into three major types, depending on the dimensions of the dispersed nanoscale fillers. In the first type, the two dimensional (2D) nanoscale fillers such as layered silicate [3], graphene [2,4] or MXene [5,6] in the form of sheets of one to a few nanometer thick and of hundreds to thousands nanometers long are present in polymeric matrices. The corresponding polymer nanocomposites can be grouped into the type of layered polymer nanocomposites. In the second type, two dimensions are in nanometer scale and the third is larger, forming an elongated one-dimensional structure, these nanoscale fillers include nanofibers or nanotubes, e.g., carbon nanofibers and nanotubes [7] or halloysite nanotubes [8] as reinforcing nanofillers to obtain materials with exceptional properties. The third type is the nanocomposites containing nanoscale fillers of three dimensions in the order of nanometers. These nanoscale fillers are iso-dimensional low aspect ratio nanoparticles such as spherical silica [1,9], semiconductor nanoclusters [10] and quantum dots [11]. Fig. 1 shows schematics of various nanoscale fillers.

Uniform dispersion of these isotropic and anisotropic nano-sized fillers can produce ultra-large interfacial area per unit volume between nanoscale fillers and host polymers. Besides the large interfacial area, the distance between the nano-elements approaches molecular dimensions at extremely low contents of nanoscale fillers. Therefore, this is a morphology controlled by nanoscale features.

Polymer nanocomposites have superior mechanical and physical properties over host polymers partially due to the large interfacial area between polymers and nano-fillers. Spherical nanoparticle-polymer system is taken as an example for the estimation of interfacial area. The interfacial area per unit volume R (m^2/cm^3) between spherical fillers and host polymers can be derived by assuming particles of a constant radius r_f (nm), that is,

---

[*] Corresponding author.

[**] Corresponding author.

E-mail addresses: syfu@cqu.edu.cn (S. Fu), yqli@cqu.edu.cn (Y. Li).

https://doi.org/10.1016/j.nanoms.2019.02.006
Received 16 January 2019; Accepted 24 February 2019

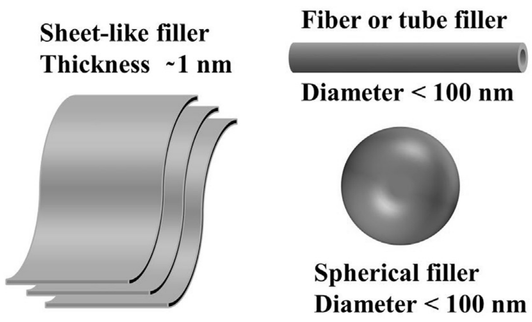

Fig. 1. Schematic diagrams of three types of nanoscale fillers.

$$R = 3000 \cdot V_f / r_f \tag{1}$$

where V_f is volume fraction of spherical nanoparticles, and R is inversely proportional to r_f. For example, when $V_f = 5\%$, $R = 15\ \mathrm{m^2/cm^3}$ if $r_f = 10\ \mathrm{nm}$, and $R = 150\ \mathrm{m^2/cm^3}$ if $r_f = 1\ \mathrm{nm}$, which is an ultra-large interfacial area. This ultra-large interfacial area and the nanoscopic dimensions of the fillers differentiate polymer nanocomposites from conventional composites. The dominance of interfacial regions resulting from the nanoscale phase dimensions has produced some unusual mechanical and physical properties not found in conventional polymer composites. Because of the ultra-large interfacial area between polymers and nanofillers, functionalization of nanofillers is used to alter interfacial states to enhance mechanical and physical properties of polymer nanocomposites [12]. Grafting of polymer molecular chains of graphene significantly improved the interfacial shear strength and interfacial mode-II fracture toughness in functionalized graphene/polymer nanocomposites [13].

So far, there have been some outstanding review papers addressing different issues of polymer nanocomposites. Albdiry et al. [3] reviewed manufacturing processes of nanoclay/polymer nanocomposites and concluded that alteration of processing (type and/or parameters) technique would greatly influence the final nanostructure, morphology and the mechanical properties of clay/polymer nanocomposites. The permeability of gas molecules in clay/polymer nanocomposites was reviewed by Choudalakis et al. [14]. The mechanics of graphene nanocomposites was surveyed by Young et al. [2] who concluded that good reinforcement could only be got at relatively low levels of graphene loading owing to difficulties in achieving good dispersions at high graphene loading. Sengupta et al. [15] surveyed the results about mechanical and electrical properties of graphite reinforced polymer composites including using various modifications of graphite in polymer matrices for creating polymer-carbon nanocomposites. Carbon nanotube (CNT)/polymer nanocomposites were reviewed by Bauhofer et al. [16] addressing electrical percolation issue, Sahoo et al. [12] discussing CNT functionalization issue, Han et al. [17] reviewing thermal conductivity and Roy et al. [18] discussing modification of CNTs and its effects on properties of polymer nanocomposites. Various techniques of experimental and modelling studies were described for carbon nanotube-polymer interactions in nanocomposites [19]. Spitalsky et al. [20] gave a survey of carbon nanotube–polymer composites: processing, chemistry, electrical and mechanical properties. Research work on halloysite nanotube/polymer nanocomposite was summarized by Liu et al. [8]. A review on polymer nanocomposites with graphene-based fillers was conducted by Kuilla et al. [21], Potts et al. [22], as well as Du et al. [4]. A short background on research work was rendered for epoxy-clay nanocomposites by Azeez et al. [23] and SiO_2/epoxy nanocomposites by Sprenger [24]. Surface modification of 0D nanoparticles to prevent particle aggregation for development of polymer nanocomposites was reviewed by Kango et al. [25].

This paper gives a comprehensive review of some basic aspects including processing, characterization and properties of various polymer nanocomposites. Since nano-fillers can be classified into three major types in terms of their morphologies including two-dimensional (2D) layered, one-dimensional (1D) fibrous and zero-dimensional (0D) spherical nanofillers, this review discusses in detail the processing, characterization and properties of the three types of polymer nanocomposites. It starts with introducing various nanoscale fillers. Then, processing of polymer nanocomposites using different methods, characterization of polymer nanocomposites using various techniques, mechanical as well physical properties of polymer nanocomposites are systematically described and discussed.

2. Nanoscale fillers and interfaces

Nanoscale fillers have various shapes and sizes; and they form ultra-large interfacial areas when bonded to polymer matrices. Since the properties of polymer nanocomposites are dependent on these factors, they will be first addressed in this section.

2.1. Sheet-like nanoscale fillers

The first example of sheet-like nano-fillers often used in polymer nanocomposites is layered silicates belonging to the structural family known as the 2:1 phyllosilicates. Montmorillonite, hectorite and saponite etc. are the usually used layered silicates and their structure is presented in Fig. 2 [26–28]. Their crystal lattice is composed of two-dimensional layers. A central octahedral sheet of alumina or magnesia is fused into two external silica tetrahedron so that the oxygen ions of octahedral sheet pertain to tetrahedral sheets. The thickness of layers is ca. 1 nm and the lateral dimensions of the layers vary from several tens of nanometers to several micrometers and even larger. These layers will form stacks with van der Waals gaps between "interlayers" or "inter-galleries". This kind of clay has a moderate cation exchange capacity and the charge of the layer is not constant since it differentiates from one layer to another and thus a mean value over the whole crystal should be taken into account.

Polymer nanocomposites may not be got by direct physical mixture of a polymer and layered silicates. This is analogous to many polymer blends in which separation of layered silicates into discrete phases may likely occur. In immiscible systems, typical with many conventional filled polymers, poor physical interaction between inorganic fillers and polymers brings about low mechanical and physical properties. Conversely, strong interactions between layered silicates and polymers may result in nanometer level dispersion of inorganic nano-phases in polymer matrices. Consequently, polymer nanocomposites will show unique mechanical and physical properties not shared by micro-composites [26, 29–33]. Pristine layered silicates usually possess hydrated Na^+ or K^+ ions [34]. In this pristine state, layered silicates are only miscible with

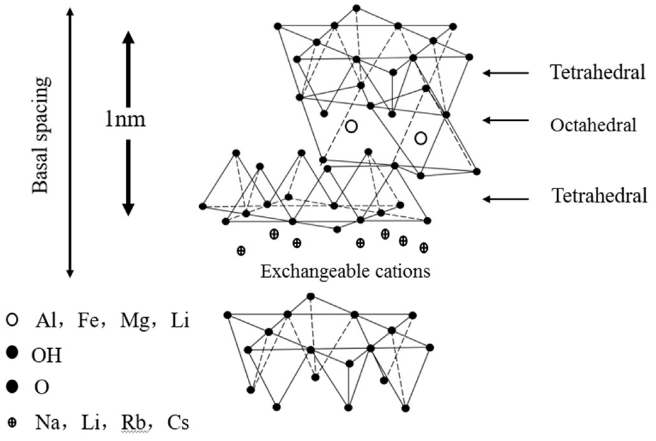

Fig. 2. Structure of commonly used 2:1 phyllosilicates [26–28].

hydrophilic polymers [35,36]. In order to mix layered silicates with other polymers, hydrophilic silicate surfaces should be modified to organophilic ones so that intercalation of various polymers can be allowed. When hydrated cations are ion-exchanged with organic cationic surfactants, e.g., alkylammonium or alkylphosphonium (onium), this usually produces a large interlayer spacing [37,38].

Alkylammonium or alkylphosphonium cations in organosilicates can reduce surface energy and enhance wetting capability of polymer matrices, and thus expand the interlayer spacing. On the other hand, alkylammonium or alkylphosphonium cations offer functional groups that can react with polymer matrices, or in some cases initiate polymerization of monomers to modify the inorganic clay-polymer matrix interface adhesion [39,40]. X-ray diffraction (XRD) is used to describe the structure of the interlayer in organoclays. According to XRD data, the organic chains are regarded to lie parallel to the silicate layer as shown in Fig. 3 [37]. The properties of layered silicates are generally unknown, and estimates are made in terms of the composite properties. For nano-scale fillers, a high aspect ratio is the most important factor to make them efficient for carrying applied loads. The layered silicates are usually impermeable to liquids and gases across the layer thickness and hence provide an excellent barrier for polymer nanocomposites to these substances.

Expanded graphite has a layered structure consisting basically of parallel boards, which can collapse and deform and result in many pores of different sizes ranging from about 10 nm to 10 μm [42,43]. The thickness of the graphite sheets in the exfoliated graphite is in the scale of ca. 100 to several hundreds of nm. It is hard to find sheets thinner than 100 nm. Graphite flakes with different sizes show the same results in forming the expanded graphite, although their expansion ratios are different. The difficulty of finding sheets with a thickness less than 100 nm by scanning electron microscopy (SEM) technique is likely caused by the nanosheets that stacked on each other or even fused at their edges (Fig. 4) [41].

Coleman et al. showed that various layered compounds such as BN, WS_2, MoS_2, $MoSe_2$, $TaSe_2$, $NbSe_2$, $MoTe_2$, $NiTe_2$ and Bi_2Te_3 can be readily dispersed in common solvents [44]. Then, these layered compounds can be deposited as individual flakes or formed into films [44]. These materials were exfoliated into individual layers and by blending them with polymer solutions, polymer nanocomposites could then be prepared. Their dispersions of 2D flakes consisting of thin nanosheets were observed typically by transmission electron microscopy (TEM) technique as shown in Fig. 5 (a to c) for BN with the lateral size of 100–5000 nm, MoS_2 and WS_2 with the lateral size of 50–1000 nm.

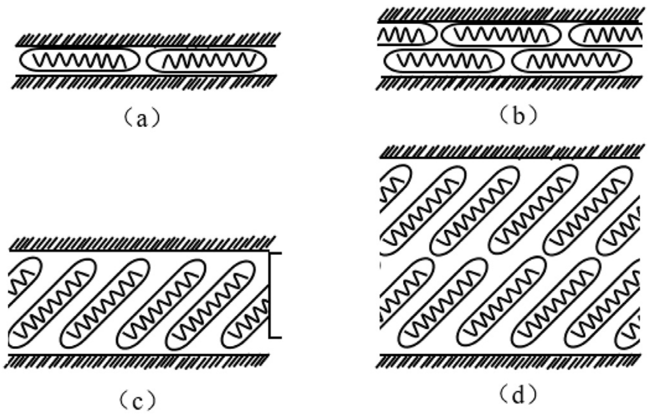

Fig. 3. Structure of the interlayered organoclays: (a) lateral monolayer; (b) lateral bilayer; (c) paraffin-type monolayer; and (d) paraffin-type bilayer [37].

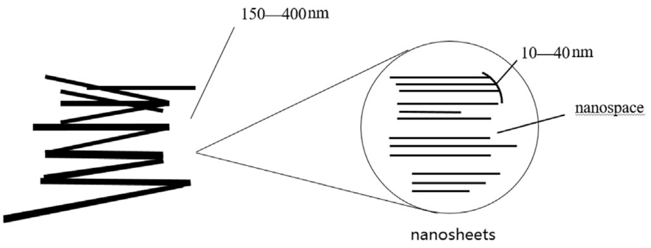

Fig. 4. Illustration for expanded graphite composing of graphite nanosheets [41].

2.2. Nanotubes and nanofibers

Carbon nanotubes are slender and long fullerenes where the walls of the tubes are of hexagonal graphite structure and often capped at each end. CNTs are basically divided into single-walled carbon nanotubes (SWCNTs) if only a graphene sheet is rolled and multi-walled carbon nanotubes (MWCNTs) if a number (≥2 for simplicity) of graphitic shells are stacked and arranged to obtain a cylindrical tube [45,46]. A single-walled carbon nanotube is hollow in structure obtained by covalently bonded carbon atoms. Multiwalled nanotubes (MWNTs) are of various morphologies depending on their preparation methods [47,48]. The spacing between neighboring graphene layers is around 0.34 nm. CNTs have quite unique mechanical and physical properties controlled by their geometry and dimensions. They have very high moduli and extremely high strength [49,50]. Theoretically, the tensile strength and modulus of a graphene layer can reach up to 200 GPa and 1 TPa, respectively. The specific strength of CNTs may be ten to one hundred times higher than that of the strongest steel [51]. In addition to their exceptional strength and modulus, they also posses superior thermal and electric properties. They are thermally stable up to 2800 °C in vacuum, and have a thermal conductivity about twice as high as that of diamond as well as an electric-current-carrying capacity 1000 times higher than that of copper wires [52]. Due to these exceptional properties, CNTs have been studied for possible applications in field-emission displays [53], scanning probe microscopy tips [54], and microelectronic devices [55,56]. Table 1 exhibits the values of Young's modulus predicted via theoretical and numerical approaches [molecular dynamic (MD) and finite element method (FEM)], and experimental measurements. These data have been widely employed for interpreting the mechanical properties of single-walled and multi-walled CNTs. The size, mechanical and electrical properties of CNTs are highly dependent on their atomic architectures. For example, armchair CNTs would show better ductility and electrical conductivity than zigzag CNTs [57]. More details for mechanical and physical properties of CNTs can be referenced to the literature [49,50,57].

Nanotubes are in general manufactured by three approaches [68]: laser furnace, arc, and chemical vapour deposition (CVD). Laser method is not suitable for large-scale production. The problem with arc method is purification. Removal of metal catalyst and non-nanotube carbon materials costs more than production itself. And infrared may be the proper method to measure purity [69]. CVD is a scalable method whereby the purity of CNTs can be controlled by careful processing and aligned arrays of carbon nanotubes with desired diameter and length. Fig. 6a and b shows the grown straight CNTs over a large area with excellent uniformity in diameter, straightness, length, and site density [70,71]. The thickness of the catalyst layer can be adjusted to control the diameter of the CNTS as shown in Fig. 7a and b.

Much work has also been done to prepare fibers by aligning CNTs. For example, nanotube/polyvinyl alcohol fibers is developed via drawing [72]. This process is taken up by Dalton et al. [73]. Alternatively, it is useful to learn from other strong fibers such as Kevlar. SWCNTs are dispersed in 102% sulfuric acid, possibly protonating the sidewalls and allowing the fibers to be drawn [74]. One method is to draw and spin CNT fibers directly from a CVD reaction chamber as shown schematically in Fig. 8 [75]. The resulting fibers from CNTs can then be post-impregnated with epoxy resin to make a nanocomposite. These

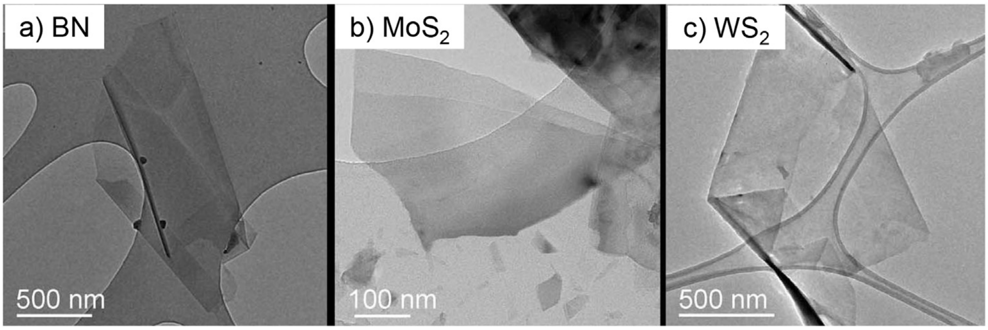

Fig. 5. TEM images of nanosheets (a to c) of flakes of BN, MoS_2, and WS_2, respectively [44].

Table 1
Comparison of the results for the Young's modulus of carbon nanotubes by various studies.

E (TPa)	Method	References
5.5	MD	[58]
4.7	Theoretical	[59]
1.325	MD	[60]
1.0	MD	[61]
0.77	Theoretical	[62]
1.25	Theoretical	[63]
1.05	FEM	[64]
0.9	Experimental	[65]
0.79	Experimental	[66]
0.27–0.95	Experimental	[67]

fibers have a failure strength up to about 1 GPa, which is much smaller than that (30–50 GPa) of a single nanotube. This is understandable since CNTs can be considered as short fibers that their load-carrying capability would be much lower than continuous counterparts. Thus, better interfacial adhesion of CNTs with polymers would be critical for CNTs to share the load better.

2.3. *Nanoscale spherical fillers*

Spherical nanoparticles have been existing since 1900's and carbon black as an example has been made available by pyrolysis in a range of surface areas. The particle sizes are between 20 and 300 nm with surface areas of 20–500 m^2g^{-1}. Silica has also been made available by different methods including wet chemical process [76], Ludox process (Dupont commercial process) and flame process [77]. The flame methods have

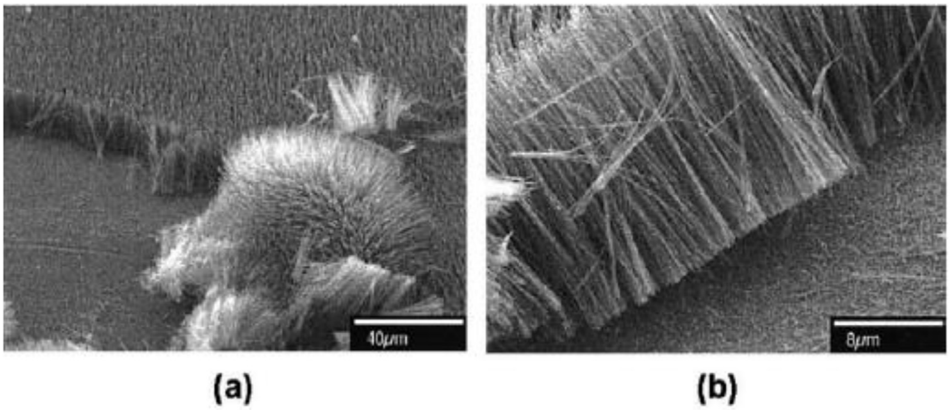

Fig. 6. Micrographs of the straight MWCNTs grown via CVD [71].

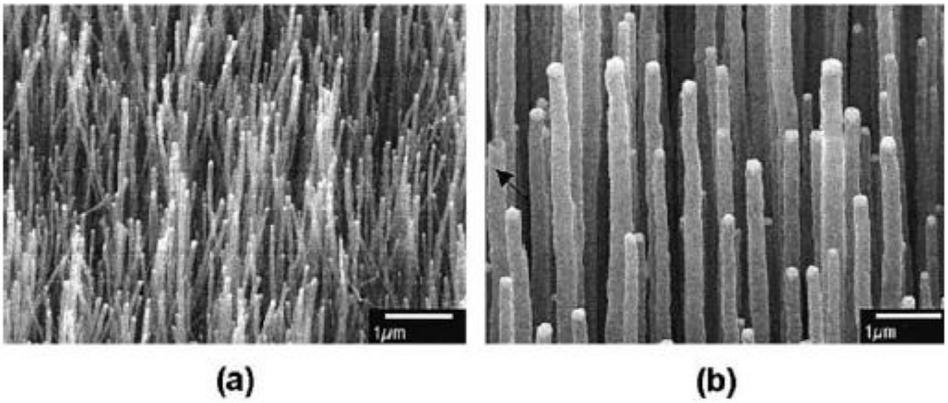

Fig. 7. Micrographs showing control over the nanotube diameter: (a) 40–50 nm and (b) 200–300 nm aligned carbon nanotubes [71].

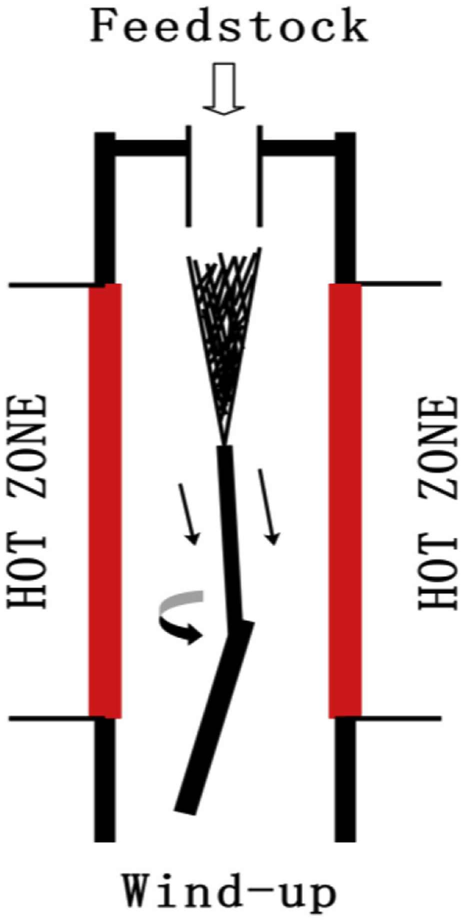

Fig. 8. Schematic diagram of how to wind nanotube fibers directly from a CVD growth chamber. A feedstock of ethanol and thiophene catalyst is used at 1100 °C [75].

been used for a long time and are still in use for ultrafine powder production. Generally, hydrogen or hydrocarbons are burned in O_2 to produce a flame in which nanoparticles form and grow. And one frequently observes particle aggregation in such flames [77]. It is particularly typical for silica particles and a number of studies concerning ultrafine silica production in flames are disclosed [78–80]. The aggregate size of ultrafine silica samples produced in hydrogen/oxygen flames is in the range of several hundreds of nm to several micron-meters while the major particles have diameters of 10–20 nm [81].

Synthesis of spherical nanoparticles with controllable size is the goal of many research efforts. The main driving force for this interest is the particle size's effect on their properties. Nanoscale fillers are dispersed in polymers to take advantage of the novel properties of these nanoscale materials. Nanofillers can lend properties to polymer matrices that they cannot achieve alone or with micro-sized fillers. For example, addition of nanoparticles at proper contents to polymers can enhance strength and modulus while maintain ductility while introduction of micro-sized fillers will very likely not achieve this balanced performance.

The particle size critically depends on the production method of the nano-particles. The thermal plasma method has been applied for preparation of ultrafine powders [82–84]. The plasma method has some advantages over the flame method. For example, small residence time of species in the plasma reactor can be reached; rapid cooling of raw vapour can be realized and high-temperature boiling substances can be produced. Moreover, the arc plasma method produces non-aggregated particles while the flame method yields large particle aggregates. In addition, mono-dispersed silica particles having a uniform size distribution can be manufactured by controllable hydrolysis of tetraethylortho-silicate (TEOS) in ethanol, followed by condensation of dispersed phase material [85].

Nanoparticles are very small and their aggregation is therefore very hard to avoid. Good dispersion of nanoparticles in polymers is critical to obtain high performance polymer nanocomposites and dispersants sometimes are used to improve dispersibility of nanoparticles. For example, two types of dispersants are used in the preparation of the water slurry of nano-ZnO particles by ball milling [86]. Dispersant A used is an ultra high molecular weight block polymer and possesses a strong affinity for pigments; dispersant B used is polyacrylate sodium with a low molecular weight of only several thousands. Fig. 9 shows TEM images of ZnO particles with a diameter of ca. 60 nm dispersed in water via ball milling for 4 h. When dispersant A is used, almost all ZnO nanoparticles are dispersed to the original size, as shown in Fig. 9a; but when dispersant B is used, a large number of ZnO nanoparticles are dispersed to nano-scale, whilst agglomerates of ZnO nanoparticles with sizes 200–300 nm are also seen in Fig. 9b. These results show that the dispersant chain length controls the dispersibility of nano-ZnO nanoparticles in water due to the steric and static stabilization effects.

Silane surface modified zinc oxide quantum dots (S—ZnO QDs) were synthesized using $Zn(CH_3COO)_2•2H_2O$ dissolved in absolute ethanol and then mixed with silane (KH-560) in LiOH ethanol solution. The morphology of the as-obtained spherical S—ZnO-QDs was shown in Fig. 10 [11]. It displays that S—ZnO-QDs with a diameter of ca. 1.8 nm are mono-dispersed in ethanol. High resolution TEM (HRTEM) image exhibits that the lattice space between the two (002) planes of ZnO is ca. 2.6 Å (see bottom inset).

2.4. Nanoscale filler-polymer interfaces

Since nanofiller-matrix interfaces in polymer nanocomposites are recognized to be important, selected surface modification is always required according to the specific objectives and the characteristics of particular polymer system. The general idea is on the basis of the concept of creating an ultra large interfacial area between the nanoscale fillers and polymer matrices. However, the interfacial area is not the only major factor determining the properties of polymer nanocomposites, interfacial interaction is also crucial in determining the nanocompoiste properties. Thus, proper surface modification is needed, and then polymer nanocomposites with tailored properties can be obtained for various engineering applications.

It is well accepted that montmorillonite (MMT) clay particles generally agglomerate within a distance ~0.5 nm. Surface treatment reduces the layer-layer attraction and expands the gallery spacing to above 2 nm. The gallery spacing can be further increased by adsorbing monomers into

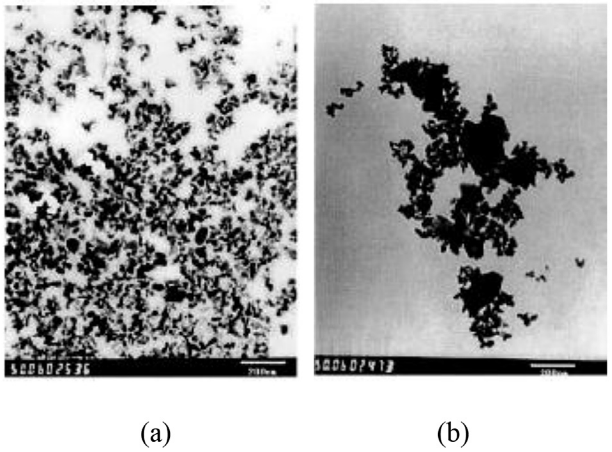

Fig. 9. TEM images of 60 nm ZnO nanoparticles dispersed in water with (a) dispersant A, (b) and dispersant B [86].

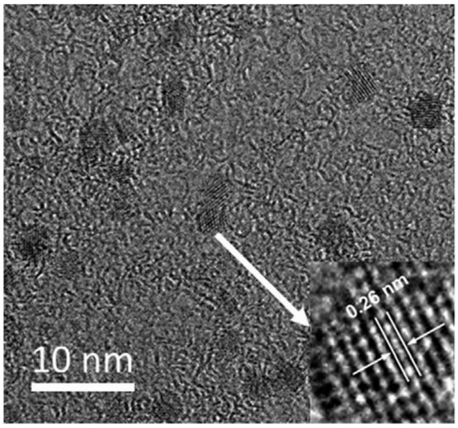

Fig. 10. TEM image of S —ZnO-QDs (bottom inset: HRTEM image of S—ZnO-QDs) [11].

the galleries prior to polymerization. A schematic of the MMT surface treatment is shown in Fig. 11.

The surface free energy of CNTs is very low and there are no reactive groups needed for coupling. The importance of interfacial interactions in preparing carbon nanotube/polymer composites is recognized as a most critical issue. Many studies have shown that the interfacial strength between single micron-diameter fibers and polymers can be evaluated directly. Such nano-scale experiment can be done on samples with nanotubes bridging voids in a polymer matrix [88]. The pullout curve resembles a typical force-displacement curve for single fiber pullout tests as shown in Fig. 12 [87]. An interfacial strength of about 50 MPa was obtained, which is about ten times larger than the adhesion between the same type of polymer and carbon micro-fibers. Silica nanotubes are used to reinforce polyimide (PI) films [89]. Coupling agent (γ-amino-propyltriethoxy silane, KH 550) was used to improve the compatibility between silica and polyimide, and hence enhance the silica-polyimide interfacial adhesion. It is noted that addition of a proper content of coupling agent leads to improvements in tensile strength and modulus.

Interface is shown below to be an influential factor in spherical nanoparticle/polymer nanocomposites. The fracture toughness of polypropylene filled with 70 nm $CaCO_3$ (0–40 vol%; both untreated and surface treated) was studied by Levita et al. [90]. The untreated fillers were shown to reduce but treated fillers increase the toughness with a maximum at ~10 vol%. These results indicate that the nanoparticle/polymer interface is critical for the fracture properties of polymer nanocomposites.

In this section, only brief discussions are given on the basics of nanoparticles and nanoscale filler-polymer interfaces. For further details and in-depth analyses of these topics, readers may refer to published relevant reviews [27,28,91].

3. Preparation of polymer nanocomposites

Preparation of good quality polymer nanocomposite samples using a proper processing method is critical to achieve high performance of polymer nanocomposites. The processing techniques developed for preparation of polymer nanocomposites [44,92–101] include: melt mixing, solution mixing, *in situ* polymerization, *in-situ* particle processing and other approaches. Creation of one universal technique for preparing all types of polymer nanocomposites is impossible due to the physical and chemical differences between polymers and various available types of facilities. Each polymer system needs specific processing conditions based on processing efficiency, nano-scale filler type and desired properties. In general, different processing technologies do not yield equivalent results [102].

Fig. 11. Schematic showing of MMT surface treatment.

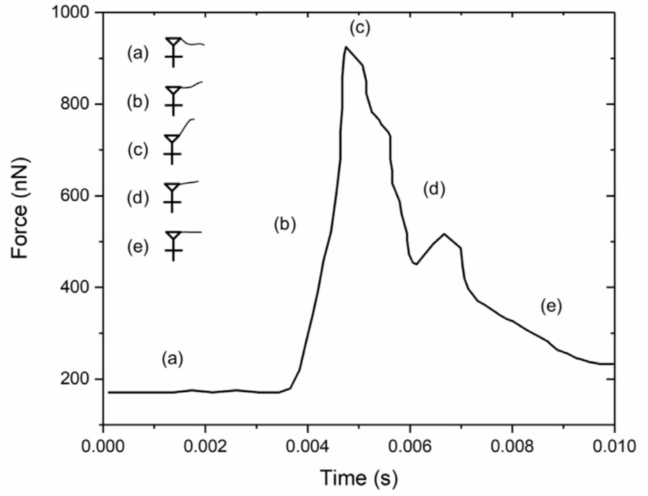

Fig. 12. CNT pullout from a polymer surface: typical plot of pullout force versus pullout time. (a) CNT is embedded in a polymer matrix; (b) as the CNT is pulled away from the polymer, the cantilever bends; (c) at the maximum force, the maximum cantilever deflection is achieved; (d) pullout then occurs; (e) eventual complete separation of the nanotube takes place from the polymer (e) [87].

3.1. Layered filler/polymer nanocomposites

Since layered silicate clays are hydrophilic, they are not suitable for mixing and interacting with most polymers. Moreover, electrostatic forces induce the tight stacking of layered clay platelets. As shown in Fig. 13, counter-ions are attracted to the net negative charge inside the clay platelets. Two neighboring platelets can share the counter-ions, leading to stacks of platelets that are tightly held together. It is not effective to use untreated clay for making polymer nanocomposites since most of the clay platelets would be stuck inside, and unable to interact with polymer matrices. Therefore, clay have to be treated before it is used to prepare polymer nanocomposites. A common and easy method for modifying clay surface is via ion exchange to make it more compatible with organic polymers. Then, clay can be compatibilized with various polymer matrices. Meanwhile, this process helps to separate the clay platelets and then these platelets can be more easily intercalated and exfoliated.

Since Usuki et al. in Toyota began their comprehensive research on clay/polymer nanocomposites, there has been extensive work on layered silicate/polymer nanocomposites [103]. Depending on the nature of the components (layered silicate, organic cation and polymer matrix) used and the preparation method, three major types of polymer nanocomposites can be achieved when layered silicates are associated with a polymer as shown in Fig. 14 [27]. When the polymer is not able to

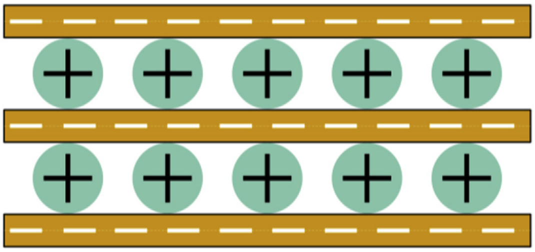

Fig. 13. Schematic showing of the layered structure of clay platelets.

intercalate between silicate sheets, a phase separated micro-composite is obtained as shown (Fig. 14a). And its characteristics behave in a similar way as traditional micro-composites. Two other types of polymer nanocomposites can be got when clay is intercalated or exfoliated. For intercalated structure (Fig. 14b), a single extended polymer chain intercalates between the silicate layers, leading to an ordered multi-layer alternating polymeric and inorganic morphology. When the silicate layers are uniformly and completely dispersed in a continuous polymer medium, an exfoliated structure can be obtained (Fig. 14c) and the resultant composite is called the exfoliated polymer nanocomposite.

Four major processes are: (1) intercalation of polymer or pre-polymer from solution, (2) *in situ* intercalative polymerization, (3) direct melt intercalation and (4) template synthesis for preparation of layered silicate/polymer nanocomposites [27,28,104]. In the first method, the polymer or pre-polymer should be soluble and the silicate layers should be expandable. First, layered silicate is swollen in a solvent such as chloroform, toluene or water. Then, layered silicate and polymer solutions are mixed, the polymer chains intercalate and displace the solvent within the silicate interlayers. The intercalated structure remains upon removing the solvent, which results in -layered silicate/polymer nanocomposites. As an example, the a,v-amino acids modified Na$^+$- montmorillonite (MMT) is swollen by ε-caprolactam monomer at 100 °C and then initiates its ring opening polymerization to get MMT/nylon 6 nanocomposites [105]. The ammonium cation of ω-amino acids is chosen for intercalation of ε-caprolactam. The number of carbon atoms in α,ω amino acids strongly affect the swelling behavior as exhibited in Fig. 15, indicating that the intercalation degree of ε-caprolactam monomer is high since the carbon atom number in the v-amino acid is large.

The second process is called *in situ* intercalative polymerization. The layered silicate is first swollen in a liquid monomer or a monomer solution so that the polymer forms between the intercalated clay sheets. Though interlamellar polymerization techniques have been known well for using layered silicates [106,107], polymer nanocomposites only gains great attention due to the work on a MMT/Nylon 6 nanocomposite from the Toyota research group [29]. Moreover, a two-step in-situ polymerization were used for preparation of exfoliated or intercalated MMT/polymer nanocomposites [108]. The two steps involve preparation of treated MMT solution and blending with polymers, respectively.

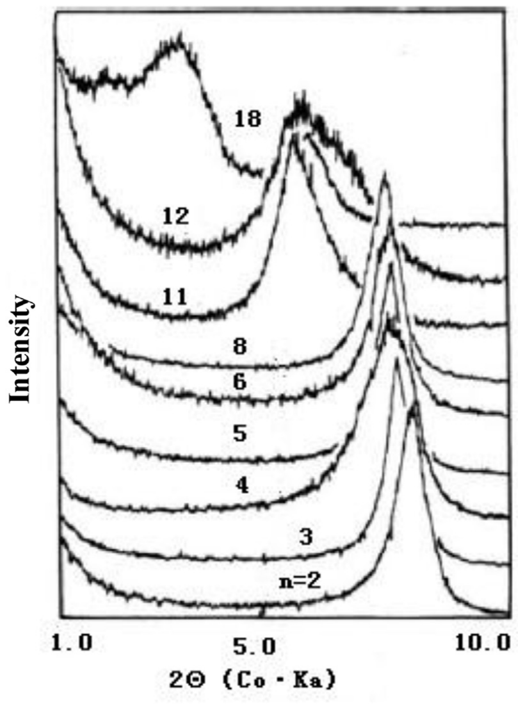

Fig. 15. XRD patterns of modified Na$^+$-MMT by v-amino acid [$NH_2(CH_2)_{n-1}COOH$] [105].

In the third technique, namely direct melt intercalation, layered silicates are blended with polymer matrices in the molten state and no solvent is required. Fig. 16 shows a schematic illustration of preparing polymer nanocomposite by direct melt intercalation in organically modified layered silicate (OMLS) [109]. A mixture of polymer and OMLS is annealed statically or by shearing above the softening point of the polymer matrix. The polymer chains diffuse into the galleries between the silicate layers from the bulk polymer melt during annealing.

In the fourth process, the polymers act as templates to form the clay layers. *In situ* hydro-thermal crystallization of the clay layers takes place in an aqueous polymer gel and layered silicate-based nanocomposites are

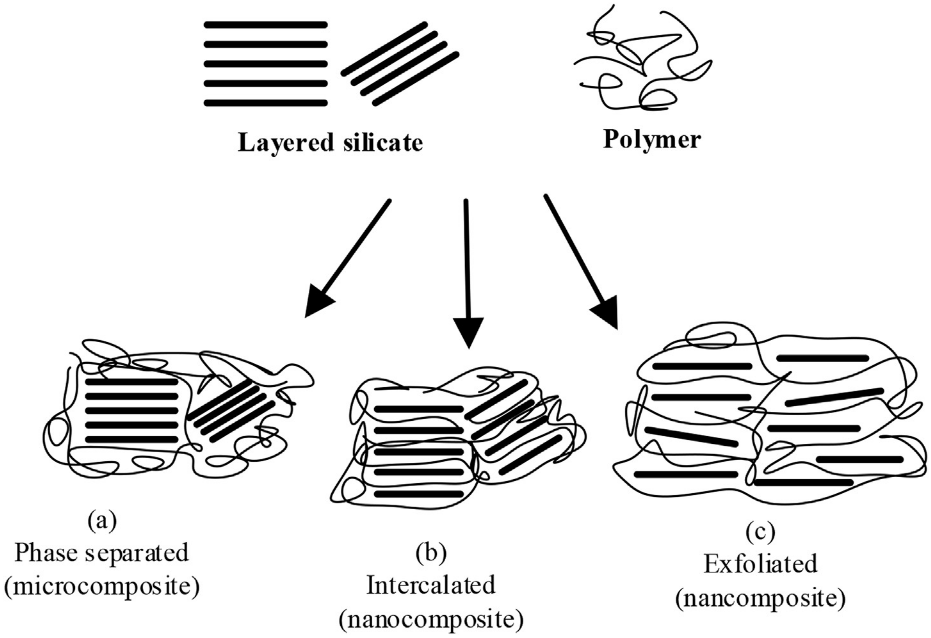

Fig. 14. Schematic illustration of three different types of nanocomposites arising from the interaction of layered silicates and polymers [27]: (a) phase separated polymer micro-composite; (b) intercalated polymer nanocomposite; and (c) exfoliated polymer nanocomposite.

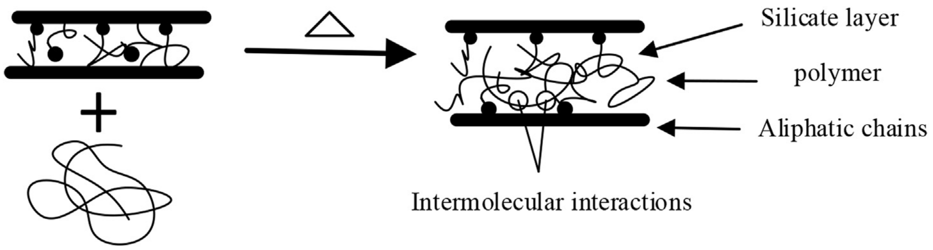

Fig. 16. Schematic of intercalation process between an OMLS and a polymer melt [109].

then prepared. This method has been used to synthesize double-layer hydroxide-based nanocomposites in which the silicates are formed *in situ* in the aqueous solution containing the silicate building blocks and the polymer [110,111]. This process is particularly suitable for water soluble polymers such as hydroxypropylmethylcellulose (HPMC), poly (vinyl-pyrrolidone) (PVPyr), poly (dimethyldi-allylammonium) (PDDA) and poly (aniline) (PANI) [112].

In-situ polymerization method can also be employed to prepare layered graphite-polymer nanocomposites [113,114]. Natural graphite flakes have excellent electrical conductivity and layered structures with a c-axis lattice constant. Because no reactive ion groups exist on the natural graphite layers, it is hard to intercalate monomers into the graphite sub-layers to prepare the graphite/polymer nanocomposites via ion exchange reaction. However, the expanded graphite contains abundant multi-pores with sizes ranging from 2 to 10 μm. Fig. 17 shows a schematic for preparing expanded graphite. First, the expanded graphite is mixed with polymer solution via *in situ* polymerization with the aid of sonication. The polymers are embedded in the pores of the expanded graphite and remain there after solvent extraction. Polymer nanocomposites are then obtained by hot pressing or dip-coating process. In addition, an electrostatic assembly process was also reported for preparing graphene/polymer nanocomposites [115]. First, polystyrene (PS) latex was made by using hexadecyl trimethyl ammonium bromide as a cationic surfactant, creating positive charges on the surfaces of PS micelles. Then, an in-situ demulsification process was performed by introducing negatively charged graphene oxide (GO) into the positively charged PS latex. Afterwards, in-situ reduction and hot pressing were conducted, the graphene agglomeration was largely prohibited by the PS microspheres and facilitated the formation of graphene networks in the PS matrix [115].

3.2. Nanofiber (or nanotube)/polymer nanocomposites

The reported exceptional properties of CNTs motivate many researchers to conduct extensive studies on the processing of CNT reinforced polymer nanocomposites. An interesting way to fabricate these composites is to spin carbon fibers from CNTs dispersed in a surfactant solution followed by recondensation in a stream of a polymer solution [72,116,117]. With this method, there is preferential orientation of the nanotubes along the fiber axis. Carbon nanofiber (CNF) reinforced polymer nanocomposites can be prepared by high shearing method like twin screw extrusion [118–121]. High shearing method is efficient for preparing a CNF well-dispersed sample. The dispersion and distribution of carbon nanofibers within the extruded PMMA nanocomposites can be observed using SEM [121]. SEM images in Fig. 18 show that the nanofibers are well dispersed in the nanocomposites, where PR-21-PS and PR-24-PS are two carbon nanofibers obtained from Applied Sciences Inc. Detailed discussions about dispersion and alignment of carbon nanotubes in polymer matrices can be found in the excellent review [122].

However, the CNF aspect ratio is largely reduced in high shear method. In order to maintain the high aspect ratio of CNTs, *in situ* ring-opening polymerization is then developed for making carbon nanofiber/polycarbonate nanocomposites [123]. The CNFs and carbonate oligomer are ground together with a mortar and pestle until a homogeneous dispersion is obtained. The warmed homogeneous mixture melted with the oligomers in a test tube is then sonicated and allowed to cool to room temperature. A methylene chloride mixture is added to the CNF/oligomer mixture and the sample is sonicated again. Finally, the ring-opening polymerization is conducted to obtain nanocomposites after the solvent is removed using vacuum. The dispersion of carbon nanofibers in polycarbonate can be seen from TEM images in Fig. 19 [123]. The CNFs seem to be well-dispersed throughout the prepared sample and a network is seen whilst there is still aggregation in the 9 wt % nanocomposite.

Moreover, CNT/polymer resin (like epoxy etc.) nanocomposites can also be prepared by hot pressing [122]. Thin membranes of nanotube networks are first obtained by multiple steps of nanotube dispersion and suspension filtration, CNT bulky-papers are then prepared as performs by resin infiltration. These bulky-papers (see Fig. 20) are thus stacked to form the final solid nanocomposites by using a hot press.

3.3. Nanoparticle/polymer nanocomposites

Good dispersion of nanoparticles in polymers is critical to achievement of high performance polymer nanocomposites. Generally, three major ways are available to achieve good dispersion of nanoparticles in polymers. The first is direct mixing of nanoparticles either as discrete phases with polymers to get polymer nanocomposites. The second is *in-situ* polymerization in the presence of nanoparticles to prepare

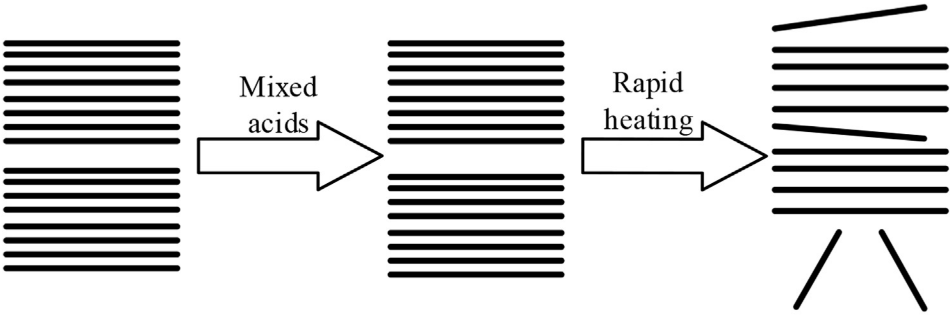

Fig. 17. Schematic of forming expanded graphite (EG) from natural flake graphite [114].

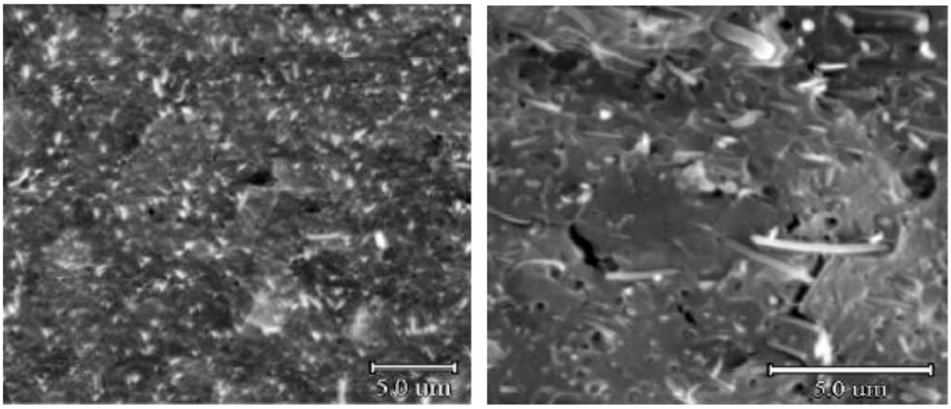

Fig. 18. SEM images of CNF/PMMA composite rod: (a) 5 wt% PR-24-PS/PMMA; (b) 5 wt% PR-21-PS/PMMA [121].

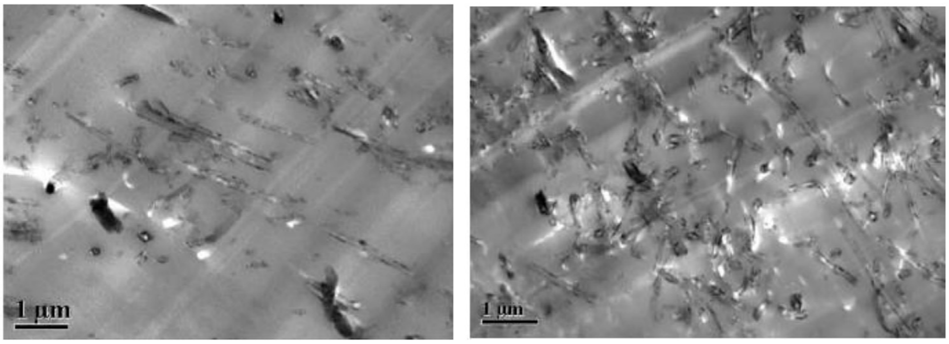

Fig. 19. TEM images of CNF/PC composites 6 wt% (left) and 9 wt% (right) [123].

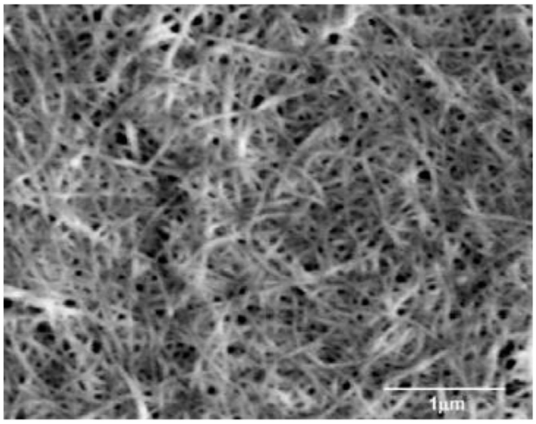

Fig. 20. SEM image of the CNT bulky-paper surface [124].

nanocomposites. The third is combination of both *in-situ* formation of nanoparticles and *in-situ* polymerization to get polymer nanocomposites.

3.3.1. Direct mixing

Well-established polymer processing techniques can be used for direct mixing. For example, nanocomposites with calcium carbonate ($CaCO_3$) and polypropylene (PP) matrix were prepared through melt mixing of the components using a Haake mixer [96]. $CaCO_3$ nanoparticles are 44 nm in diameter. This technique produces reasonably well-dispersed nanocomposite samples at relatively low filler volume fractions of 4.8% and 9.2%, but aggregation occurs at a relatively high volume fraction of 12%. A form of melt-mixing was also used to produce nanocomposites. Silica-polyurethane nanocomposites were made by Petrovic et al. by first mixing silica with polyol [95]. Then, the mixture was cured with diisocyanate at 100 °C for 16 h aided by 0.1% catalyst. The spherical particles have an average diameter of 12 nm and a narrow size distribution (10–20 nm). Good quality samples were produced at 10, 20, 30 and 40 wt.%, but not at 50% filler weight fraction.

Good dispersion of nanoparticles in polymer matrices is one of the major issues in producing good quality polymer nanocomposite samples. Rong et al. show that grafting of monomers made of styrene to surround nanoparticles yields good dispersion. Isotactic polypropylene is used as the matrix and silica of a size of ca. 7 nm is employed as nanofiller [97]. First, the particles are heated to remove water absorbed on their surfaces and then one of the monomers is mixed with solvent. Afterwards, this mixture is irradiated to remove the solvent. Nanocomposite samples with good dispersion of silica are finally prepared by adding polypropylene via tumble mixing, compounding and extruding. The samples produced by this technique show no aggregation and in addition, the particle–polymer matrix interfacial interaction is greatly improved.

3.3.2. In-situ polymerization

Another technique that has been well accepted to prepare polymer nanocomposites is *in situ* polymerization [98–100,125,126]. In this method, nanoparticles are first dispersed in monomer and the resultant mixture is then polymerized. In the work of Yang et al. (1998), silica/polyamide-6 nanocomposites are produced by first drying the silica particles to eliminate water absorbed on their surfaces [98]. Then, the particles are blended with ε-caproamide and a suitable polymerization initiator is added concurrently. The obtained mixture is finally polymerized at a high temperature under nitrogen [98]. This technique gives well-dispersed nanocomposite samples containing silica of ~50 nm, but aggregates are observed for smaller particles with a size ~12 nm [100]. This is most likely because of the increased surface energy for smaller nanoparticles, which favors further particle aggregation.

3.3.3. Solution mixing

Solution mixing method is another technique for producing particulate polymer nanocomposites. The solution mixing technique is used to produce polymethylmethacrylate (PMMA) nanocomposites with good dispersion of alumina nanoparticles [127,128]. The alumina nanoparticles are first added to methylmethacrylate (MMA) monomer and dispersed in a lowly viscous solution through sonication. A chain transfer agent and an initiator are later added. Afterwards, the mixture is polymerized under nitrogen and dried in vacuum. Further processing to make samples are conducted by conventional techniques.

3.3.4. *In-situ particle processing*

This method, namely *in-situ* sol-gel processing of nanoparticles inside polymers, allows design of organic–inorganic nanocomposites. This process has been employed for producing particulate polymer nanocomposites with silica and titania in a variety of polymer matrices [101,129–136]. In this technique, several ways can be employed to produce polymer nanocomposites. The first is to mix silica precursor with a copolymer of polymer matrix and then the sol-gel reaction progresses to produce silica. During drying, the polymer blocks phase-separation and the silica regions coalesce [129]. The second is to mix a silica precursor such as tetraethylorthosilicate (TEOS) with a polymer matrix such as polyimide and epoxy [134,137]. This approach has also been applied to preparation of TiO_2/polymer nanocomposites. Direct addition of TiO_2 nanoparticles to poly (styrene maleic anhydride) (PSMA) results in serious aggregation. Thus, PSMA is first dissolved in tetrahydrofuran (THF), and tetrabutyl titanate is then added under appropriate conditions to prepare nanocomposites with good dispersion of TiO_2 nanoparticles [135]. Since the uncondensed TiOH and maleic anhydride can react, the polymer coats the titania nanoparticles as they form to prevent agglomeration. In this way, good dispersion of TiO_2 in PSMA can be readily achieved. Nano-TiO_2/polyimide nanocomposite films are obtained using the sol-gel process [101,136]. Combination of the above two ways has also been used for making polymer nanocomposites such as silica/polydimethylsiloxane (PDMS) composites [138]. The PDMS network is first formed with TEOS as an end-linking agent. Then, the network is swollen with TEOS and the sol-gel reaction catalyzed.

Silica and titania are ceramic nanoparticles and *in-situ* processing of ceramic/polymer nanocomposites is given above. Particulate metal/polymer nanocomposites can also be produced through *in-situ* formation of metal nanoparticles in polymers using *in-situ* particle processing technique. A review on the *in-situ* formation of metal nanoparticles in polymers has been given by Mayer [139]. Important factors include metal precursor and metal/polymer interaction in terms of particle size, stability and morphology. For hydrophobic polymers, metal precursors with a more hydrophobic characteristic usually lead to stronger interactions and hence smaller particle sizes. If a stronger interaction takes place between the polymer and the precursor, the particles tend to be smaller. Faster reduction methods also bring about smaller particles.

The details of specific preparation methods discussed above can be referenced to corresponding references. In general, no single process can be followed for producing all types of polymer nanocomposites. From the above summary, it is clear that the most important factor to consider in deciding between different processing techniques is the main requirements of good particle dispersion and control of particle size in final polymer nanocomposites.

4. Characterization of polymer nanocomposites

Characterization of polymer nanocomposites can be conducted using wide angle x-ray diffraction (WAXD) analysis, small angle X-ray scattering (SAXS), scanning electron microscopy (SEM), transmission electron microscopy (TEM), thermal gravimetric analysis (TGA), atomic force microscopy (AFM) and solid-state nuclear magnetic resonance (NMR) techniques as well as a dynamic mechanical thermal analyzer (DMTA) etc. In this section, some examples will be presented to show how to characterize polymer nanocomposites with these techniques.

4.1. *Layered filler/polymer nanocomposites*

The structure of layered silicate/polymer nanocompositesis is often characterized using WAXD analysis and TEM observation. Due to its easiness and availability, WAXD is often used to probe the structure of polymer nanocomposites [26,30–33] and occasionally to study the kinetics of polymer melt intercalation [140]. In contrast, TEM technique gives a qualitative understanding of internal structure of nanocomposites, spatial distribution of different phases and any defects by direct observation. However, it is cautioned that only a representative cross-section is studied on the sample. Also, TEM is time-intensive and only gives qualitative characterization on the sample as a whole; but low-angle peaks in WAXD yield quantified changes in layer spacing. Simultaneous SAXS and WAXD studies yield quantitative information of nanostructure and crystallite structure in polymer nanocomposites [141]. NMR can be employed as a tool to gain greater insight about surface chemistry, morphology, and to a very limited extent, dynamics of the polymer nanocomposites [142]. The main objective in solid-state NMR analysis is to connect the measured longitudinal relaxations with the quality of nanoparticle dispersion. NMR can also be used to find out the phase structure of polymer nanocomposites [141]. SEM technique is most commonly used to observe the fracture surfaces of polymer nanocomposites to obtain insight of failure modes and sometimes to see the dispersion of nanoparticles in polymers across the failed surface [137]. AFM technique can serve as a good tool to observe dispersability of nanoparticles in polymers [143].

Two complementary techniques, XRD and TEM, are used to characterize the structures of polymer nanocomposites. XRD is often used to identify intercalated structures. In layered silicate/polymer nanocomposites, the repeating multilayer structure is well preserved, which allows the interlayer spacing to be calculated. The interlayer spacing can be increased by intercalation of polymer chains as shown in Fig. 21, causing the diffraction peak to shift towards lower angle values [26]. Layer spacing is related to angle through Bragg's relation: $\lambda = 2d \sin\theta$, in which λ is wave length of X-ray radiation used in diffraction experiment, d spacing between diffraction lattice planes and θ diffraction or glancing angle. For an exfoliated structure, diffraction peaks cannot be seen in the XRD diffractograms either because there is a much larger spacing between the exfoliated layers (i.e. exceeding 8 nm for ordered exfoliated structure) or because the nanocomposite does not have ordered structures. In the latter case, TEM is often used to characterize the morphologies of the polymer nanocomposites. Besides these two well-defined (intercalated and exfoliated) structures, other intermediate structures with both intercalation and exfoliation can also exist. Thus, a broadening

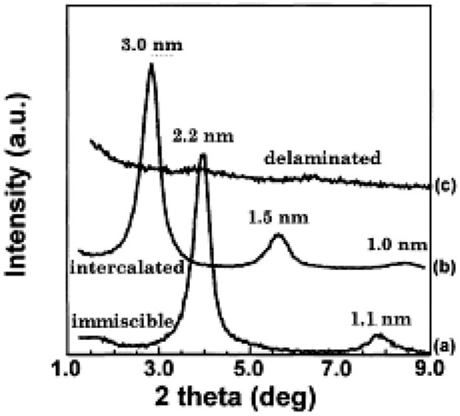

Fig. 21. XRD patterns for (a) phase separated micro-composite (organo-modified fluorohectorite in a HDPE matrix), (b) intercalated nanocomposite (same organo-modified fluorohectorite in a PS matrix) and (c) exfoliated nanocomposite (same organo-modified fluorohectorite in a silicone rubber matrix) [26].

of the diffraction peak is often seen and it is necessary to use TEM observations to define the overall structure [144,145]. Fig. 22 shows TEM images respectively for intercalated and exfoliated nanocomposites [144].

The clay dispersions are characterized by TEM images as shown in in Fig. 23 [146]. The dark lines and the bright areas represent the clay layers and thermoset matrix. TEM analysis display that simultaneously existing exfoliated and intercalated morphologies are achieved upon addition of nanoclay for both the samples. The well dispersed individual clay layers in the polymer matrix are observed, while the large intercalated tactoids are seen in NC-1 (1 wt% nanoclay) and NC-5 (5 wt% nanoclay). The simultaneous presence of exfoliated and intercalated structures in nanocomposites suggests that the van der Waals and Coulombic forces between silicate layers, high specific surface area and surface energy tend to maintain them tightly rather than to disperse them homogeneously in the epoxy matrix.

Fig. 24a and b represent, respectively, the WAXD patterns of various organo-modified layered silicates (OMLSs) and corresponding nanocomposites of polyimide (PI) in the range $2\theta = 2–10°$ [147]. WAXD patterns (see Fig. 24b) reveal that the MMT or mica/PI nanocomposites do not have any peaks corresponding to the exfoliated structure, but the hectorite or saponite/PI nanocomposites have small peaks, suggesting that some portions of OMLSs are stacked. It is known that OMLS particles are dispersed homogeneously in the PI matrix and oriented parallel to the film surface when MMT or mica-based OMLS is used for preparing nanocomposites, whereas most of the OMLS are dispersed homogeneously with small stacks in the saponite/PI nanocomposite. Conversely, aggregates of OMLSs usually appear in the nanocomposite when hectorite is used as nanofiller. These observations are well correlated with the WAXD patterns as shown in Fig. 24b. In another work, the rigid-rod MMT/PI nanocomposites are characterized by TEM and WAXD [148]. The MMT/PI nanocomposites are exfoliated at low contents and partially exfoliated at high contents. In the case of MMT/poly (L-lactide) (PLLA) nanocomposites [149], WAXD and SAXS results exhibit that the silicate layers of clay cannot be intercalated in the PLLA-MMT blends prepared by the solvent-cast method. That is, clay exists in the form of tactoids. The tactoids consist of several stacked silicate monolayers and these tactoids help form remarkable geometrical structures in the blends, leading to superstructures in the thickness of the blended composite film, which increases the Young's modulus of the blend. Similar result was observed for the 2C18-MMT/poly (ε-caprolactone) (PCL) blend [150]. Based on WAXD analyses of clay/nylon 6 nanocomposiets [151], it is concluded thatthe organoclay galleries amplify systematically to adapt the molecular size and amount of amine surfactant exchanges for Na^+-MMT. And three identified distinct surfactant effects include: (a) one long alkyl tail rather than two on the ammonium ion; (b) methyl groups rather than 2-hydroxy-ethyl groups on the amine; and (c) an equivalent on the clay rather than excess amount of amine surfactant. These effects bring about greater extents of exfoliation, increased stiffness and higher yield strength for nanocomposites.

TEM is used to characterize polymer-layered graphite nanocomposites such as expanded graphite/poly (St–MMA) nanocomposites as shown in Fig. 25, [41]. The solid lines are the exfoliated graphite sheets viewed from their side direction, whereas the domains represent the poly (St–MMA) matrix. Obviously, the thickness of graphite sheets in the polymer matrix is ca. 10–20 nm. The graphite sheets are almost

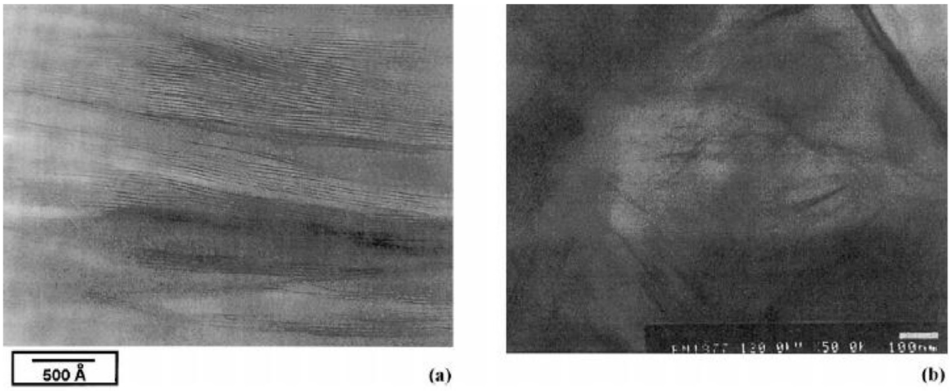

Fig. 22. TEM images respectively for (a) intercalated and (b) exfoliated poly (styrene)-based nanocomposites [144].

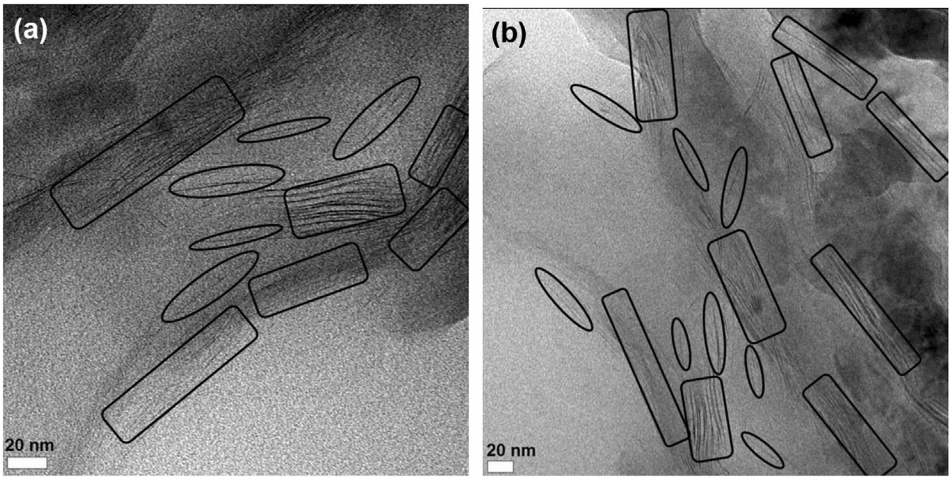

Fig. 23. TEM micrographs of (a) 1 wt% nanoclay/epoxy nanocomposite (NC-1) and (b) 5 wt% nanoclay/epoxy nanocomposite (NC-5) (circle denotes exfoliated layers and rectangle indicates intercalated layers) [146].

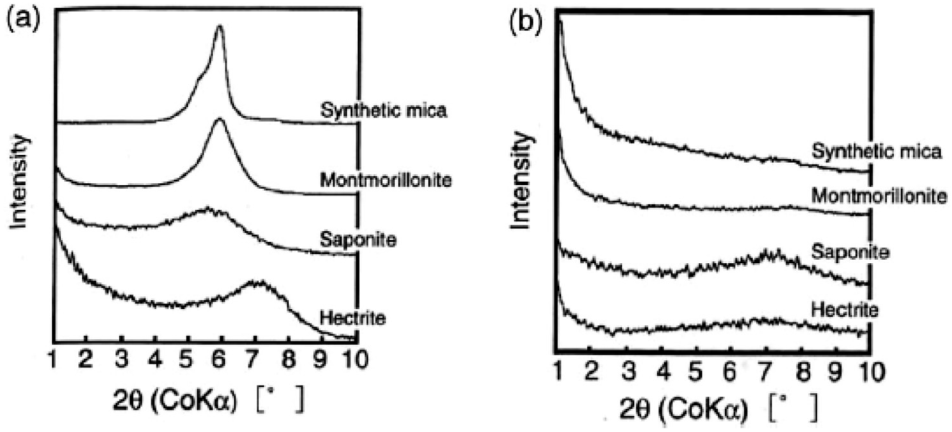

Fig. 24. WAXD patterns for (a) various organoclays and (b) corresponding nanocomposites based on polyimide [147].

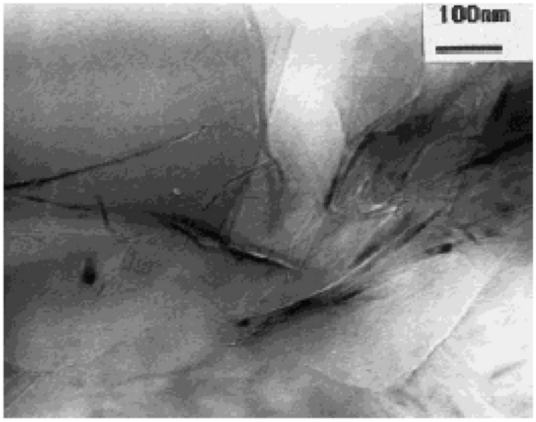

Fig. 25. TEM image of graphite/poly (St–MMA) nanocomposite [41].

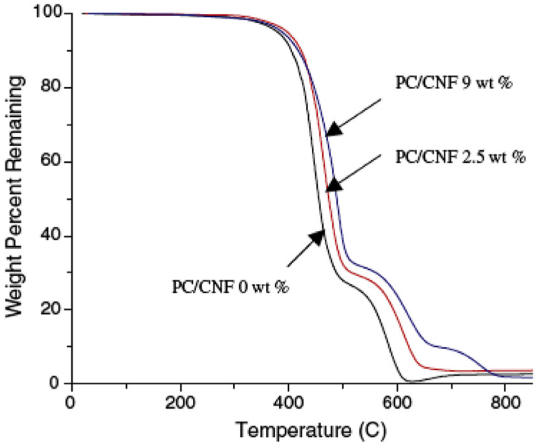

Fig. 26. TGA results for the PC/CNF composites [123].

homogeneously dispersed in the polymer matrix although there are still some graphite sheets existing in the form of micrometer sized particles.

4.2. Nanofiber or nanotube/polymer nanocomposites

TGA can be used to characterize thermal behaviors of polymer nanocomposites and then investigate the thermal stability of CNF or CNT-polymer nanocomposites [123]. TGA (Fig. 26) analysis shows a slight increase in thermal stability of CNF/polymer composites with increasing CNF content [123]. At 9 wt% CNF, 5 wt% loss of polycarbonate (PC) occurs at 382 °C compared to 379 °C for the control pure polymer. The secondary decomposition of PC has a more significant difference between 9 wt % CNF (577 °C) and pure polymer (512 °C). In CNF (or CNT)/polymer nanocomposites, the increased thermal stability is often attributed to restricted macro-molecule mobility imposed by the CNFs [152,153]. The purpose here is to show characterization means for polymer nanocomposites and more details will be presented in Section 4 on thermal stability of nanocomposites.

In Section 2.4, nanocomposite interfaces are briefly introduced. TEM technique can be well used to characterize CNT or CNF/polymer interfaces. Thin films are microtomed at room temperature from tensile bars from both directions perpendicular and parallel to flow direction. The samples cut from the outer regions show cylindrical nanofibre cross-sections, whereas more oval shaped cross-sections can be seen in the centre part, testifying the different alignments is dependent on the shear flow experienced during processing. Also, the nanofibre cross-sections are all well-separated, verifying the good dispersion quality of nanofibers. Fig. 27 exhibits a TEM micrograph of a CNF wall (left) and the interfacial bonding to the PEEK matrix [154]. The interface maintained during sample preparation is considered as an indication of good interfacial bonding between the vapour-grown CNFs and the PEEK.

4.3. Nanoparticle/polymer nanocomposites

TEM technique has been well accepted for characterizing the dispersibility of nanoparticles in polymers. Fig. 28 shows TEM images of the nano-ZnO/poly (styrene butylacrylate) latex composites with various nano-ZnO contents [86]. It can be clearly seen that the dispersibility of the nanoparticles in the nanocomposites decreases with increasing nano-ZnO content. Most of the nanoparticles inside the nanocomposite with 3 wt % ZnO content are well dispersed to nano-scale as exhibited in Fig. 28 (a). As more nano-ZnO particles are introduced into the polymer matrix, more agglomerates of nano-ZnO are observed as displayed in Fig. 28(b–d).

SEM can also be employed to characterize the dispersibility of particles in polymers. The morphology of the cryogenic tensile fracture surfaces of silica/PI nanocomposite films is studied using SEM and shown in Fig. 29 [137]. Particle dispersions are shown to be uniform in all samples and the particle size increases with increasing silica content in the polyimide hybrid films.

Dispersion of metal nanoparticles in polymers can be characterized using AFM technique. Since the resonant frequency of the AFM tip interacting with the polymer crystal is different from that of the metal nanoparticles, the tapping frequency is slightly increased in order to differentiate metal nanoparticles from polymer matrix. Fairly uniform nanoparticles with diameters between 10 and 40 nm are observed in Fig. 30 throughout the Pd nanoparticle/FEP composite film, and particle

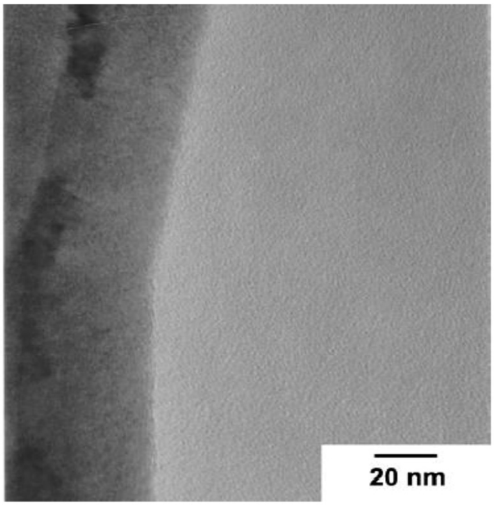

Fig. 27. High-resolution TEM micrograph for the interfacial bonding between a vapour grown CNF wall (left) and the PEEK [154].

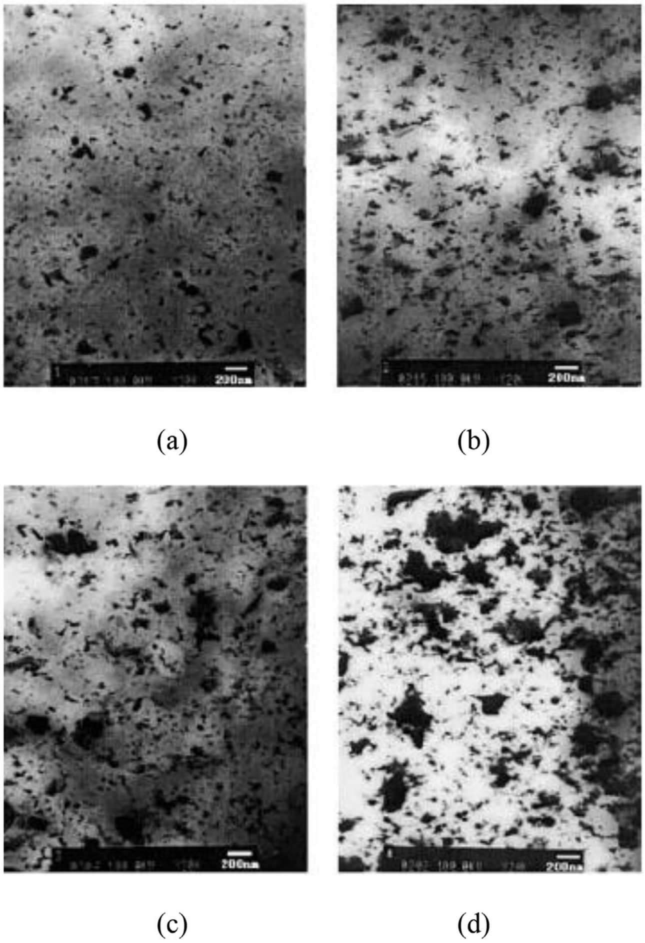

Fig. 28. TEM micrographs of PSB nanocomposites with nano-ZnO contents of: (a) 3 wt %, (b) 5 wt %, (c) 7 wt %, and (d) 9 wt % [86].

distribution does not vary much through the thickness of the composite film [143].

5. Properties of polymer nanocomposites

Polymers have relatively insufficient modulus and strength as engineering materials. Inorganic inclusions such as fibers, whiskers, platelets or particles are often employed to improve their mechanical properties. Traditionally, polymer composites are reinforced with micron-sized inclusions. In recent years, the inclusion size is allowed to go down to nanoscale. Research work is still ongoing and a definite conclusion is not yet clear on the effect of nano filler size on properties of polymer systems. The properties of polymers that can be enhanced dramatically by inctroducing nanoscale fillers at fairly low concentration include mechanical properties, thermal stability, heat distortion temperature, fire retardancy, gas barrier properties, ionic conductivity and magnetic properties etc. In this section, the effects of nanoscale filler incorporation on these properties of polymer nanocomposites are discussed.

5.1. Mechanical properties

5.1.1. Layered nanofiller/polymer nanocomposites

Clay minerals have a layer structure with a typical thickness of ~1 nm. If properly exfoliated, clay can reach to platelets having a high aspect ratio (an average length of 120 nm reported). Organoclay/nylon 6 nanocomposites are made via direct melt compounding using a conventional twin screw extruder [155]. The strength of the nanocomposites is significantly increased and shows much higher values than that of glass fiber composites [155]. The yield strength of nylon-6/organoclay nanocomposites increases dramatically with the increase of organoclay content and has a higher value than the nylon-6/glass fiber composites with a higher weight percentage as shown in Table 2, [155]. Moreover, the modulus of nylon 6/organoclay nanocomposites increases dramatically with the increase of organoclay content as shown in Fig. 31, [155]. This can be explained in terms of platelet aspect ratio. The platelets resulting from exfoliation of clay minerals have a high aspect ratio in the nanocomposites. As shown previously for short fiber reinforced polymer composites, the composite strength and modulus generally increases with the increase of filler aspect ratio [156,157]. So a high aspect ratio of clay platelets is important to the achievement of the high strength and modulus. Table 3 shows that the tensile strength and Young's modulus of clay/nylon 1012 nanocomposites increases dramatically with increasing the particle content [158]. Similar results are obtained for polyurethane/clay nanocomposites [159,160].

The mechanical properties of layered silicate/polymer nanocomposites are dependent on whether they are intercalated or exfoliated nanocomposites or micro-composites. For intercalated nanocomposites, the strength can be enhanced by the addition of clay nanoparticles. The tensile strength results of intercalated clay (MMT)/elastomeric polyurethane (MMT/PU) nanocomposite are shown in Fig. 32, [161]. The tensile strength increases with increasing the clay content in the range 0–8 wt%. The maximum value of the tensile strength is reached when the content of clay is 8 wt %. When the clay content is increased further over 8 wt %, the tensile strength decreases. This is because when the clay content is lower than 8 wt %, the nanometer clay layers have strong interaction with the PU matrix and show a good dispersion in the PU matrix; however, when the clay content is greater than 8 wt %, the clay begins to aggregate [161]. Furthermore, the exfoliated nano-composites have higher strength than the intercalated counterparts. As shown in Table 4, the strength of nylon 6/clay exfoliated nanocomposites is significantly increased by adding only a few wt % of clay particles [161,162]. Intercalated nanocomposites show a lower absolute improvement in strength, if any. Magadiite exfoliation in reinforcement of the polymer is illustrated by the tensile strength *vs* silicate content results in Fig. 33, [163]. Moreover, the tensile strength of the exfoliated magadiite nanocomposites is better than that of the conventional composites prepared from Na^{+}-magadiite and C18-magadiite-LM. These results are expected because silicate nanolayers have been well dispersed in the polymer and each nanolayer contributes to the reinforcement effect. Exfoliated nanocomposites are microscopically homogeneous, which is superior to the macroscopic homogeneity of traditional composites.

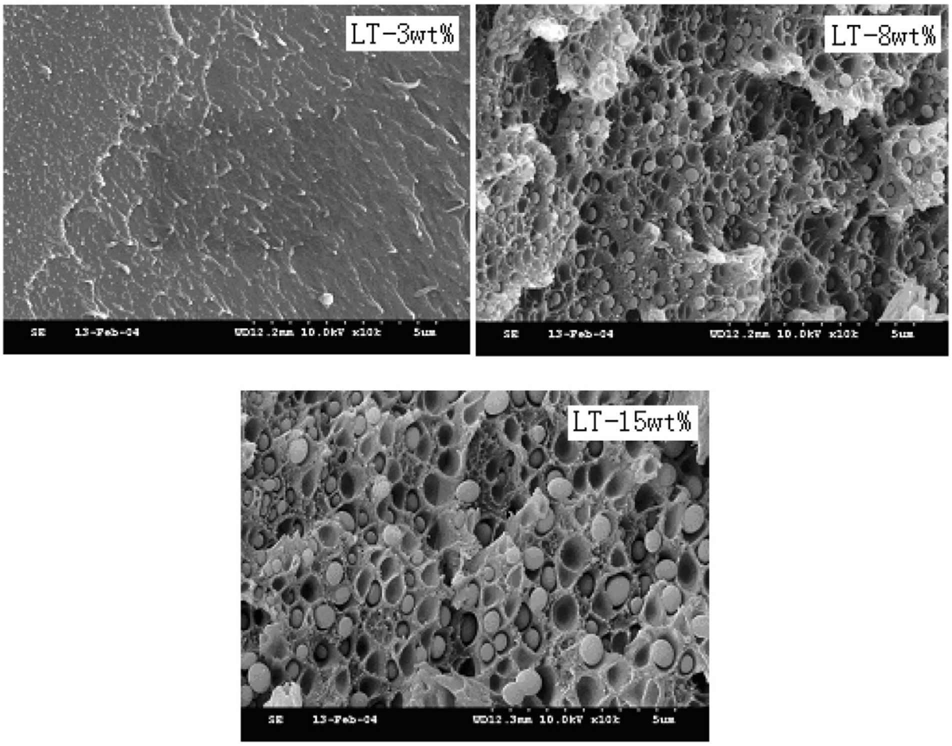

Fig. 29. SEM photographs of the tensile fracture surfaces at 77 K of silica/PI hybrid films with (a) 3 wt % silica, (b) 8 wt % silica, and (c) 15 wt % silica [137].

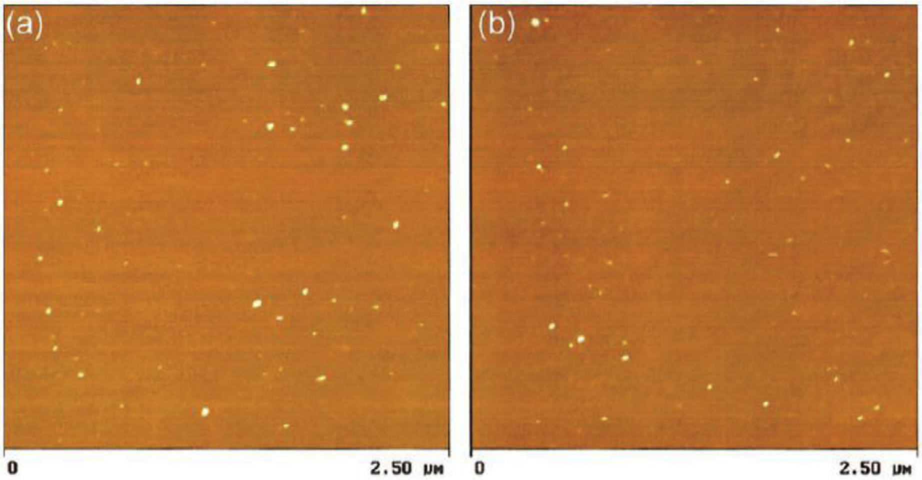

Fig. 30. AFM phase images of fluorinated ethylene-propylene (FEP) composite film infused with Pd nano-particles: (a) edge of the film; (b) centre of the film [143].

Table 2
Comparison of the yield strength of organoclay/polyamide 6 nanocomposites and glass fiber/polyamide 6 composites [155].

Polyamide composites	Filler content (wt %)	Yield strength (MPa)
Nylon 6 (N6)	0	64.2±0.8
Glass fiber/N6	5	72.6±0.8
Organoclay/N6	16	84±0.7

Fracture energy and toughness of clay-modified glassy epoxy composites have been determined with compact tension specimens [164]. The results are given in Fig. 34 for a range of clay concentrations. At low concentrations, less than 5 wt%, there is little improvement in fracture energy/toughness, since the clay domains are isolated and offer little resistance to fracture. However, at 5 wt % and above, there is a significant jump in fracture energy/toughness. The fracture energy of the composites is shown to be improved by 100% at the clay conctent of 5 wt %. In contrast, however, the results for the notched Izod impact strength of neat nylon 66, binary and ternary nanocomposites toughened with SEBS-g-MA and filled with clay show that the nanocomposites have been embrittled [165]. This is possibly caused by the constraining effect of the matrix on the clay layers limiting the toughening mechanisms that could occur similar to the case of short fiber reinforced thermoplastic composites [166].

Exfoliated molybdenum disulfide (MoS_2) nanoplatelets are dispersed in an epoxy resin at the filler content up to 1 wt.% [167]. The results show that MoS_2 nanoplatelets are effective in increasing tensile strength and elastic modulus of the epoxy at very low MoS_2 contents (0.1–0.2% by weight). However, beyond ~0.2% content, a reduction in performance is observed and at ~1% MoS_2 content, the performance of the nanocomposite is only comparable to that of pure epoxy. This is because at

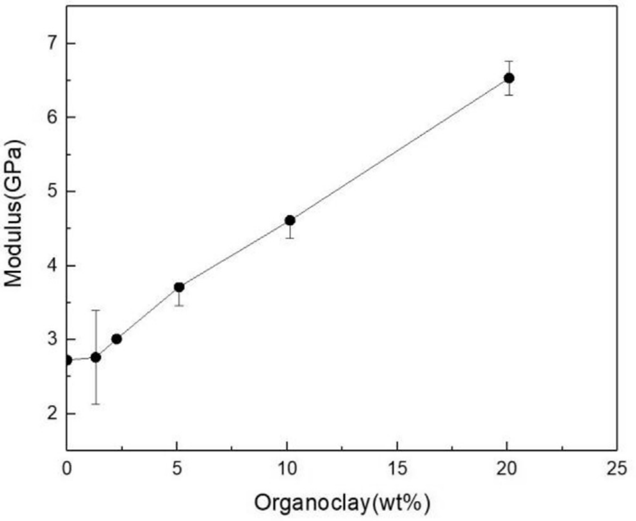

Fig. 31. Young's modulus of melt processed organoclay/nylon 6 nanocomposites as a function of organoclay content [155].

Table 3
Tensile strength of nylon 1012 and clay/nylon 1012 nanocomposites [158].

Material	Tensile strength (MPa)	Tensile modulus (GPa)
Nylon 1012	31.67±0.5	2.02±0.2
Clay (1)/nylon 1012	34.1±0.5	2.11±0.2
Clay (3)/nylon 1012	38.86±0.5	2.93±0.2
Clay (5)/nylon 1012	47.4±0.6	31±0.2

Note: Numbers in parentheses indicate the percentage of clay in weight in the nanocomposites.

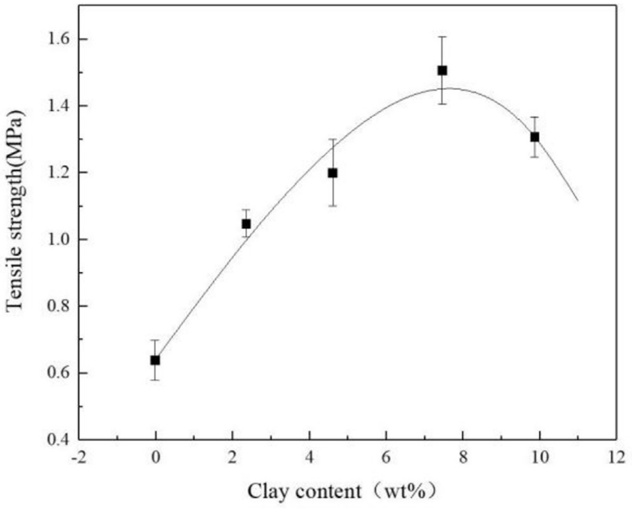

Fig. 32. Effect of clay content on the tensile strength of MMT/PU nanocomposites [161].

Table 4
Tensile strength of nanocomposites based on various thermoplastic matrices and nano-silicate particles [27,162].

Matrix type	Matrix tensile strength (MPa)	Nanocomposite type	Nanofiller content (wt %)	Composite tensile strength (MPa)
Nylon-6	68.6	Exfoliated	4.7	97.2
	68.6		5.3	97.3
	68.6		4.1	102
	68.2		4.2	91.3
PMMA	59	Intercalated	12.6	62.0
	59		20.7	62.0
PP	31.4		5.0	29.5
	32.6		4.8	31.7
PS	28.7		11.3	21.7
	28.7		17.2	24
	28.7		24.6	16.6
	28.7		34.1	16.0

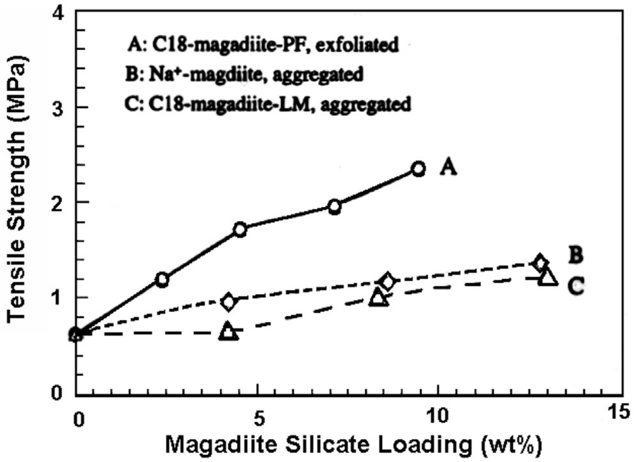

Fig. 33. Comparison of tensile strength of an exfoliated magadiite/epoxy nanocomposite prepared from C18-magadiite-PF and conventional magadiite composites prepared from Na^+-magadiite and C18-magadiite-LM [163].

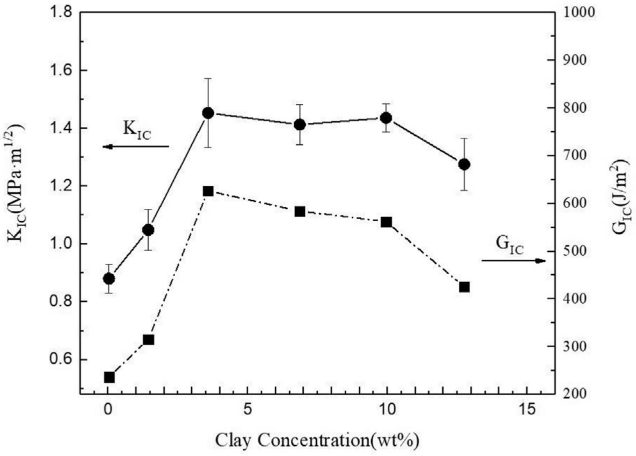

Fig. 34. Variance of fracture toughness with clay concentration [164].

higher loading fractions, MoS_2 nanoplatelets would form agglomerates, resulting in fewer interfacial interactions. Moreover, epoxy-based nanocomposites with Mg—Al layered double hydroxides (Mg—Al LDHs) were prepared under high shear mechanical agitation [168]. Epoxy/Mg—Al LDH system revealed higher values of storage modulus and elastic modulus but the strength was not enhanced by addition of LHDs.

Ultra-high molecular weight polyethylene (UHMWPE) nanocomposites were fabricated by the addition of Ti_3C_2, a two-dimensional nanomaterial (Mxene) using a hot compression mold technique [169]. The frictional coefficient was greatly lowered but the yield and ultimate strength was only slightly enhanced by the introduction of Mxene at 0.25 wt%-2.0 wt%. However, on the other hand, the $Ti_3C_2T_x$ films could be fabricated by vacuum-assisted filtration (VAF) [170] and the VAF was then employed to manufacture highly flexible $Ti_3C_2T_x$/polyvinyl alcohol (PVA) nanocomposite films. The cross-section of the composites shows parallel stacking of $Ti_3C_2T_x$ flakes. The tensile strength of the

$Ti_3C_2T_x$/PVA nanocomposites was greatly increased compared to that of pure $Ti_3C_2T_x$ or PVA films. It seems that different preparation methods leads to different strengthening effects for MXene/polymer nanocomposites.

Among the various factors influencing the mechanical properties of polymer nanocomposites, the interfacial interaction and thus the stress transfer from the matrix to the nanoparticles play the major role [171]. A poor interface/interphase induces the debonding of nanoscale fillers from the polymer matrix during loading [172], possibly weakening the polymer matrix. Theoretical results showed that the mechanical properties of polymer nanocomposites depend critically on the interface/interphase characteristics such as thickness, modulus and strength [173,174]. Two types of graphene nanoplatelet (GNP)/epoxy nanocomposites with different interface strengths were prepared using the combination of sonication and chemical modification [175]. Surface-modified GNP/epoxy nanocomposites exhibited a remarkable enhanced fracture energy release rate in comparison with neat epoxy. Nonetheless, though the case of 2D layered nanocomposites is discussed here, it should be pointed out that the interfaces/interphases are not only critical for mechanical properties of 2D layered nanofiller/polymer nanocomposites but also for those of 1D fibrous and 0D spherical polymer nanocomposites.

5.1.2. Nanofiber or nanotube/polymer nanocomposites

As pointed out in the section on nanoscale fillers, carbon nanotubes or nanofibers have very high mechanical properties. It is then of interest to find out the mechanical properties of the resultant nanocomposites after carbon nanotubes or nanofibers are incorporated into polymers. The mechanical behavior of such nanocomposites is presented below with examples.

As discussed earlier, when carbon nanotubes are assembled in ropes, slipping of CNTs would greatly affect the elastic properties [176]. Except slipping of CNTs, the aggregation of CNT ropes also effectively reduce the length/diameter ratio (aspect ratio) of the reinforcement. CNT/PVA composite films are processed for studying mechanical properties [177]. The tensile elastic modulus and damping properties of the PVA composite films are estimated with a DMTA as a function of CNT content and temperature. From the theory developed for short-fiber composites, a nanotube elastic modulus of 150 MPa has been estimated from the experimental data. This value in a microscopic composite is well below the values reported for isolated nanotubes. Two possible reasons are: (1) carbon nanotubes are generally curved when dispersed in polymer matrices, leading to lowered elastic properties while in the theory for short fiber composites, short fibers are assumed straight [2]; (2) carbon nanotube-polymer interfacial adhesion is generally poor but the theory for short fiber composites assumes the interfacial adhesion perfect [156,178]. Hence, the elastic modulus of carbon nanotubes would lead to significant underestimation.

Another example is carbon-nanotube/polystyrene composites [179]. When only 1 wt % (about 0.5 vol %) of nanotubes is added, 25% increase in tensile strength and 36–42% increase in elastic stiffness are achieved. Fig. 35 is the TEM image of the nanotubes film showing the fracture mechanisms. Similar to traditional fiber composites, nanotube pullout, nanotube fracture and nanotube crack-bridging are observed. Short fiber composite theory is used to demonstrate that 10 wt % carbon fibers (about 5 vol %) are required to achieve the same enhancement in elastic modulus with 1 wt% CNTs [180].

An interesting composite is macroscopic carbon fiber made of nanotubes and a traditional material. single-walled nanotubes at 5 wt.% are dispersed in isotropic petroleum pitch [117]. Compared to traditional isotropic pitch fibers, the tensile strength of the carbon fibers containing CNTs is improved by ~90%, elastic modulus by ~150% and electrical conductivity by ~340%.Further efforts will lead to the creation of a new form of carbon fibers that have extraordinary flexibility, stiffness and strength. Fig. 36 shows the exceptional flexibility of the as-prepared nanotube-based fibers produced by Vigolo and coworkers [72].

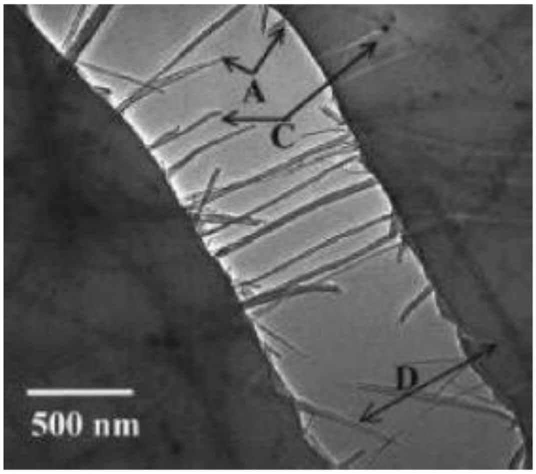

Fig. 35. SEM image showing fracture mechanisms of nanotube-based composites [179].

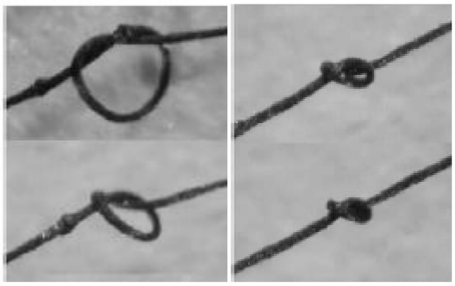

Fig. 36. Carbon nanotube-based fibers with exceptional flexibility [72].

The stress-strain curves at cryogenic temperature (liquid nitrogen temperature, 77 K) of neat epoxy and MWCNT/poly (ethersulfone) (PES)/epoxy composites prepared by three roll milling technique are exhibited in Fig. 37a [181]. It displays the linear relationship between stress and strain for both epoxy resin and MWCNT/epoxy composites, and thus these samples exhibit brittle behaviors at 77 K. Incorporation of MWCNTs at proper contents led to enhancements in cryogenic tensile properties. However, as the CNT content increases further to 1.0 wt% and above, the tensile strength and failure strain are lowered due to the aggregation of CNTs at high contents.

The fracture toughness expressed by critical stress intensity factor K_{IC} at 77 K of MWCNT/PES/epoxy composites is presented in Fig. 37b as a function of the CNT content [181]. It is shown that as the CNT content increases, the fracture toughness initially increases and reaches the maximum value of 2.02 MPa $m^{1/2}$ with an improvement of 13.5% at 0.5 wt.% MWCNT content. However, aggregates of MWCNTs would appear at high CNT contents and this could give rise to weak MWCNT-epoxy interactions and high stress concentrations. Therefore, the slight decrease of K_{IC} at 77 K was caused by the aggregation of MWCNTs with 1.0 and 2.5 wt.%. Although the K_{IC} at 77 K of the composites was reduced by further increasing the MWCNT content to 1.0 wt.% and 2.5 wt.%, it was still higher than that of the matrix.

Incorporation of carbon nanotubes does not always enhance the mechanical properties of polymers. For example, the incorporation of nanofibres significantly reduced the impact properties of polycarbonate [182], the failure strain of polypropylene and PEEK at 15 wt% nanofibre loading [152,154]. This is mainly due to poor adhesion of carbon nanotubes to polymer matrices and restricted matrix deformation imposed by carbon nanotubes.

The fracture toughness enhancement of carbon nanotube (CNT)-reinforced polymer composites was analysed based on atomistic

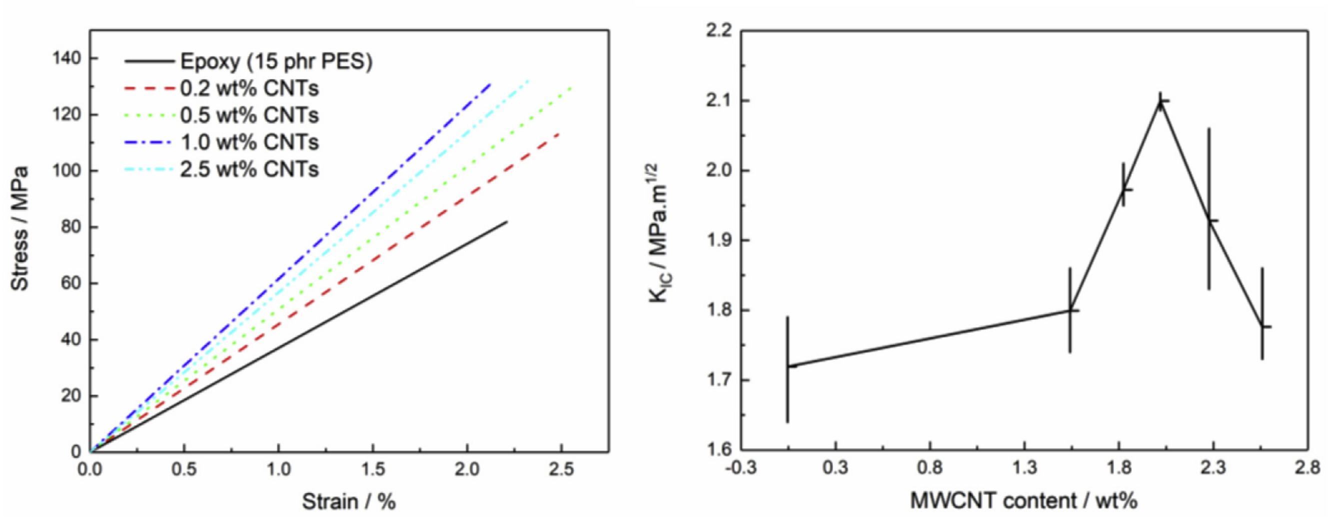

(a)

(b)

Fig. 37. (a) Typical stress-strain cures and (b) fracture toughness K_{IC} of MWCNT/PES/epoxy composites at 77 K [181].

simulation, shear-lag theory and facture mechanics [183]. Fig. 38 shows the theoretical results for normalized fracture toughness enhancement versus normalized interface length [183], where the normalized interface length is defined as a function of interface strength and shear displacement. It is interesting to note from Fig. 38 that when normalized interface length is larger than 5, the normalized fracture toughness enhancement approaches a plateau. Therefore, the fracture toughness enhancement is insensitive to a further increase in normalized interface length. It was thus suggested that the normalized interface length of 5 is long enough to achieve good toughness enhancement. Further, for CNTs with finite length, it was regarded that there existed an optimal interface strength which led to pull-out failure for optimal fracture toughness. Therefore, optimal CNT length and optimal interface strength would lead to optimal fracture toughness for CNT/polymer nanocomposites. In addition, the same authors investigated the effect of CNT diameter on the fracture toughness of CNT reinforced composites and it was found that the reduction in CNT diameter could lead to a sudden drop in composite fracture toughness due to the transition of dominant failure mode [184]. Smaller CNTs did not definitely confer a higher fracture toughness on their reinforced composites, and the optimal diameter of CNTs might exist in the transition from interfacial debonding to CNT breaking. The above results are similar to those of short fiber reinforced polymer composites [178]. Optimal interface bonding and short fiber aspect ratio hold true for achieving high fracture toughness of short fiber composites. However, a stronger interface adhesion generally corresponds to a higher strength of discontinuous polymer composite [178].

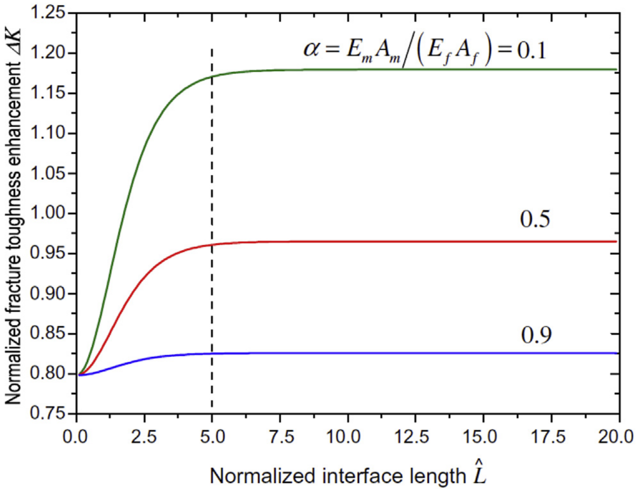

Fig. 38. Dependence of normalized fracture toughness enhancement on normalized interface length with different α values[183]. Here E_f and E_m are Young's modulus while A_f and A_m are the cross-section areas of CNTs and the matrix, respectively.

5.1.3. *Spherical nanoparticle/polymer nanocomposites*

The effect of particle size (particle diameter) on tensile strength of $CaCO_3$/PP composites is presented in Fig. 39 [185]. The particle size varies in a wide range from 0.01 μm (10 nm), 0.08 μm and 1.3 μm–58 μm. Clearly, the composite strength increases with decreasing particle size. Since smaller particles have higher total surface areas for a given particle volume fraction, the strength increases with increasing the surface area of filled particles. Because the stress transfer from a polymer matrix to particle fillers takes place via the filler-matrix interface, higher surface area and hence higher interfacial area will help enhance the efficiency of stress transfer.

The role of particle/matrix interfacial adhesion is also of interest on the composite strength. When silica nanoparticle surfaces are modified by aminobutyric acid to improve filler/matrix adhesion, the tensile strength of silica filled nylon 6 nano-composites shows a bell-shape with increasing silica content, Fig. 40, where the size of most particles varies from 50 to 110 nm [99]. It is also shown that the tensile strength has the maximum value at 5 wt % silica. This can be explained by the separation-to-aggregation process of inorganic particles with increasing particle content. When the surface of the particles is not modified, the strength decreases with increasing particle loading. The modified composites have good dispersion and good interfacial adhesion between silica particles and polymer matrix. So, when an external stress is applied on the nanocomposites, the stress transfer at the interface should be better for the silica-modified nanocomposite and hence an improvement in composite strength is observed. Similarly, the impact fracture energy of silica filled nylon 6 nanocomposites also shows the same trend as the tensile strength data with respect to increase of silica content.

Significant improvement in modulus has also been observed by the addition of nanoparticles to a polymer matrix. This has been

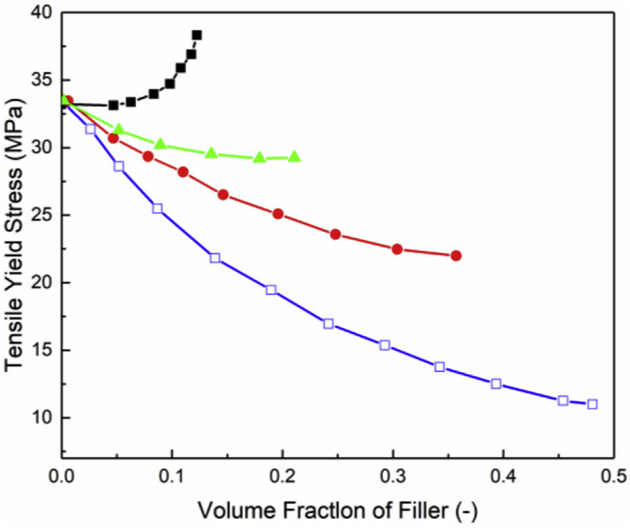

Fig. 39. Effect of spherical particle size on the tensile strength of$CaCO_3$/PP composites [185]. Particle diameter: (■) 0.01 µm, (Δ) 0.08 µm, (◯) 1.3 µm and (☐) 58 µm.

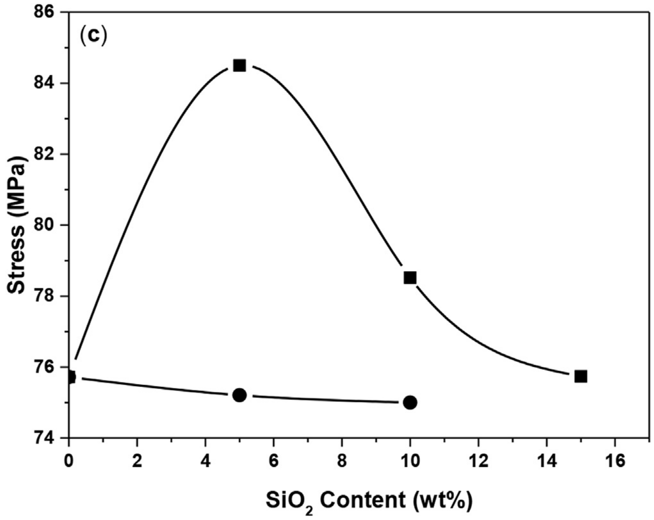

Fig. 40. Tensile strength of nanocomposites based on nylon 6 filled with modified (■) and unmodified (●) silica (SiO_2) particles, respectively [99].

demonstrated by Ou et al. on silica filled nylon 6 nanocomposites, where the particle size ranges from 50 to 110 nm [99]. Results for tensile modulus of silica/PI composites are shown in Fig. 41 [186]. The Young's modulus of the PI nanocomposites increases linearly with increasing silica content. This trend is the same as for constant-size particle filled composites. However, the particle size is 100–200 nm at a silica content of 5 wt%, 200–450 nm and 1–2 µm, respectively, when the silica content is increased to 10 and 20 wt %. Therefore, the dependence of the composite modulus on the particle size is not significant as the composite strength does. Otherwise, the relationship between Young's modulus and particle content will be nonlinear.

The results for the tensile properties of silica/epoxy nanocomposites are given in Table 5 [134]. At ambient temperature, the strength (only a slight change) is insensitive to silica nanoparticle content. However, at cryogenic temperature, the composite strength increases greatly with increasing silica content. This is because at cryogenic temperature, the compressive stress at the silica/epoxy interface caused by different thermal expansions between silica nanoparticles and epoxy resin would lead to largely improved silica/epoxy interface adhesion. Nonetheless, the elongation at break at cryogenic temperature is only slightly improved by the addition of silica nanoparticles while the elongation at break at ambient temperature is greatly enhanced by the addition of silica nanoparticles.

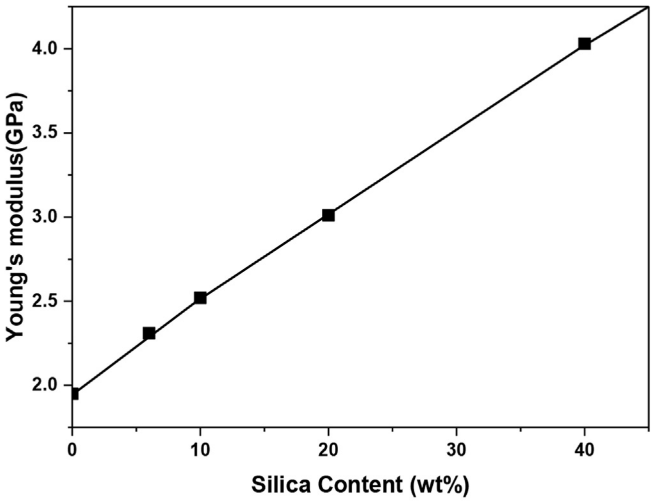

Fig. 41. Influence of silica content on the Young's modulus of silica/polyimide (PI) composites [186].

5.2. Dynamic mechanical analysis

5.2.1. Layered nanofiller/polymer nanocomposites

The dynamic mechanical properties of neat polypropylene (PP) and nano-composites (PPCNs) prepared with organo-clay are exhibited in Fig. 42, [187]. Clearly, addition of EM-MMT to the PP matrix leads to a remarkable increase in stiffness and a reduction in tan δ. The E′ curves display an improved rubbery plateau, indicating that organo-clay induces a reinforcing effect. Moreover, at very high temperatures, this reinforcing effect becomes stronger. These observations further confirm the improved thermal–mechanical stability by the layered nano-fillers at high temperature. The PPCNs exhibit two peaks in tan δ (see Fig. 42c). The dominating relaxation process at ~10 °C is the glass–rubber relaxation of the amorphous region of PP. The weak peak at ~100 °C is associated with the crystalline regions of polypropylene. Moreover, it is interesting to observe that the glass transition temperature (T_g) of PPCNs does not further decrease above an organo-clay content of 3 wt%.

5.2.2. Nanofiber or nanotube/polymer nanocomposites

The results for storage modulus of CNT/epoxy composites are shown in Fig. 43 and Table 6, [124]. The storage modulus of the nanocomposites is increased by 349–492% compared to that of neat resin. Nonetheless, the storage modulus is much lower than that predicted by the rule of mixtures for randomly oriented SWCNT-reinforced composites. Particularly, the formation of large ropes in the composites can significantly reduce aspect ratio and thus decrease stress transfer capability. It is experimentally displayed that the elastic and shear moduli of SWCNT ropes are decreased from 900 GPa to around 100 GPa due to possible tube slippage in the ropes when SWNT rope diameters increase from 3 to 20 nm [176]. Thus, the carbon nanotube rope-reinforced composites would yield poor mechanical properties. Also, a notable observation of the DMA results shows that the structures and mechanical properties of the nanocomposites are highly dependent on the dispersion of the nanotubes, which directly affects the molecular interactions of nanotube/nanotube and nanotube/resin in the composites. Such molecular interactions are critical in stress transfer and interfacial bonding that finally determine the nanocomposite mechanical properties.

Table 5
Dependence of tensile strength and failure strain of silica/epoxy nanocomposites on silica content [134].

Sample No.	Silica content (wt %)	Tensile strength (MPa)		Failure strain (%)	
		77 K	298 K	77 K	298 K
1	0	72.7±4.5	47.5±1.5	1.6±0.1	6.5±2.4
2	2	84.6±0.9	50.2±0.8	1.8±0.15	16.5±1.6
3	4	102.5±4	46.2±0.8	2.3±0.1	15.2±2.1

5.2.3. Nanoparticle/polymer nanocomposites

Fig. 44 shows storage modulus versus temperature for pristine poly (vinyl chloride) (PVC) and nano-$CaCO_3$/PVC nanocomposites [188]. The storage modulus in the studied temperature range (<60 °C) of pure PVC is lower than that of the $CaCO_3$/PVC nanocomposites. It verifies that well-dispersed $CaCO_3$ nanoparticles can stiffen the polymer matrix. However, at the 7.5 wt% $CaCO_3$ nanoparticle loading, the stiffening effect decreases with increasing temperature, most probably resulting from agglomeration of the $CaCO_3$ nanoparticles.

5.3. Thermal stability and flame retardancy

Thermal stability of biodegradable poly (ε-caprolactone) (PCL) nanocomposites filled with layered silicates (montmorillonite, MMT) was studied by using TGA. Generally, the degradation of PCL obeys a 2-step mechanism (Alexandre and Dubois, 2000; Lepoittevin et al., 2002): firstly, random chain scission via pyrolysis of the ester groups, releasing CO_2, H_2O and hexanoic acid, then secondly, ε-caprolactone (cyclic monomer) is formed due to an unzipping depolymerization process. The thermograms of MMT/PLC nanocomposites are presented in Fig. 45 [189]. Both intercalated and exfoliated nanocomposites display greater thermal stability compared to pure PCL or corresponding micro-composites. This may be caused by reductions in permeability/diffusivity of oxygen and other degraded volatile products due to the homogeneously distributed clay sheets, which have a high-aspect ratio, and to char formation. The thermal stability of the nanocomposites consistently increases as the clay content increases up to 5 wt%.

Heat release rate curves of the PA6 and clay/PaA6 composite samples are displayed in Fig. 46 [190]. Slight increase in the ignition delay time and significant reduction in the peak heat release rate are observed for the nanocomposite samples in comparison to pristine PA6. The heat release rate decreases with increasing the clay content. Also, the mass loss rate is proportional to the heat release rate for all the samples. Therefore, the specific heat of combustion got from the heat release rate divided by the mass loss rate is obtained to be 30 ± 2 kJ/g for the three samples [190].

Thermogravimetric analysis shown in Fig. 47 displays that the decomposition onset of CNFs is approximately equal to 550 °C, while poly (methyl methacrylate) (PMMA) begins to degrade at about 300 °C. CNF/PMMA composite obviously shows an onset degradation temperature higher than that of pure PMMA [121]. This is because the addition of high temperature nanoparticles such as smectic clays etc. to a polymer

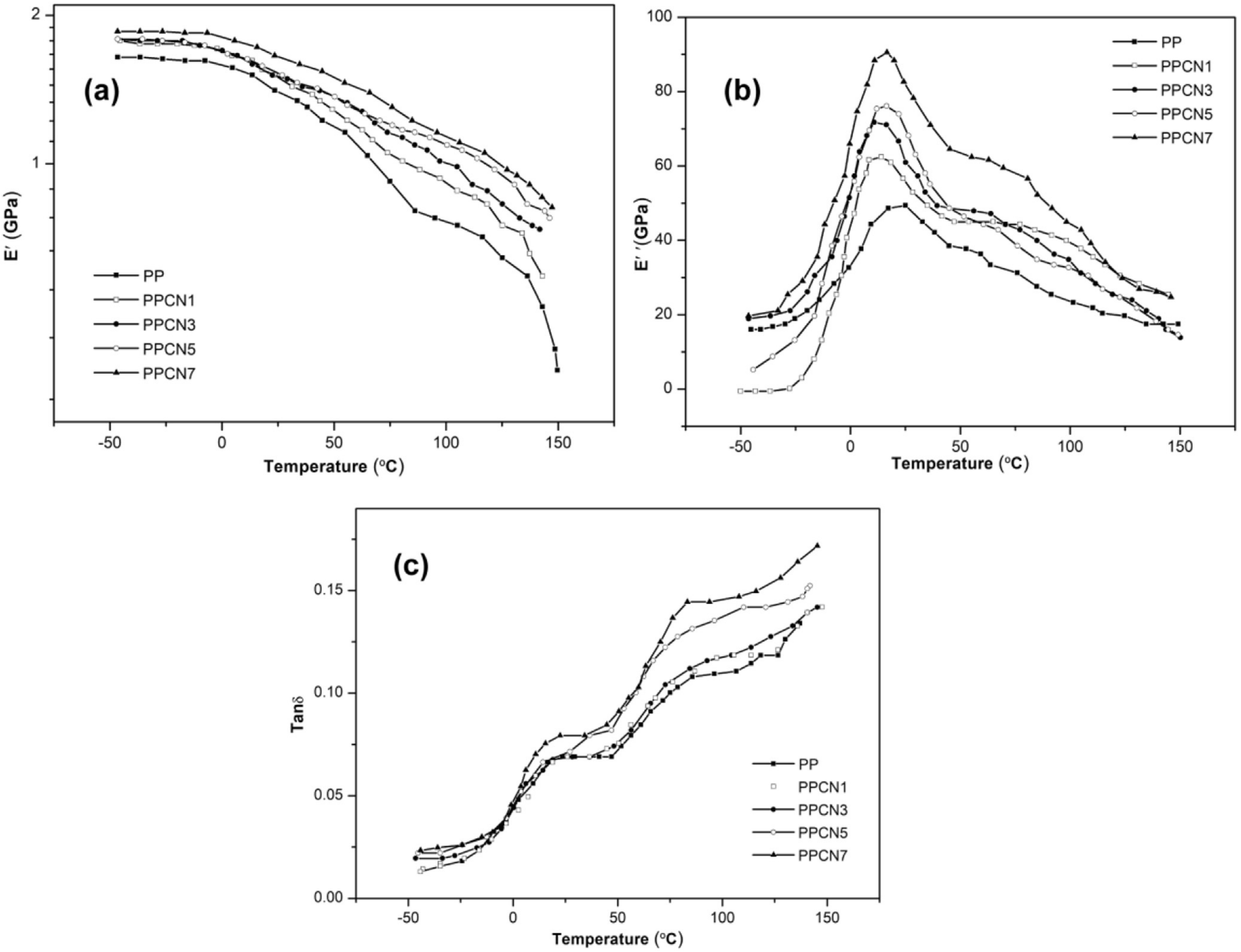

Fig. 42. DMA results: (a) storage modulus, E′; (b) loss modulus, E′′; and (c) loss factor tan δ for neat PP and PPCN as a function of temperature [187].

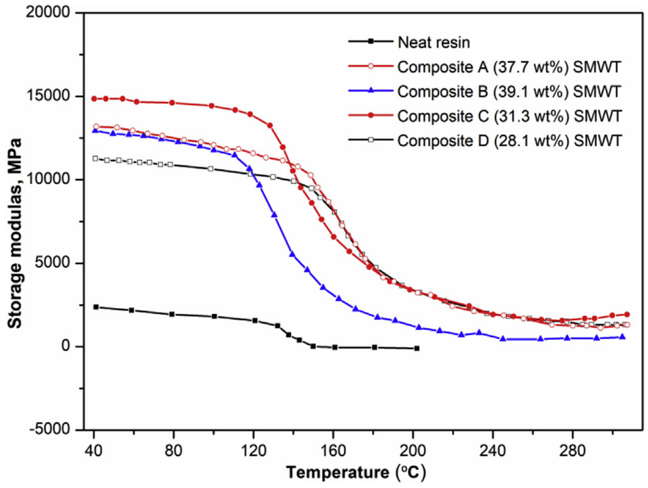

Fig. 43. DMA storage modulus curves of nanocomposites [124].

Table 6
Results for DMA storage modulus [124].

SWCNT content (wt%)	Storage modulus (GPa)	Increase (%)
0	2.6	0
28.1	11.5	349
31.3	15.1	492
37.7	13.5	429
39.1	13.2	419

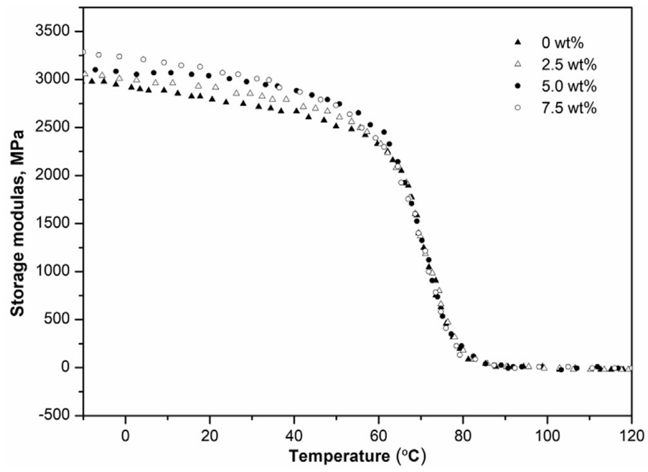

Fig. 44. Storage modulus versus temperature for PVC and $CaCO_3$/PVC nanocomposites [188].

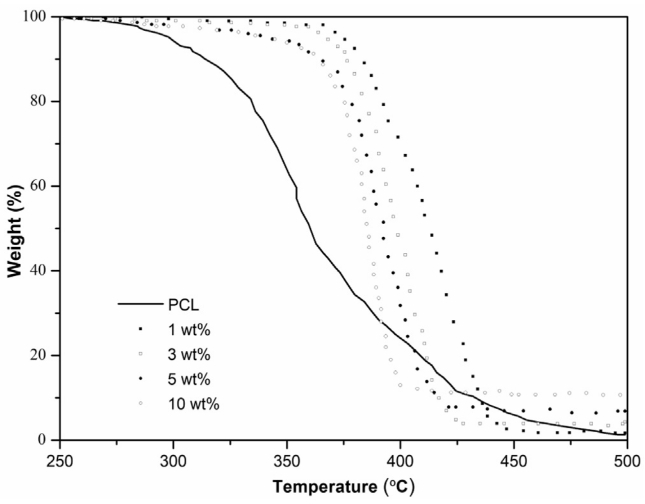

Fig. 45. Temperature dependence of the weight loss under an air flow for neat PCL and MMT/PCL nanocomposites [189].

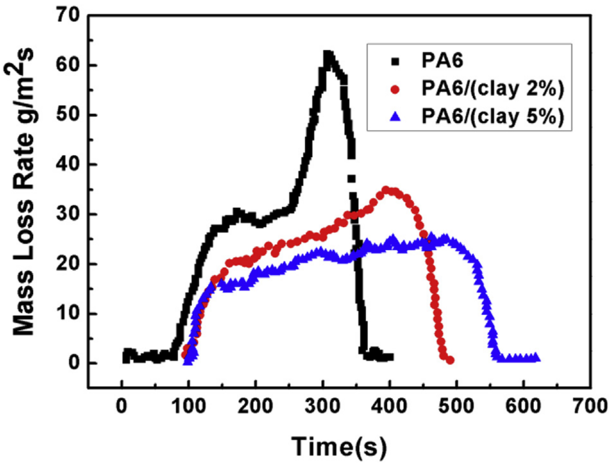

Fig. 46. Mass burning rate of PA6 and composite samples (8 mm thick) at 50 kW/m^2 [190].

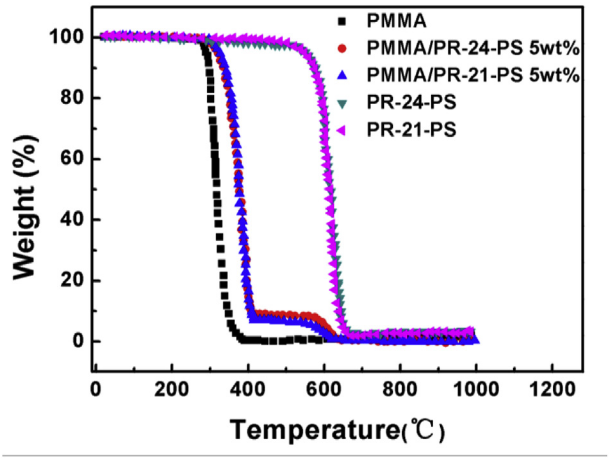

Fig. 47. Weight loss in PMMA, carbon nanofibers and carbon nanofiber/PMMA composites when heated in air at 10 °C/min [121].

usually increases thermal decomposition temperature.

When clay and carbon nanotubes are simultaneously used, some interesting results are obtained. The flame retardant behavior of 4.8 wt% organo-modified clay and/or purified MWCNT filled ethylene vinyl acetate (EVA) nanocomposites is presented in Table 7, [191]. Table 7 shows that the polymer nanocomposites exhibit improved flame retardant properties since the peak of heat release rate (PHRR) is decreased for all the samples. For the same filler content, the purified MWCNTs with a more reduced PHRR serve as better flame retardant than the organo-clay. However, the largest reduction (36%) in the PHRR is observed for the ternary nanocomposite with 2.4 wt% purified MWCNTs and 2.4 wt% organo-modified clay. Combination of these two nanofillers has reduced the ignition time dropping from 84 s for pure EVA to 71 s for the ternary nanocomposite, and not far away from 67 s for the binary organo-modified clay/EVA nanocomposite. Moreover, a synergistic effect between organoclays and nanotubes exists for flame retardant properties. The improved flame retardant properties may be explained by the observation of residues recovered after combustion. The char formed

Table 7
Flame retardant behavior by cone calorimetry test (heat flux = 35 kW/m^2) showing the effects of organo-modified clay and purified MWCNTs on peak of heat release rate (PHRR), ignition time (T_i) and surface crack density of EVA nanocomposites [191].

Sample composition		Ti (s)	PHRR (kW/m^2)	Crack density[a]
Organo-modified clay (wt%)	Purified MWCNTs (wt%)			
–	–	84	580	[a]
4.8	–	67	470	[c]
–	4.8	83	405	[b]
2.4	2.4	71	370	0

[a] , almost complete elimination/volatilization of EVA matrix.
[b] , formation of holes.
[c] , presence of cracks; 0, almost no visible cracks on the surface.

is much less cracked in the ternary composite compared to that for the corresponding binary composites. The flammability is decreased owing to the uniform crust formed on the top surface of the burning sample.

Table 8 gives the results for the glass transition temperatures (T_g) of the PVC phases of pristine PVC and $CaCO_3$/PVC nanocomposites [188]. It is clear that the glass transition peak of the PVC phases in $CaCO_3$/PVC nanocomposites tends to shift towards a marginal but definitely higher temperature as the $CaCO_3$ weight fraction increases up to 7.5 wt%. These results result from the restricting of the motion of PVC segmental chains by the good dispersion of $CaCO_3$ nanoparticles. T_g is reduced to 81.9 °C when 7.5 wt% $CaCO_3$ nanoparticles are added since agglomeration of $CaCO_3$ nanoparticles would take place for this high nanoparticle content and then weaken the interaction between PVC chains and nanoparticles so that.

The glass transition temperature (T_g) of SiO_2/epoxy nanocomposites prepared using sol-gel method is exhibited in Fig. 48 as a function of silica nanoparticle content [134]. Obviously, the glass transition temperature (T_g) has been increased by the addition of silica nanoparticles prepared via the sol-gel method. The main reason for the increase in T_g is likely due to a loss in the mobility of chain segments of epoxy resin resulting from the silica/epoxy interactions. This phenomenon has also been observed for silica/PA 6 nanocomposites [99].

The thermal stability of the SiO_2/PI composite films by TG is showed in Table 9 [137]. It is seen that the initial thermal decomposition temperature (T_d) increases as silica content increases. The improved thermal stability should result from the high thermal stability of silica and the crosslink point nature of the silica particles. The initial thermal decomposition temperature is further improved by using a new sol-gel route which leads to smaller (nanoscale) particle size (PS2 samples). The reduction in the size of the SiO_2 particles leads to the great increase in the interfacial area at a given silica fraction. Further, the reduced size of the SiO_2 particles leads to an increase in the cross-linking density to some extent. All these effects bring about higher T_d for SiO_2/PI composites prepared by the new process than for their counterparts.

Layered double hydroxide (LDH)/poly (methyl-ether-imide) (PMEI) nanocomposites were manufactured via solution intercalation method [192]. Thermogravimetric analysis in both nitrogen and air atmospheres shows that thermal stability of the nanocomposites was improved compared to neat PMEI. In-situ polymerization technique was employed for synthesis of LDH/polyacrylonitrile (PAN) nanocomposites with different LDH concentrations [193]. It was found that the thermal property of PAN was substantially enhanced due to strong interfacial adhesion of Mg—Al-LDH with PAN matrix. In addition, influences of the interlayer anions of LDHs on the thermal stability and flame retardancy of polymere nanocomposites were studied [194]. Results exhibited that both the thermal stability and the flame retardancy could be significantly enhanced, and the enhanced extent was highly dependent on the type of interlayer anions that were intercalated in LDHs [194].

Table 8
T_g of PVC and $CaCO_3$/PVC nanocomposites [188].

Samples	T_g (°C)
Pure PVC	81.7
PVC/2.5 wt % $CaCO_3$	82.8
PVC/5.0 wt % $CaCO_3$	83.1
PVC/7.5 wt % $CaCO_3$	81.9

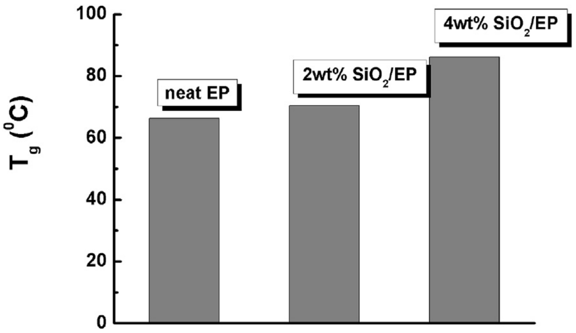

Fig. 48. T_g of neat epoxy and silica/epoxy nanocomposites [134].

Table 9
Thermal stability of SiO_2/PI composite films by TG [137].

Sample code	PI	PS1-3 wt %	PS1-10 wt %	PS2-3 wt %	PS2-10 wt %
T_d (°C)	495.5	513	559.7	550	567.2
Weight lost (%)	44	39	36	39	36.7

Flame resistance of the PMMA samples uncoated and coated with poly (ε-caprolactone) (PCL)/SiO_2 nanocomposites can be tested using a Glow Wire Test apparatus. The necessary time for flame ignition after the contact of the specimen with the hot glow wire (730 °C) is measured, and the results are shown in Table 10 [195]. In all cases, a great increase (from 70 to 120%) of flame resistance is observed for the case of uncoated PMMA. Nonetheless, a direct correlation between molecular structure (namely molecular weight and/or functionality)/composition and time-to-flame is not evidently clear. Furthermore, the flame resistance results got after UV radiation exposure indicate that this treatment is bad for the uncoated PMMA. Conversely, the time to flame for the coated PMMA subjected to the same UV radiation exposure time is almost not changed, indicating that the hybrid coating can enhance the UV resistance of PMMA. On the other hand, the flame retardant characteristics of the generated Novolac type phenolic/TEOS hybrids are examined by measuring their limited oxygen index (LOI) [196]. A great increase (from 33 to 44) in LOI is observed when TEOS is incorporated

Table 10
Flame resistance of PMMA uncoated and coated with different nanocomposites as a function of SiO_2/PCL ratio before and after 50 days exposed to UV radiation [195].

Coating code	SiO_2/PCL ratio (wt/wt)	Time to flame (s)	Time to flame (s) after UV exposure
None	–	6.3	4.8
α-PCL(20)Si/SiO_2	2/1	12.7	11.0
α-PCL(20)Si/SiO_2	1/1	12.3	–
α-PCL(20)Si/SiO_2	1/2	11.7	–
α-PCL(50)Si/SiO_2	2/1	11.3	–
α-PCL(50)Si/SiO_2	1/1	10.7	–
α-PCL(50)Si/SiO_2	1/2	11.3	–

into the phenolic resin. This variance suggests that incorporation of silicon greatly promotes the flame retardance of the resin.

5.4. Gas barrier and separation properties

The films prepared from exfoliated nanocomposites contain high aspect ratio layered silicates that are capable of reducing gas permeability. Measurement of the permeability to carbon dioxide was conducted for the partially-exfoliated PI-based nanocomposite films by Lan et al. [197]. It is interesting to observe that the relative permeability values of P_c/P_p, where P_c and P_p stand respectively for the permeability for the composite and the unfilled polymer, decreases with increasing the filler volume fraction (Fig. 49) [197]. A theoretical equation is obtained, which allows the predictions of gas permeability as a function of the filler length and width as well as volume fraction within the PI matrix. When an aspect ratio (width/thickness) of 192 is used, the best fitting is achieved. This aspect ratio is much smaller than what could be expected for a truly exfoliated structure, namely an aspect ratio of ca. 2000 for montmorillonite single layers [197].

The barrier property of polymer nanocomposites was investigated theoretically on the intercalation (or exfoliation) extent, orientation and dispersion of nanometer-sized silicate platelets in a polymer matrix by Lu and Mai [198]. There exists a critical volume fraction ϕ_c of silicate platelets over which the platelet system acts as a barrier. ϕ_c is expressed by

$$\phi_c = \frac{2}{2S+1}\frac{W}{L}P_c \tag{2}$$

where S is the orientation parameter and $P_c = 0.718$. L and W denote the length and thickness of platelets, respectively. Fig. 50 shows the critical volume fraction ϕ_c versus the orientation parameter S of silicate platelets with $L/W = 100$, where the insets denote three typical patterns (S = 1/2, 0, and 1) of silicate platelets in a polymer matrix. In general, S has a value from 0 to 1.

The silica content in the poly (1-trimethylsilyl-1-propyne) (PTMSP) nanocomposite membranes is increased by increasing the ratio of silane to polymer (see Fig. 51) [199]. The increase of silane to 30 wt.% based on polymer content in the sol–gel tetraethoxysilane (TEOS)/methyltriethoxysilane (MTEOS) copolymerization with different molar ratios (1:0 and 1:1) leads to the formation of heterogeneous membranes. A homogeneous membrane can be obtained with 20 wt.% silane employed in TEOS/MTEOS copolymerization with molar ratio (1:1). When the conversion is incomplete, the final silica content is not increased even if the amount of silane is increased. Residual silane is left in the composite membrane, bringing about a decrease of butane permeability coefficient. However, the selectivity is significantly improved, namely almost three-fold related to the PTMSP membrane. Fig. 51 show the permeation property for mixture gas in the PTMSP nanocomposite membranes [199].

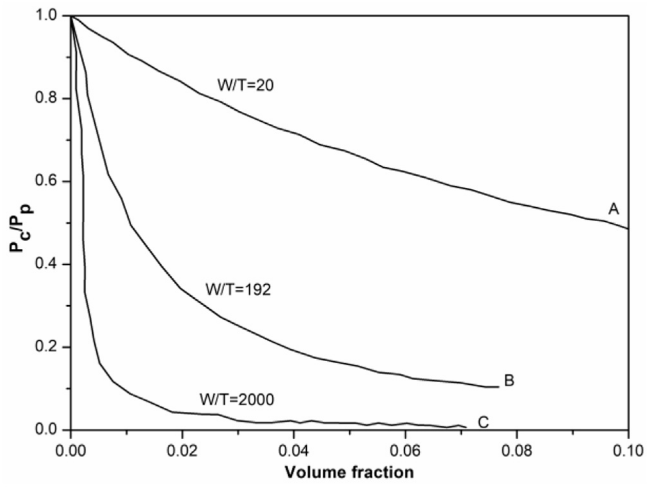

Fig. 49. CO_2 permeability of clay/PI composites. Curves A and C are estimated for fillers with an aspect ratio of 20 and 2000, respectively, Curve B is created by least squares fitting of the permeability equation to the experimental data [197].

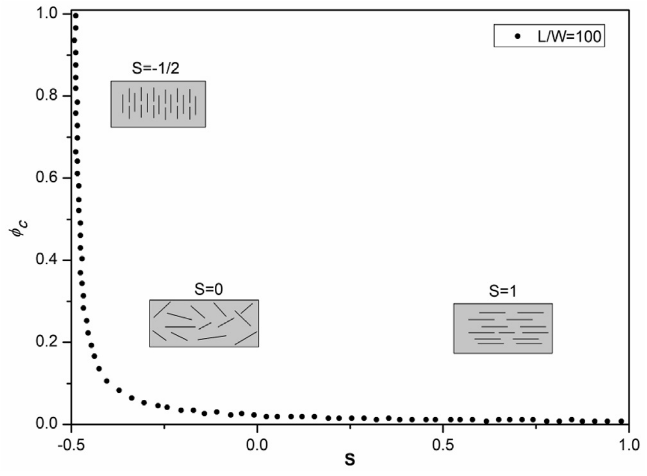

Fig. 50. Dependence of critical volume fraction ϕ_c on orientation S of silicate platelets with $L/W = 100$. The insets are three typical patterns of silicate platelets in a polymer matrix for $S = -1/2$, 0 and 1, respectively [198].

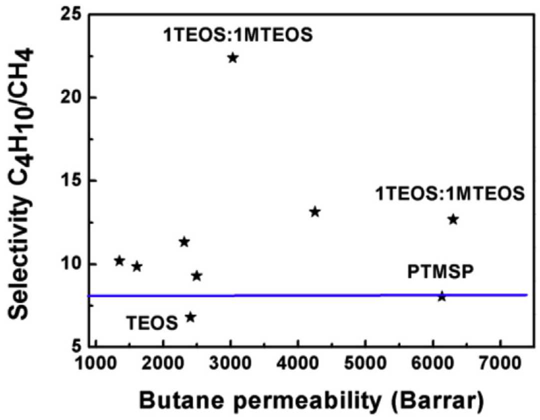

Fig. 51. Selectivity data acquired at 30 °C with feed pressure of 1.4 bar and permeate pressure of 1 bar for mixture gas in silica/PTMSP nanocomposite membranes prepared by sol–gel copolymerization as a function of silane and TEOS/silane molar ratio (1:0, 1:1 and 0:1) [199].

5.5. Miscellaneous

5.5.1. Magnetic properties

The magnetic property of cobalt oxide/polymer nanocomposite is shown in Fig. 52 [200]. The measured magnetization is divided by the total mass of the used film. It is clear from Fig. 52 that the nanocomposite films are weakly ferri-magnetic at room temperature. The magnetization at an applied field of 8 kOe is 0.28 emu/g of the nanocomposite, which corresponds to 22 emu/g of Co_3O_4 since the nanocomposite contains 8.7 wt % Co_3O_4.

The variation of magnetization as a function of applied field at a temperature of 300 K is shown in Fig. 52a–c for nickel ferrite powders, nickel ferrite/polyethylene and nickel ferrite/polystyrene nanocomposites [201]. Typical superparamagnetic behaviors, e.g. no hysteresis, almost immeasurable coercivity and remanence, and non-saturation even at high magnetic field of 50 kOe, are seen. The non-saturation of M − H loop and the absence of hysteresis, remanence and coercivity

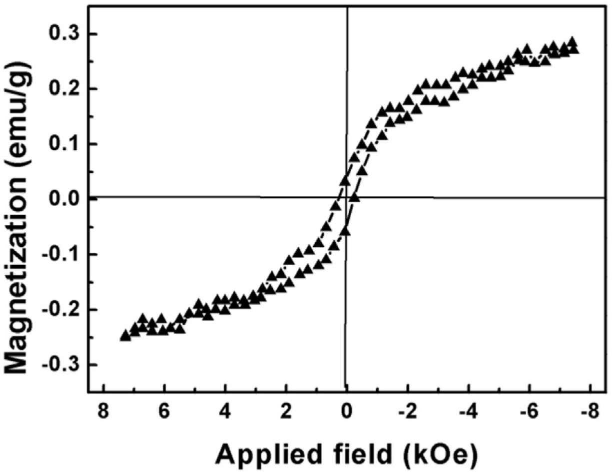

Fig. 52. Magnetic property of cobalt oxide/polymer nanocomposite films [200].

(Fig. 53a–c) at 300 K indicate the presence of superparamagnetic and single domain particles for each of the three materials. The value of saturation magnetization can be obtained to be 25.4, 24, and 28 emu/g, for nickel ferrite, nickel ferrite/polyethylene ball-milled nanocomposite and nickel ferrite/polystyrene nanocomposite, respectively by fitting the high field data to the function $\sigma = \sigma_S\ (1\ - \alpha/H)$, where α is a fitting parameter and H is applied magnetic field. The behavior seen in the nickel ferrite-polystyrene nanocomposite is typical of assembled nanoparticles whose moments thermally fluctuate between easy directions.

5.5.2. Dimensional stability

Dimensional stability is a critical issue in many applications. Incorporation of a low content of nanoscale fillers into polymers can significantly reduce coefficient of thermal expansion (CTE), and then improve thermal stability. Fig. 54 shows that the average coefficient of thermal expansion (CTE) from 298 K to 77 K of the nanocomposites decreases with increasing silica content [134]. The introduction of silica nanoparticles dramatically reduces the CTE. This is due to the fact that the CTE of silica nanoparticles is much lower than that of epoxy resins. The decrease in the CTE by addition of silica nanoparticles is desirable for cryogenic engineering applications.

The reduced segmental movement of PI matrix with introduction of MMT would also result in a decrease in the CTE. Fig. 55 shows the relationship between the CTE of the nanocomposite films and the MMT content [202]. It is clear that the introduction of a small amount of MMT can dramatically reduce the CTE. The dramatic decrease in the CTE (namely significant increase in dimensional stability) is extremely desired when PI is applied in microelectronic and optoelectronic fields.

5.5.3. Transmittance and refractive index

Fig. 56a shows that the silane surface-modified ZnO-quantum dot (S—ZnO-QD)/silicone nanocomposite containing 1.0 wt% 1.8 nm S—ZnO-QDs displays an approximately 88% transmittance in the visible wavelength range, which is only very slightly lower than that (90% transmittance) for the pure silicone resin due to the excellent dispersion and increased refractive index (closer to that of silicone resin) of modified ZnO-QDs [11]. The transmittance below ca. 350 nm is sharply reduced due to the UV shielding effect of ZnO-QDs. As the size of ZnO-QDs increases from 1.8 to 4.5 nm, the transmittance of the nanocomposites decreases but to a small degree only. In spite of this decrease in transmittance by increased QD size, the 4.5 nm S—ZnO QD/silicone nanocomposite still maintains a high transmittance of ca. 75%. This value is much higher than that of the nanocomposite containing un-modified ZnO-QDs [203].

Fig. 56b shows only a slight decrease in the transmittance when the S—ZnO-QD content is increased from 0.5 wt% to 1.0 wt% in the nanocomposites. However, when the S—ZnO-QD content is increased to 5.0 wt%, the nanocomposite transmittance is dramatically decreased to 20% by increased scattering effect due to formation of S—ZnO-QD aggregates at high loadings.

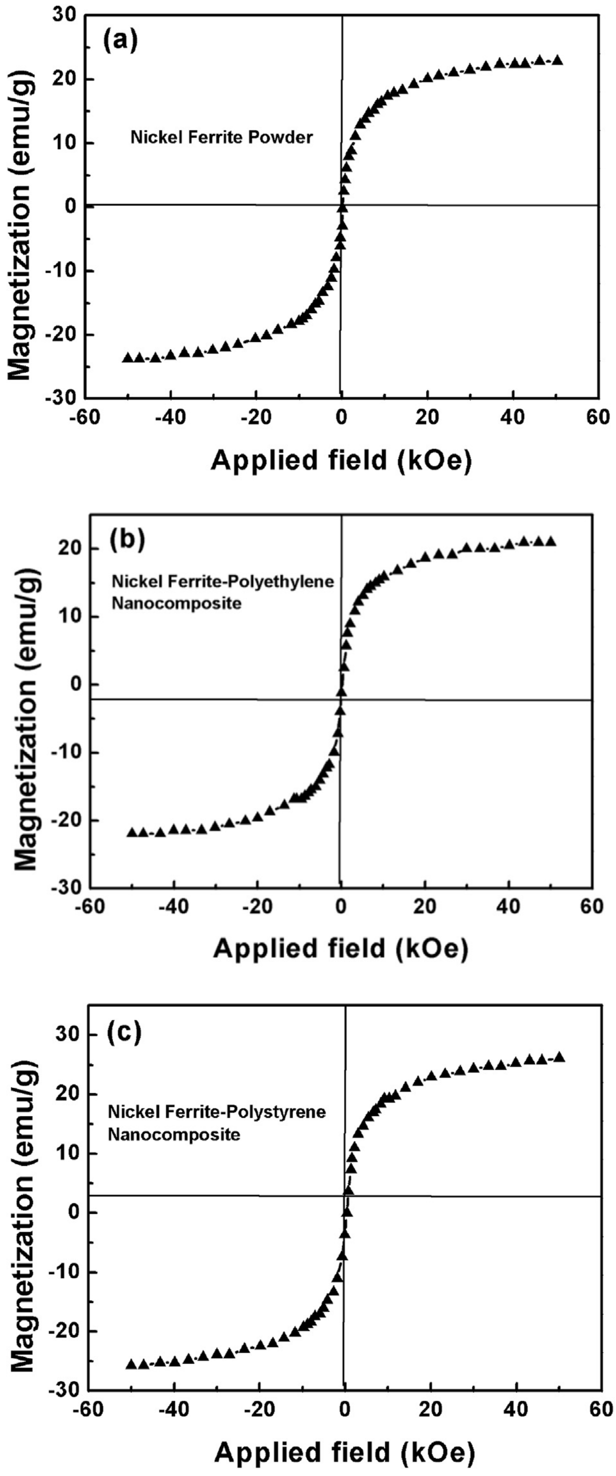

Fig. 53. Variation of magnetization with applied field at 300 K for nanocrystalline nickel ferrite (a), nanocrystalline nickel ferrite/polyethylene ball-milled nanocomposite (b), and nanocrystalline nickel ferrite/polystyrene nanocomposite (c) [201].

In-situ polymerization was used to prepare transparent ZnO/epoxy nanocomposites from transparent epoxy (EP-400) and ZnO

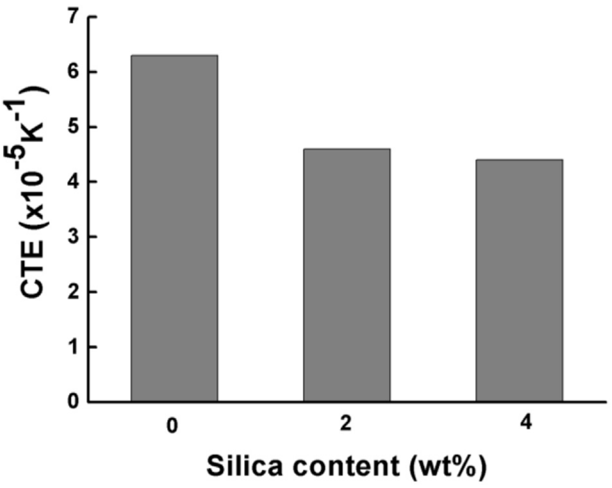

Fig. 54. Average coefficient of thermal expansion from 298 K to 77 K of silica/epoxy nanocomposites [134].

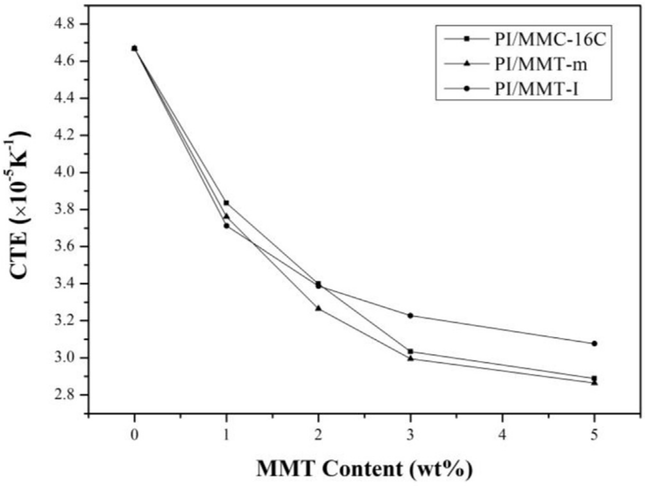

Fig. 55. Effect of MMT content on the coefficient of thermal expansion of PI/MMT-l, PI/MMT-m and PI/MMT-16C nanocomposite films [202].

nanoparticles. Mean particle size of ZnO nanoparticles varies from 15.9 to 71.9 nm listed in Table 11, [204]. Fig. 57a shows the UV–vis transmittance spectra of epoxy and 0.07 wt% ZnO/epoxy nanocomposites [204]. It can be seen from Fig. 57a that the visible light transparency decreases while the UV shielding efficiency of nanocomposites increases with increasing the ZnO particle size. The Z5-ZnO/epoxy nanocomposite exhibits not only high UV light shielding (~96% at 320 nm) but also high-visible light transmittance. Moreover, Fig. 57b displays that UV light absorbance increases generally with increasing the ZnO particle size. This observation in consistent with the transmittance result (Fig. 57a).

It is well known that the large difference in refractive index (RI) between packaging materials and LED chips results in a great loss in lighting transmission, and thus a reduction in the lighting efficiency of LEDs. It is an easy but smart way to increase the RI of the packaging materials by incorporation of inorganic fillers with much higher RI compared to packing materials. Fig. 58a shows the relationship between the RI of S—ZnO-QD/silicone nanocomposite and the S—ZnO-QD content [11]. It is seen that the RI of silica nanocomposites as packing materials dramatically increases as the S—ZnO-QD content increases and changes from 1.42 to 1.52 and 1.56, respectively at loading levels of 0.5 wt% and 1.0 wt%. Nonetheless, a further increase in the content of S—ZnO-QDs to 5.0 wt% leads to only 4% increase in the RI, indicating a limited enhancement at high S—ZnO-QD contents. This is mainly caused by the light scattering between the S—ZnO-QDs and the silicone resin resulting from the aggregation of the S—ZnO-QDs at high loadings. Furthermore, Fig. 58b shows that the refractive index of the nanocomposite is insensible to the size of ZnO QDs, suggesting no obvious dependence of RI on the QD size.

5.5.4. *Electrical conductivity and other properties*

The high aspect ratio and high conductivity of CNTs makes them excellent fillers for conducting nanocomposites. If the volume fraction of the conducting phase exceeds a ‘percolation threshold’ at which there is a continuous conducting path, the composites will become conducting. This threshold does not depend on the size and shape of conducting phase

Table 11
Crystallite size of ZnO nanoparticles [204].

ZnO nanoparticle code	Z2	Z3	Z4	Z5	Z6	Z7	Z8
Mean particle size (nm)	15.9	18.6	22.1	26.7	45.9	63.6	71.9

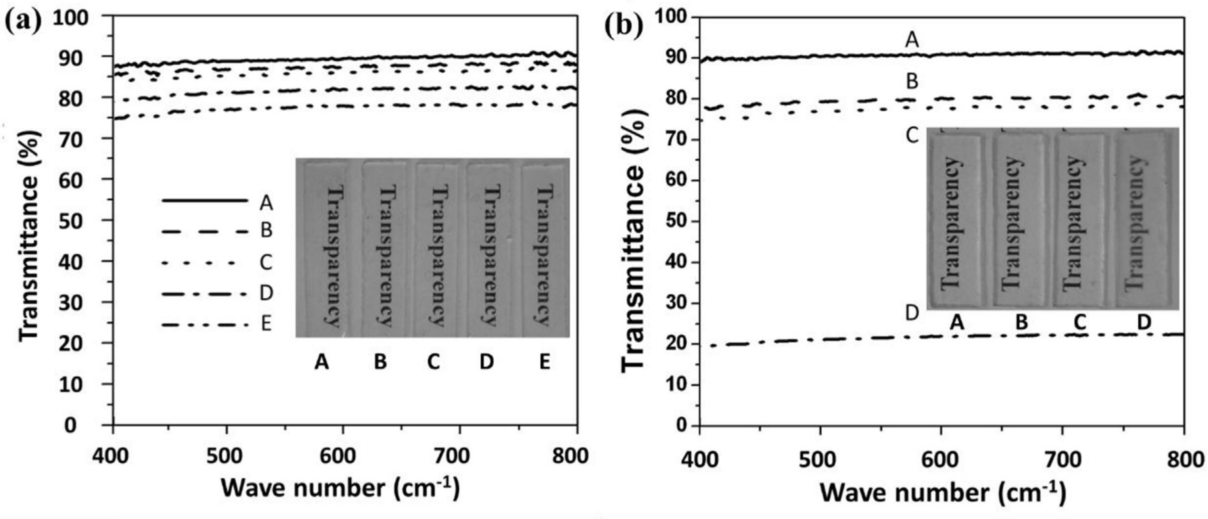

Fig. 56. Transmittance of S—ZnO-QD/silicone nanocomposites containing QDs of (a) various sizes: A) 1.8, B) 2.0, C) 2.2, D) 3.3 and E) 4.5 nm, where the S—ZnO-QD content is fixed at 1 wt%; and (b) different contents: A) 0.0, B) 0.5, C) 1.0, and D) 5.0 wt%, in which the S—ZnO-QD size is fixed as 4.5 nm [11].

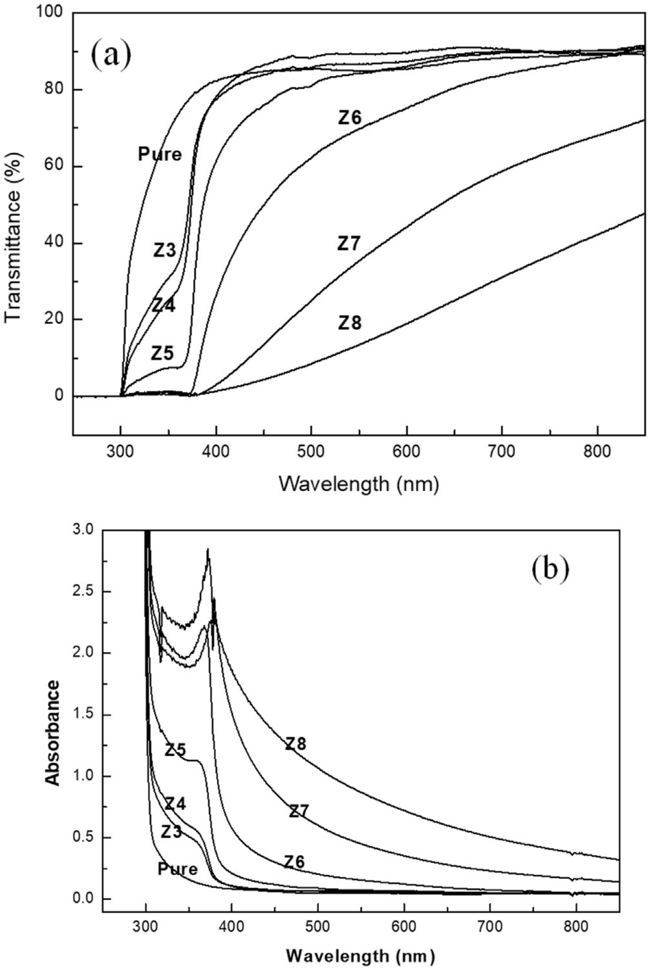

Fig. 57. UV–vis spectra of epoxy matrix and ZnO/epoxy nanocomposites containing 0.07 wt% ZnO nanoparticles [204]. (a) Transmittance, and (b) absorbance.

if its particles are equiaxed. With long thin particles, the contact chance increases, thus decreasing the percolation threshold so that conduction takes place at a much lower filler loading. Conventional conducting composites are made of carbon black in polymers. This requires ~16% of carbon but can be much decreased by smart processing. Fig. 59 shows that MWCNT filled epoxy composites achieve percolation at the loadings of 0.01 vol.% and even 0.004 vol.% with careful processing [92]. These are extremely low filler contents. Thermal conductivity of carbon nanotube filled nanocomposites is also of great interest but no percolation was observed for thermal conduction [205,206]. Nonetheless, for 2D carbon nano-filler namely graphene based polymer nanocomposites, the thermal conductivity was studied experimentally [207] and theoretically [208]. They announced there was possible percolation threshold for graphene/polymer nanocomposites.

Mixture of Ti_3C_2Tx MXene with either a charged polydiallyldimethylammonium chloride (PDDA) or an electrically neutral PVA was made to prepare $Ti_3C_2T_x$/polymer nanocomposites [170]. High aspect ratio of delaminated MXene rendered it promising nanofiller for preparing high performance multifunctional polymer nanocomposites. The as-fabricated Ti_3C_2Tx/PVA nanocomposite films are flexible and have a high electrical conductivity of ca. 2.2×10^4 S/m.

Poly (p-phenylene vinylene) (PPV) nanocomposites are made by adding silicon oxide (SiO_2) or titanium (TiO_2) nanoparticles and their electrical properties have been reported [209]. The composite thin film was deposited onto indium tin oxide (ITO) substrates followed by thermal evaporation of a MgAg cathode of thickness 500 nm to make diodes. Current-voltage characteristics were measured for the indium tin oxide (ITO)-composite-MgAg diodes. Their electrical behavior was different from that of the composites, depending on particle size and nature of used oxide. The variations in the electrical behaviors of the diodes are dependent on the composite-electrode contact morphology, polymer–dielectric particle contact, and change in polymer chain length.

Polymer nanocomposites have also been used as electrorheological sensitive additive [210]. Their addition leads to improvement of ablative properties in aeronautics and the combination of dispersed layered silicates in a liquid crystal medium for production of stable electro-optical devices leads to a bi-stable and reversible electro-optical effect between a light scattering opaque state and a transparent state [140,211]. Nanocomposites have also been considered to tune ionic conductivity of poly- (ethylene oxide) (PEO) [212]. The intercalated nanocomposite achieved by melt intercalation of PEO (40 wt.%) into Li-montmorillonite (60 wt.%) shows an enhanced stability of the ionic conductivity at ambient temperature compared to the more common PEO/$LiBF_4$ electrolytes. This enhancement is due to the fact that PEO cannot crystallize when intercalated, hence eliminating the crystallites that are non-conductive. The high ionic conductivity at ambient temperature combined with a single ionic conductor character of the nanocomposites make them promising electrolyte materials.

Polymer nanocomposite electrolytes (PNEs) are made by incorporating hydrophilic fumed silica with different ratios up to 5 wt.% into gel polymeric electrolyte (GPE) comprising 15 wt.% poly (methyl methacrylate) (PMMA)-immobilized liquid electrolyte [213]. The resulting PNEs display high ionic conductivity and electrical conductivity as high as 8 mS/cm along with a viscosity of 370 Pa-s by adding 2 wt.% SiO_2. In addition, high thermal stability, shear thinning (namely easy processablity) and low volatility all make PNEs a potential candidate as solid-like electrolytes for electrochemical devices.

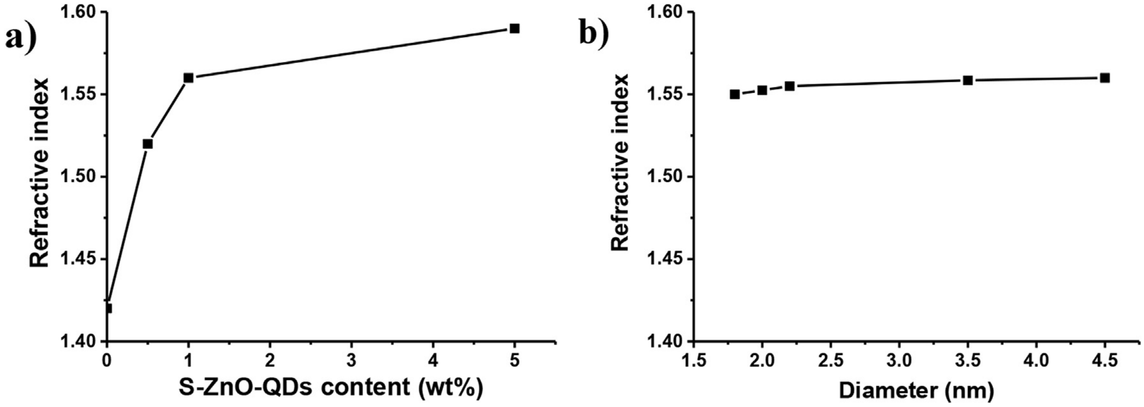

Fig. 58. Refractive index of S—ZnO-QD/silicone nanocomposites with (a) various contents of 1.8 nm S—ZnO-QDs and (b) various particle sizes of ZnO-QDs [11].

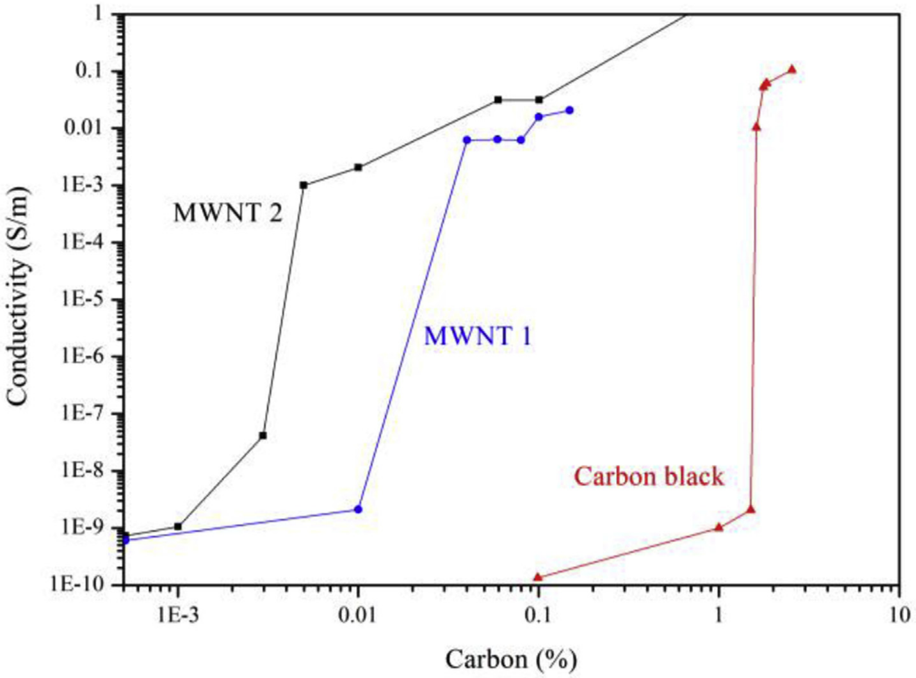

Fig. 59. Dependence of conductivity on carbon content for three different carbon/epoxy composite systems showing a rapid increase in conductivity corresponding to percolation threshold [92].

Reduced graphene oxide (RGO)/PbTiO$_3$/poly (3,4-ethylenedioxythiophene) (PEDOT) nanocomposites were prepared by employing facile in-situ chemical oxidative polymerization method [214]. Ferro-electric PbTiO$_3$ and RGO induced dielectric loss in the nanocomposites and PEDOT established a conducting network over PbTiO$_3$ nanoparticles and RGO layer, leading to the improved electromagnetic shielding performance by augmenting dielectric loss [136].

6. Summary

It has been clearly shown that incorporation of a low content of nanoscale fillers into polymers leads to enhancements in mechanical and physical properties. Introduction to various nanoscale fillers of two dimensional, one dimensional and zero dimensional morphologies used in polymer nanocomposites has been given in this review paper. It provides a basic level of understanding how polymer nanocomposites are processed using different methods. Also, the characterization of polymer nanocomposites has been presented by using various techniques. Then, their mechanical and physical properties were discussed in detail in terms of the nanoscale filler type, particle size and dispersion degree. The effect of interface strength was also presented on mechanical properties of polymer nanocomposites. It is believed that this review can provide guiding significance for design of high performance polymer nanocomposites from three aspects of processing, characterization and properties.

Acknowledgements

We would like to thank National Natural Science Foundation of China (Nos. 51573200, 11872132 and U183720015) for financial support.

References

[1] E. Reynaud, C. Gauthier, J. Perez, Nanophases in polymers, Rev. Métall. 96 (1999) 169–176.

[2] R.J. Young, I.A. Kinloch, L. Gong, K.S. Novoselov, The mechanics of graphene nanocomposites: a review, Compos. Sci. Technol. 72 (2012) 1459–1476.

[3] M.T. Albdiry, B.F. Yousif, H. Ku, K.T. Lau, A critical review on the manufacturing processes in relation to the properties of nanoclay/polymer composites, J. Compos. Mater. 47 (2013) 1093–1115.

[4] J.H. Du, H.M. Cheng, The fabrication, properties, and uses of graphene/polymer composites, Macromol. Chem. Phys. 213 (2012) 1060–1077.

[5] X.Q. Li, C.Y. Wang, Y. Cao, G.X. Wang, Functional MXene materials: progress of their applications, Chem. Asian J. 13 (2018) 2742–2757.

[6] S.B. Tu, Q. Jiang, X.X. Zhang, H.N. Alshareef, Large dielectric constant enhancement in MXene percolative polymer composites, ACS Nano 12 (2018) 3369–3377.

[7] P. Calvert, Nanotube composites - a recipe for strength, Nature 399 (1999) 210–211.

[8] M.X. Liu, Z.X. Jia, D.M. Jia, C.R. Zhou, Recent advance in research on halloysite nanotubes-polymer nanocomposite, Prog. Polym. Sci. 39 (2014) 1498–1525.

[9] J.E. Mark, Ceramic-reinforced polymers and polymer-modified ceramics, Polym. Eng. Sci. 36 (1996) 2905–2920.

[10] N. Herron, D.L. Thorn, Nanoparticles: uses and relationships to molecular cluster compounds, Adv. Mater. 10 (1998) 1173–1184.

[11] P. Huang, H.Q. Shi, S.Y. Fu, H.M. Xiao, N. Hu, Y.Q. Li, Greatly decreased redshift and largely enhanced refractive index of mono-dispersed ZnO-QD/silicone nanocomposites, J. Mater. Chem. 4 (2016) 8663–8669.

[12] N.G. Sahoo, S. Rana, J.W. Cho, L. Li, S.H. Chan, Polymer nanocomposites based on functionalized carbon nanotubes, Prog. Polym. Sci. 35 (2010) 837–867.

[13] F. Liu, N. Hu, J.Y. Zhang, S. Atobe, S.Y. Weng, H.M. Ning, Y.L. Liu, L.K. Wu, Y.X. Zhao, F.H. Mo, S.Y. Fu, C.H. Xu, Alamusi, W. Yuan, The interfacial mechanical properties of functionalized graphene-polymer nanocomposites, RSC Adv. 6 (2016) 66658–66664.

[14] G. Choudalakis, A.D. Gotsis, Permeability of polymer/clay nanocomposites: a review, Eur. Polym. J. 45 (2009) 967–984.

[15] R. Sengupta, M. Bhattacharya, S. Bandyopadhyay, A.K. Bhowmick, A review on the mechanical and electrical properties of graphite and modified graphite reinforced polymer composites, Prog. Polym. Sci. 36 (2011) 638–670.

[16] W. Bauhofer, J.Z. Kovacs, A review and analysis of electrical percolation in carbon nanotube polymer composites, Compos. Sci. Technol. 69 (2009) 1486–1498.

[17] Z.D. Han, A. Fina, Thermal conductivity of carbon nanotubes and their polymer nanocomposites: a review, Prog. Polym. Sci. 36 (2011) 914–944.

[18] N. Roy, R. Sengupta, A.K. Bhowmick, Modifications of carbon for polymer composites and nanocomposites, Prog. Polym. Sci. 37 (2012) 781–819.

[19] M. Rahmat, P. Hubert, Carbon nanotube-polymer interactions in nanocomposites: a review, Compos. Sci. Technol. 72 (2011) 72–84.

[20] Z. Spitalsky, D. Tasis, K. Papagelis, C. Galiotis, Carbon nanotube-polymer composites: chemistry, processing, mechanical and electrical properties, Prog. Polym. Sci. 35 (2010) 357–401.

[21] T. Kuilla, S. Bhadra, D.H. Yao, N.H. Kim, S. Bose, J.H. Lee, Recent advances in graphene based polymer composites, Prog. Polym. Sci. 35 (2010) 1350–1375.

[22] J.R. Potts, D.R. Dreyer, C.W. Bielawski, R.S. Ruoff, Graphene-based polymer nanocomposites, Polymer 52 (2011) 5–25.

[23] A.A. Azeez, K.Y. Rhee, S.J. Park, D. Hui, Epoxy clay nanocomposites - processing, properties and applications: a review, Composites Part B 45 (2013) 308–320.

[24] S. Sprenger, Epoxy resin composites with surface-modified silicon dioxide nanoparticles: a review, J. Appl. Polym. Sci. 130 (2013) 1421–1428.

[25] S. Kango, S. Kalia, A. Celli, J. Njuguna, Y. Habibi, R. Kumar, Surface modification of inorganic nanoparticles for development of organic-inorganic nanocomposites-A review, Prog. Polym. Sci. 38 (2013) 1232–1261.

[26] E.P. Giannelis, R. Krishnamoorti, E. Manias, Polymer-silicate nanocomposites: model systems for confined polymers and polymer brushes, in: S. Granick, K. Binder, P.G. de Gennes, E.P. Giannelis, G.S. Grest, H. Hervet, R. Krishnamoorti, L. Léger, E. Manias, E. Raphaël, S.Q. Wang (Eds.), Polymers in Confined Environments, Springer, Berlin, Heidelberg, 1999, pp. 107–147.

[27] M. Alexandre, P. Dubois, Polymer-layered silicate nanocomposites: preparation, properties and uses of a new class of materials, Mater. Sci. Eng. R 28 (2000) 1–63.

[28] S.S. Ray, M. Okamoto, Polymer/layered silicate nanocomposites: a review from preparation to processing, Prog. Polym. Sci. 28 (2003) 1539–1641.

[29] A. Okada, M. Kawasumi, A. Usuki, Y. Kojima, T. Kurauchi, O. Kamigaito, Synthesis and properties of nylon-6/clay hybrids, in: D.W. Schaefer, J.E. Mark (Eds.), Polymer Based Molecular Composites, MRS Symposium Proceedings, 1990, pp. 45–50. Pittsburgh.

[30] E.P. Giannelis, Polymer layered silicate nanocomposites, Adv. Mater. 8 (1996) 1–9.

[31] P.C. Lebaron, Z. Wang, T.J. Pinnavaia, Polymer-layered silicate nanocomposites: an overview, Appl. Clay Sci. 15 (1999) 11–29.

[32] R.A. Vaia, G. Price, P.N. Ruth, H.T. Nguyen, J. Lichtenhan, Polymer/layered silicate nanocomposites as high performance ablative materials, Appl. Clay Sci. 15 (1999) 67–92.

[33] M. Biswas, S.S. Ray, Recent progress in synthesis and evaluation of polymer-montmorillonite nanocomposites, Adv. Polym. Sci. 155 (2001) 167–221.

[34] S.W. Brindly, G. Brown, Crystal Structure of Clay Minerals and Their X-Ray Diffraction, Mineralogical Society, London, 1980.

[35] P. Aranda, E. Ruizhitzky, Poly(ethylene oxide)-silicate intercalation materials, Chem. Mater. 4 (1992) 1395–1403.

[36] D.J. Greenland, Adsorption of polyvinyl alcohols by montmorillonite, J. Colloid Sci. 18 (1963) 647–664.

[37] G. Lagaly, Interaction of alkylamines with different types of layered compounds, Solid State Ionics 22 (1986) 43–51.

[38] Y.H. Zhang, J.T. Wu, S.Y. Fu, S.Y. Yang, Y. Li, L. Fan, R.K.Y. Li, L.F. Li, Q. Yan, Studies on characterization and cryogenic mechanical properties of polyimide-layered silicate nanocomposite films, Polymer 45 (2004) 7579–7587.

[39] A. Blumstein, Polymerization of adsorbed monolayers: II. Thermal degradation of the inserted polymers, J. Polym. Sci., Part A: Polym. Chem. 3 (1965) 2665–2673.

[40] R. Krishnamoorti, A.V. Ramanan, E.P. Giannelis, Structure and dynamics of polymer-layered silicate nanocomposites, Chem. Mater. 8 (1996) 1728–1734.

[41] G.H. Chen, D.J. Wu, W.G. Weng, W.L. Yan, Preparation of polymer/graphite conducting nanocomposite by intercalation polymerization, J. Appl. Polym. Sci. 82 (2001) 2506–2513.

[42] D.D.L. Chung, Exfoliation of graphite, J. Mater. Sci. 22 (1987) 4190–4198.

[43] X.Y. Chuan, D. Chen, X. Zhou, Intercalation of $CuCl_2$ into expanded graphite, Carbon 35 (1997) 311–313.

[44] J.N. Coleman, M. Lotya, A. O'Neill, S.D. Bergin, P.J. King, U. Khan, K. Young, A. Gaucher, S. De, R.J. Smith, Two-dimensional nanosheets produced by liquid exfoliation of layered materials, Science 42 (2011) 568–571.

[45] S. Lijima, T. Ichihashi, Erratum: single-shell carbon nanotubes of 1-nm diameter, Nature 364 (1993), 737-737.

[46] S. Lijima, Helical microtubules of graphitic carbon, Nature 354 (1991) 56–58.

[47] M.S. Dresselhaus, G. Dresselhaus, P.C. Eklund, Science of Fullerenes and Carbon Nanotubes, Academic Press, San Diego, 1995.

[48] V.Z. Mordkovich, M. Baxendale, S. Yoshimura, R.P.H. Chang, Intercalation into carbon nanotubes, Carbon 34 (1996) 1301–1303.

[49] M.M.J. Treacy, T.W. Ebbesen, J.M. Gibson, Exceptionally high Young's modulus observed for individual carbon nanotubes, Nature 381 (1996) 678–680.

[50] E.W. Wong, P.E. Sheehan, C.M. Lieber, Nanobeam mechanics: elasticity, strength and toughness of nanorods and nanotubes, Science 277 (1997) 1971–1975.

[51] H.W. Kroto, J.R. Heath, S.C. O'Brien, R.F. Curl, R.E. Smalley, C60: buckminsterfullerene, Nature 318 (1985) 162–163.

[52] P.G. Collins, P. Avouris, Nanotubes for electronics, Sci. Am. 283 (2000) 62–69.

[53] S. Fan, M.G. Chapline, N.R. Franklin, T.W. Tombler, A.M. Cassell, H. Dai, Self-oriented regular arrays of carbon nanotubes and their field emission properties, Science 283 (1999) 512–514.

[54] S.S. Wong, E. Joselevich, A.T. Woolley, C.L. Cheung, C.M. Lieber, Covalently functionalized nanotubes as nanometre-sized probes in chemistry and biology, Nature 394 (1998) 52.

[55] T. Rueckes, K. Kim, E. Joselevich, G.Y. Tseng, C.L. Cheung, C.M. Lieber, Carbon nanotube-based nonvolatile random access memory for molecular computing, Science 289 (2000) 94–97.

[56] Z. Yao, H.W.C. Postma, L. Balents, C. Dekker, Carbon nanotube intramolecular junctions, Nature 402 (1999) 273–276.

[57] M.B. Nardelli, B.I. Yakobson, J. Bernholc, Brittle and ductile behavior in carbon nanotubes, Phys. Rev. Lett. 81 (1998) 4656–4659.

[58] B.I. Yakobson, C.J. Brabec, J. Berhnolc, Nanomechanics of carbon tubes: instabilities beyond linear response, J. phys. rev. lett 76 (1996) 2511.

[59] Z.C. Tu, Y.Z.C. Ou, Single-walled and multiwalled carbon nanotubes viewed as elastic tubes with the effective Young's moduli dependent on layer number, Phys. Rev. B Condens. Matter 65 (2002) 233407.

[60] T. Chang, J. Geng, X. Guo, Prediction of Chirality- and size-dependent elastic properties of single-walled carbon nanotubes via a molecular mechanics model, Proc. Math. Phys. Eng. 462 (2006) 2523–2540.

[61] J.P. Lu, Elastic properties of single and multilayered nanotubes, J. Phys. Chem. Solids 58 (1997) 1649–1652.

[62] G. Zhou, W.H. Duan, B.L. Gu, First-principles study on morphology and mechanical properties of single-walled carbon nanotube, Chem. Phys. Lett. 333 (2001) 344–349.

[63] A. Krishnan, E. Dujardin, T.W. Ebbesen, P.N. Yianilos, M.M.J. Treacy, Young's modulus of single-walled nanotubes, Phys. Rev. B Condens. Matter 58 (1998) 14013.

[64] C.Y. Li, T.W. Chou, Elastic moduli of multi-walled carbon nanotubes and the effect of van der Waals forces, Compos. Sci. Technol. 63 (2003) 1517–1524.

[65] B.G. Demczyk, Y.M. Wang, J. Cumings, M. Hetman, W. Han, A. Zettl, R.O. Ritchie, Direct mechanical measurement of the tensile strength and elastic modulus of multiwalled carbon nanotubes, Mater. Sci. Eng., A 334 (2002) 173–178.

[66] F. Li, H.M. Cheng, S. Bai, G. Su, M.S. Dresselhaus, Tensile strength of single-walled carbon nanotubes directly measured from their macroscopic ropes, Appl. Phys. Lett. 77 (2000) 3161–3163.

[67] M.F. Yu, O. Lourie, M.J. Dyer, K. Moloni, T.F. Kelly, R.S. Ruoff, Strength and breaking mechanism of multiwalled carbon nanotubes under tensile load, Science 287 (2000) 637–640.

[68] J. Robertson, Realistic applications of CNTs, mater, Today Off. 7 (2004) 46–52.

[69] R.C. Haddon, J. Sippel, A.G. Rinzler, F. Papadimitrakopoulos, Purification and separation of carbon nanotubes, MRS Bull. 29 (2004) 252–259.

[70] Z.F. Ren, Z.P. Huang, D.Z. Wang, J.G. Wen, J.H. Wang, L.E. Calvet, J. Chen, J.F. Klemic, M.A. Reed, Growth of a single freestanding multiwall carbon nanotube on each nanonickel dot, Appl. Phys. Lett. 75 (1999) 1086–1088.

[71] Z.F. Ren, Z.P. Huang, J.W. Xu, J.H. Wang, P. Bush, M.P. Siegal, P.N. Provencio, Synthesis of large arrays of well-aligned carbon nanotubes on glass, Science 282 (1998) 1105–1107.

[72] B. Vigolo, A. Pénicaud, C. Coulon, C. Sauder, R. Pailler, C. Journet, P. Bernier, P. Poulin, Macroscopic fibers and ribbons of oriented carbon nanotubes, Science 290 (2000) 1331–1334.

[73] A.B. Dalton, S. Collins, E. Munoz, J.M. Razal, V.H. Ebron, J.P. Ferraris, J.N. Coleman, B.G. Kim, R.H. Baughman, Super-tough carbon-nanotube fibres, Nature 423 (2003) 703.

[74] V.A. Davis, L.M. Ericson, F. Hua, Y. Wang, V. Prieto, J.A. Longoria, S. Ramesh, R.K. Saini, C. Kittrell, Phase behavior and rheology of SWNTs in superacids, Macromolecules 37 (2004) 154–160.

[75] Y.L. Li, I.A. Kinloch, A.H. Windle, Direct spinning of carbon nanotube fibers from chemical vapor deposition synthesis, Science 304 (2004) 276–278.

[76] W. Stöber, A. Fink, E. Bohn, Controlled growth of monodisperse silica spheres in the micron size range, J. Colloid Interface Sci. 26 (1968) 62–69.

[77] F.E. Kruis, First Joint ESF-NST Symposium on Aerosols for Nanostructured Materials and Devices, 1998. Edinburgh, Scotland.

[78] G.D. Ulrich, J.W. Rieh, Aggregation and growth of submicron oxide particles in flames, J. Colloid Interface Sci. 87 (1982) 257–265.

[79] G.D. Ulrich, N.S. Subramanian III., Coalescence as a rate-controlling process, Combust. Sci. Technol. 17 (1977) 119–126.

[80] D. Schaefer, A. Hurd, Growth and structure of combustion aerosols: fumed silica, Aerosol Sci. Technol. 12 (1990) 876–890.

[81] H. Barthel, M. Heinemann, M. Stintz, B. Wessely, Particle sizes of fumed silica, Part. Part. Syst. Char. 16 (2015) 169–176.

[82] P. Fauchais, E. Bourdin, J.F. Coudert, R. McPherson, High pressure plasmas and their application to ceramic technology, in: F.L. Boschke (Ed.), Topics in Current Chemistry (Plasma Chemistry IV), Springer, Berlin, 1983, pp. 59–183.

[83] R.M. Young, E. Pfender, Generation and behavior of fine particles in thermal plasmas—a review, Plasma Chem. Plasma Process. 5 (1985) 1–37.

[84] G. Dransfield, in: I. Birkby, Sterling (Eds.), Plasma Production and Novel Processing to Ultrafine Ceramic Powders, Ceram. Technol. Int., Malaysia, 1992, pp. 71–74.

[85] G.H. Bogush, M.A. Tracy, C.F. Zukoski, Preparation of monodisperse silica particles: control of size and mass fraction, J. Non-Cryst. Solids 104 (1988) 95–106.

[86] M. Xiong, G. Gu, B. You, L. Wu, Preparation and characterization of poly(styrene butylacrylate) latex/nano-ZnO nanocomposites, J. Appl. Polym. Sci. 90 (2010) 1923–1931.

[87] A.H. Barber, S.R. Cohen, H.D. Wagner, Measurement of carbon nanotube–polymer interfacial strength, Appl. Phys. Lett. 82 (2003) 4140–4142.

[88] C.A. Cooper, S.R. Cohen, A.H. Barber, H.D. Wagner, Detachment of nanotubes from a polymer matrix, Appl. Phys. Lett. 81 (2002) 3873–3875.

[89] Y.Q. Li, Q.Y. Pan, M. Li, S.Y. Fu, Preparation and mechanical properties of novel polyimide/T-silica hybrid films, Compos. Sci. Technol. 67 (2007) 54–60.

[90] G. Levita, A. Marchetti, A. Lazzeri, Fracture of ultrafine calcium carbonate/polypropylene composites, Polym. Compos. 10 (1989) 39–43.

[91] V.A. Buryachenko, A. Roy, K. Lafdi, K.L. Anderson, S. Chellapilla, Multi-scale mechanics of nanocomposites including interface: experimental and numerical investigation, Compos. Sci. Technol. 65 (2005) 2435–2465.

[92] J.K.W. Sandler, J.E. Kirk, I.A. Kinloch, M.S.P. Shaffer, A.H. Windle, Ultra-low electrical percolation threshold in carbon-nanotube-epoxy composites, Polymer 44 (2003) 5893–5899.

[93] E.A. Mayerberger, O. Urbanek, R.M. McDaniel, R.M. Street, M.W. Barsoum, C.L. Schauer, Preparation and characterization of polymer-$Ti_3C_2T_x$ (MXene) composite nanofibers produced via electrospinning, J. Appl. Polym. Sci. 134 (2017).

[94] Y.Q. Li, S.Y. Fu, Y.W. Mai, Preparation and characterization of transparent ZnO/epoxy nanocomposites with high-UV shielding efficiency, Polymer 47 (2006) 2127–2132.

[95] Z.S. Petrović, I. Javni, A. Waddon, G. Bánhegyi, Structure and properties of polyurethane–silica nanocomposites, J. Appl. Polym. Sci. 76 (2015) 133–151.

[96] C.M. Chan, J. Wu, J.X. Li, Y.K. Cheung, Polypropylene/calcium carbonate nanocomposites, Polymer 43 (2002) 2981–2992.

[97] M.Z. Rong, M.Q. Zhang, Y.X. Zheng, H.M. Zeng, R. Walter, K. Friedrich, Structure–property relationships of irradiation grafted nano-inorganic particle filled polypropylene composites, Polymer 42 (2001) 167–183.

[98] F. Yang, Y. Ou, Z. Yu, Polyamide 6/silica nanocomposites prepared by in situ polymerization, J. Appl. Polym. Sci. 69 (2015) 355–361.

[99] Y. Ou, F. Yang, Z. Yu, A new conception on the toughness of nylon 6/silica nanocomposite prepared via in situ polymerization, J. Polym. Sci., Part B: Polym. Phys. 36 (2015) 789–795.

[100] E. Reynaud, T. Jouen, C. Gauthier, G. Vigier, J. Varlet, Nanofillers in polymeric matrix: a study on silica reinforced PA6, Polymer 42 (2001) 8759–8768.

[101] M. Li, Y.Q. Li, S.Y. Fu, Cryogenic mechanical properties and thermal stability of polyimide hybrid films filled with MMT-TiO_2 nano-particles, Acta Mater. Compos. Sin. 23 (2006) 69–74.

[102] S.K. Park, K.D. Kim, H.T. Kim, Preparation of silica nanoparticles: determination of the optimal synthesis conditions for small and uniform particles, Colloids Surf., A 197 (2002) 7–17.

[103] A. Usuki, M. Kawasumi, Y. Kojima, A. Okada, T. Kurauchi, O. Kamigaito, Swelling behavior of montmorillonite cation exchanged for ω-amino acids by ε-caprolactam, J. Mater. Res. 8 (2011) 1174–1178.

[104] C. Oriakhi, Nano sandwiches, Chem. Br. 34 (1998) 59–62.

[105] U. Arimitsu, K. Yoshitsugu, K. Masaya, O. Akane, F. Yoshiaki, K. Toshio, K. Osami, Synthesis of nylon 6-clay hybrid, J. Mater. Res. 8 (1993) 1179–1184.

[106] R. Xu, E. Manias, A.J. Snyder, J. Runt, New biomedical poly(urethane urea)−layered silicate nanocomposites, Macromolecules 34 (2001) 337–339.

[107] R.K. Bharadwaj, Modeling the barrier properties of polymer-layered silicate nanocomposites, Macromolecules 34 (2001) 9189–9192.

[108] J. Ma, J. Xu, J.H. Ren, Z.Z. Yu, Y.W. Mai, A new approach to polymer/montmorillonite nanocomposites, Polymer, Polymer 44 (2003) 4619–4624.

[109] R.A. Vaia, E.P. Giannelis, Lattice model of polymer melt intercalation in organically-modified layered silicates, Macromolecules 30 (1997) 7990–7999.

[110] O.C. Wilson Jr., T. Olorunyolemi, A. Jaworski, L. Borum, D. Young, A. Siriwat, E. Dickens, C. Oriakhi, M. Lerner, Surface and interfacial properties of polymer-intercalated layered double hydroxide nanocomposites, Appl. Clay Sci. 15 (1999) 265–279.

[111] C.O. Oriakhi, Thermal characterization of poly(styrene sulfonate)/layered double hydroxide nanocomposites, Clay Clay Miner. 45 (1997) 194–202.

[112] K.A. Carrado, L.Q. Xu, In situ synthesis of polymer−clay nanocomposites from silicate gels, Chem. Mater. 10 (1998) 1440–1445.

[113] G.H. Chen, C.L. Wu, W.G. Weng, D.J. Wu, W.L. Yan, Preparation of polystyrene/graphite nanosheet composite, Polymer 44 (2003) 1781–1784.

[114] W. Zheng, S.C. Wong, Electrical conductivity and dielectric properties of PMMA/expanded graphite composites, Compos. Sci. Technol. 63 (2003) 225–235.

[115] Z.K. Tu, J. Wang, C.J. Yu, H.W. Xiao, T. Jiang, Y.K. Yang, D.A. Shi, Y.W. Mai, R.K.Y. Li, A facile approach for preparation of polystyrene/graphene nanocomposites with ultra-low percolation threshold through an electrostatic assembly process, Compos. Sci. Technol. 134 (2016) 49–56.

[116] H.H. Gommans, J.W. Alldredge, H. Tashiro, J. Park, J. Magnuson, A.G. Rinzler, Fibers of aligned single-walled carbon nanotubes: polarized Raman spectroscopy, J. Appl. Phys. 88 (2000) 2509–2514.

[117] R. Andrews, D. Jacques, A. Rao, T. Rantell, F. Derbyshire, Y. Chen, J. Chen, R.C. Haddon, Nanotube composite carbon fibers, Appl. Phys. Lett. 75 (1999) 1329–1331.

[118] P. Pötschke, T.D. Fornes, D.R. Paul, Rheological behavior of multiwalled carbon nanotube/polycarbonate composites, Polymer 43 (2002) 3247–3255.

[119] E. Hammel, X. Tang, M. Trampert, T. Schmitt, K. Mauthner, A. Eder, P. Pötschke, Carbon nanofibers for composite applications, Carbon 42 (2004) 1153–1158.

[120] M. Sennett, E. Welsh, J.B. Wright, W.Z. Li, J.G. Wen, Z.F. Ren, Dispersion and alignment of carbon nanotubes in polycarbonate, Appl. Phys. Mater. Sci. Process 76 (2003) 111–113.

[121] J. Zeng, B. Saltysiak, W.S. Johnson, D.A. Schiraldi, S. Kumar, Processing and properties of poly(methyl methacrylate)/carbon nano fiber composites, Composites Part B 35 (2004) 173–178.

[122] X.L. Xie, Y.W. Mai, X.P. Zhou, Dispersion and alignment of carbon nanotubes in polymer matrix: a review, Mater. Sci. Eng. R 49 (2005) 89–112.

[123] B.A. Higgins, W.J. Brittain, Polycarbonate carbon nanofiber composites, Eur. Polym. J. 41 (2005) 889–893.

[124] Z. Wang, Z. Liang, B. Wang, C. Zhang, L. Kramer, Processing and property investigation of single-walled carbon nanotube(SWNT) buckypaper/epoxy resin matrix nanocomposites, Composites Part A 35 (2004) 1225–1232.

[125] C. Zeng, L.J. Lee, Poly(methyl methacrylate) and polystyrene/clay nanocomposites prepared by in-situ polymerization, Macromolecules 34 (2001) 4098–4103.

[126] Y. Li, J. Yu, Z.X. Guo, The influence of silane treatment on nylon 6/nano-SiO_2 in situ polymerization, J. Appl. Polym. Sci. 84 (2002) 827–834.

[127] B.J. Ash, L.S. Schadler, R.W. Siegel, Glass transition behavior of alumina/polymethylmethacrylate nanocomposites, Mater. Lett. 55 (2002) 83–87.

[128] R.W. Siegel, S.K. Chang, B.J. Ash, J. Stone, P.M. Ajayan, R.W. Doremus, L.S. Schadler, Mechanical behavior of polymer and ceramic matrix nanocomposites, Scripta Mater. 44 (2001) 2061–2064.

[129] G.H. Hsiue, W.J. Kuo, Y.P. Huang, R.J. Jeng, Microstructural and morphological characteristics of PS–SiO_2 nanocomposites, Polymer 41 (2000) 2813–2825.

[130] M. Smaihi, J.C. Schrotter, C. Lesimple, I. Prevost, C. Guizard, Gas separation properties of hybrid imide–siloxane copolymers with various silica contents, J. Membr. Sci. 161 (1999) 157–170.

[131] C.J. Cornelius, E. Marand, Hybrid silica-polyimide composite membranes: gas transport properties, J. Membr. Sci. 202 (2002) 97–118.

[132] P. Musto, G. Ragosta, G. Scarinzi, L. Mascia, Toughness enhancement of polyimides by in situ generation of silica particles, Polymer 45 (2004) 4265–4274.

[133] Y. Zhu, D.X. Sun, Preparation of silicon dioxide/polyurethane nanocomposites by a sol-gel process, J. Appl. Polym. Sci. 92 (2010) 2013–2016.

[134] C.J. Huang, S.Y. Fu, Y.H. Zhang, B. Lauke, L.F. Li, L. Ye, Cryogenic properties of SiO_2/epoxy nanocomposites, Cryogenics 45 (2005) 450–454.

[135] S. Wang, M. Wang, Y. Lei, L. Zhang, "Anchor effect" in poly(styrene maleic anhydride)/TiO_2 nanocomposites, J. Mater. Sci. Lett. 18 (1999) 2009–2012.

[136] Y. Kong, H. Du, J. Yang, D. Shi, Y. Wang, Y. Zhang, W. Xin, Study on polyimide/TiO_2 nanocomposite membranes for gas separation, Desalination 146 (2002) 49–55.

[137] Y. Li, S.Y. Fu, D.J. Lin, Y.H. Zhang, Q.Y. Pan, Mechanical properties of polymide composites filled with SiO_2 nano-particles at room and cryogenic temperature, Acta Mater. Compos. Sin. 22 (2005) 11–15.

[138] D.W. Mccarthy, J.E. Mark, D.W. Schaefer, Synthesis, structure and properties of hybrid organic–inorganic composites based on polysiloxanes. I. Poly(dimethylsiloxane) elastomers containing silica, J. Polym. Sci., Part B: Polym. Phys. 36 (2015) 1167–1189.

[139] A.B.R. Mayer, Formation of noble metal nanoparticles within a polymeric matrix: nanoparticle features and overall morphologies, Mater. Sci. Eng. C 6 (1998) 155–166.

[140] R.A. Vaia, K.D. Jant, E.J. Kramer, Microstructural evaluation of melt-intercalated polymer-organically modified layered silicate nanocomposites, Chem. Mater. 8 (1996) 2628–2635.

[141] L.J. Mathias, R.D. Davis, W.L. Jarrett, Observation of alpha and gamma crystal forms and amorphous regions of nylon 6 clay nanocomposites using solid-state15N nuclear magnetic resonance, Macromolecules 32 (2012) 7958–7960.

[142] D.L. Vanderhart, A. Asano, J.W. Gilman, NMR measurements related to clay-dispersion quality and organic-modifier stability in nylon-6/clay nanocomposites, Macromolecules 34 (2001) 3819–3822.

[143] J. Yu, R.Y.F. Liu, B. Poon, S. Nazarenko, T. Koloski, T. Vargo, A. Hiltner, E. Baer, Polymers with palladium nanoparticles as active membrane materials, J. Appl. Polym. Sci. 92 (2004) 749–756.

[144] J.G. Doh, I. Cho, Synthesis and properties of polystyrene-organoammonium montmorillonite hybrid, Polym. Bull. 41 (1998) 511–518.

[145] M.W. Weimer, H. Chen, E.P. Giannelis, D.Y. Sogah, Direct synthesis of dispersed nanocomposites by in situ living free radical polymerization using a silicate-anchored initiator, J. Am. Chem. Soc. 121 (1999) 1615–1616.

[146] O.P. Koc, S.B. Acar, T. Uyar, M.A. Tasdelen, In situ preparation of thermoset/clay nanocomposites via thiol-epoxy click chemistry, Polym. Bull. 75 (2018) 1–11.

[147] K. Yano, A. Usuki, A. Okada, T. Kurauchi, O. Kamigaito, Synthesis and properties of polyimide–clay hybrid, J. Polym. Sci., Part A: Polym. Chem. 35 (1997) 2289–2294.

[148] R. Magaraphan, W. Lilayuthalert, A. Sirivat, J.W. Schwank, Preparation, structure, properties and thermal behavior of rigid-rod polyimide/montmorillonite nanocomposites, Compos. Sci. Technol. 61 (2001) 1253–1264.

[149] N. Ogata, G. Jimenez, H. Kawai, T. Ogihara, Structure and thermal/mechanical properties of poly(l-lactide)-clay blend, J. Polym. Sci., Part B: Polym. Phys. 35 (2015) 389–396.

[150] G. Jimenez, N. Ogata, H. Kawai, T. Ogihara, Structure and thermal/mechanical properties of poly(1 -caprolactone)–clay blend, J. Appl. Polym. Sci. 64 (1997) 2211–2220.

[151] T.D. Fornes, P.J. Yoon, D.L. Hunter, H. Keskkula, D.R. Paul, Effect of organoclay structure on nylon 6 nanocomposite morphology and properties, Polymer 43 (2002) 5915–5933.

[152] K. Lozano, E.V. Barrera, Nanofiber-reinforced thermoplastic composites. I. Thermoanalytical and mechanical analyses, J. Appl. Polym. Sci. 79 (2015) 125–133.

[153] Z. Jin, K.P. Pramoda, G. Xu, S.H. Goh, Dynamic mechanical behavior of melt-processed multi-walled carbon nanotube/poly(methyl methacrylate) composites, Chem. Phys. Lett. 337 (2001) 43–47.

[154] J. Sandler, P. Werner, M.S.P. Shaffer, V. Demchuk, V. Altstädt, A.H. Windle, Carbon-nanofibre-reinforced poly(ether ether ketone) composites, Composites Part A 33 (2002) 1033–1039.

[155] J.W. Cho, D.R. Paul, Nylon 6 nanocomposites by melt compounding, Polymer 42 (2001) 1083–1094.

[156] S.Y. Fu, X. Hu, C.Y. Yue, The flexural modulus of misaligned short-fiber-reinforced polymers, Compos. Sci. Technol. 59 (1999) 1533–1542.

[157] S.Y. Fu, B. Lauke, Effects of fiber length and fiber orientation distributions on the tensile strength of short-fiber-reinforced polymers, Compos. Sci. Technol. 56 (1996) 1179–1190.

[158] Z.G. Wu, C.X. Zhou, R.R. Qi, H.B. Zhang, Synthesis and characterization of nylon 1012/clay nanocomposite, J. Appl. Polym. Sci. 83 (2002) 2403–2410.

[159] Z. Wang, T.J. Pinnavaia, Hybrid organic−inorganic nanocomposites: exfoliation of magadiite nanolayers in an elastomeric epoxy polymer, Chem. Mater. 10 (1998) 38–39.

[160] Z. Wang, T.J. Pinnavaia, Nanolayer reinforcement of elastomeric polyurethane, Chem. Mater. 10 (1998) 3769–3771.

[161] J. Ma, S. Zhang, Z. Qi, Synthesis and characterization of elastomeric polyurethane/clay nanocomposites, J. Appl. Polym. Sci. 82 (2001) 1444–1448.
[162] L. Liu, Z. Qi, X. Zhu, Studies on nylon 6/clay nanocomposites by melt-intercalation process, J. Appl. Polym. Sci. 71 (2015) 1133–1138.
[163] Z. Wang, L. Tie, T.J. Pinnavaia, Hybrid organic−inorganic nanocomposites formed from an epoxy polymer and a layered silicic acid (magadiite), Chem. Mater. 8 (1996) 346–353.
[164] A.S. Zerda, A. J, Lesser, Intercalated clay nanocomposites: morphology, mechanics, and fracture behavior, MRS Proceedings 661 (2000) 1137–1146.
[165] A. Dasari, Z.Z. Yu, M.S. Yang, Q.X. Zhang, X.L. Xie, Y.W. Mai, Micro- and nano-scale deformation behavior of nylon 66-based binary and ternary nanocomposites, Compos. Sci. Technol. 66 (2006) 3097–3114.
[166] S.Y. Fu, B. Lauke, The fibre pull-out energy of misaligned short fibre composites, J. Mater. Sci. 32 (1997) 1985–1993.
[167] O. Eksik, J. Gao, S.A. Shojaee, A. Thomas, P. Chow, S.F. Bartolucci, D.A. Lucca, N. Koratkar, Epoxy nanocomposites with two-dimensional transition metal dichalcogen de Additives, ACS Nano 8 (5) (2014) 5282–5289.
[168] H. Rastina, M.R. Saebb, M. Nonahala, M. Shabanianc, H. Vahabid, K. Formelae, X. Gabrionf, F. Seidig, P. Zarrintaja, M.G. Sarih, P. Laheurtei, Transparent nanocomposite coatings based on epoxy and layered double hydroxide: nonisothermal cure kinetics and viscoelastic behavior assessments, Prog. Org. Coating 113 (2017) 126–135.
[169] H. Zhang, L.B. Wang, Q. Chen, P. Li, A.G. Zhou, X.X. Cao, Q.K. Hu, Preparation, mechanical and anti-friction performance of MXene/polymer composites, Mater. Des. 92 (2016) 682–689.
[170] Z. Ling, C.E. Ren, M.Q. Zhao, J. Yang, J.M. Giammarco, J. Qiu, M.W. Barsoum, Y. Gogotsi, Flexible and conductive MXene films and nanocomposites with high capacitance, Proc. Natl. Acad. Sci. Unit. States Am. 111 (2014) 16676–16681.
[171] Y. Zare, A model for tensile strength of polymer/clay nanocomposites assuming complete and incomplete interfacial adhesion between the polymer matrix and nanoparticles by the average normal stress in clay platelets, RSC Adv. 6 (2016) 57969–57976.
[172] D. Shia, C. Hui, S. Burnside, E. Giannelis, An interface model for the prediction of Young's modulus of layered silicate–elastomer nanocomposites, Polym. Compos. 19 (1998) 608–617.
[173] Y. Zare, H. Garmabi, A developed model to assume the interphase properties in a ternary polymer nanocomposite reinforced with two nanofillers, Compos. B Eng. 75 (2015) 29–35.
[174] Y. Zare, H. Garmabi, Thickness, modulus and strength of interphase in clay/polymer nanocomposites, Appl. Clay Sci. 105–106 (2015) 66–70.
[175] I. Zaman, T.T. Phan, H.C. Kuan, Q.S. Meng, L.T.B. La, L. Luong, O. Youssf, J. Ma, Epoxy/graphene platelets nanocomposites with two levels of interface strength, Polymer 52 (2011) 1603–1611.
[176] J.P. Salvetat, G.A.D. Briggs, J.M. Bonard, R.R. Bacsa, A.J. Kulik, Elastic and shear moduli of single-walled carbon nanotube ropes, Phys. Rev. Lett. 82 (1999) 944–947.
[177] M.S.P. Shaffer, A.H. Windle, Fabrication and characterization of carbon nanotube/poly(vinyl alcohol) composites, Adv. Mater. 1512 (1999) 320–321.
[178] S.Y. Fu, B. Lauke, Y.W. Mai, Science and Engineering of Short Fibre Reinforced Polymer Composites, Woodhead Pub., Oxford, 2009.
[179] D. Qian, E.C. Dickey, R. Andrews, T. Rantell, Load transfer and deformation mechanisms in carbon nanotube-polystyrene composites, Appl. Phys. Lett. 76 (2000) 2868–2870.
[180] G.G. Tibbetts, J.J. Mchugh, Mechanical properties of vapor-grown carbon fiber composites with thermoplastic matrices, J. Mater. Res. 14 (1999) 2871–2880.
[181] J.P. Yang, Z.K. Chen, Q.P. Feng, Y.H. Deng, Y. Liu, Q.Q. Ni, S.Y. Fu, Cryogenic mechanical behaviors of carbon nanotube reinforced composites based on modified epoxy by poly(ethersulfone), Composites Part B 43 (2012) 22–26.
[182] C.A. Bernardo, G. Caldeira, Production and assessment of polycarbonate composites reinforced with vapour-grown carbon fibres, Compos. Sci. Technol. 58 (1998) 401–407.
[183] Y.L. Chen, B. Liu, X.Q. He, Y. Huang, K.C. Hwang, Failure analysis and the optimal toughness design of carbon nanotube-reinforced composites, Compos. Sci. Technol. 70 (2010) 1360–1367.
[184] Y.L. Chen, Z.Y. Wang, S.T. Wang, Z.G. Zhou, J.Y. Zhang, B. Zhou, Carbon nanotube reinforced composites: the smaller diameter, the higher fracture toughness? J. Appl. Mech. 82 (2015) 081009, 1-14.
[185] B. Pukanszky, G. Voros, Mechanism of interfacial interactions in particulate filled composites, Compos. Interfac. 1 (2015) 411–427.
[186] Z.K. Zhu, Y. Yang, J. Yin, Z.N. Qi, Preparation and properties of organosoluble polyimide/silica hybrid materials by sol–gel process, J. Appl. Polym. Sci. 73 (1999) 2977–2984.
[187] X.H. Liu, Q.J. Wu, PP/clay nanocomposites prepared by grafting-melt intercalation, Polymer 42 (2001) 10013–10019.
[188] X.L. Xie, Q.X. Liu, K. Li, X.P. Zhou, Q.X. Zhang, Z.Z. Yu, Y.W. Mai, Rheological and mechanical properties of PVC/$CaCO_3$ nanocomposites prepared by in situ polymerization, Polymer 45 (2004) 6665–6673.
[189] B. Lepoittevin, M. Devalckenaere, N. Pantoustier, M. Alexandre, D. Kubies, C. Calberg, R. Jérôme, P. Dubois, Poly(ε-caprolactone)/clay nanocomposites prepared by melt intercalation: mechanical, thermal and rheological properties, Polymer 43 (2002) 4017–4023.
[190] T. Kashiwagi, R.H. Harris Jr., X. Zhang, R.M. Briber, B.H. Cipriano, S.R. Raghavan, W.H. Awad, J.R. Shields, Flame retardant mechanism of polyamide 6–clay nanocomposites, Polymer 45 (2004) 881–891.
[191] S. Peeterbroeck, M. Alexandre, J.B. Nagy, N. Moreau, A. Destrée, F. Monteverde, A. Rulmont, R. Jérôme, P. Dubois, Polymer layered silicate/carbon nanotube nanocomposites: morphological and rheological properties, Macromol. Symp. 221 (2005) 115–126.
[192] M. Shabanian, H. Ardeshir, S. Haji-Ali, H. Moghaniand, M. Hajibeygi, K. Faghihi, H.A. Khonakdar, H. Salimi, Efficient poly(methyl-ether-imide)/LDH nanocomposite derived from a methyl rich bisphenol: from synthesis to properties, Appl, Clay Sci. 123 (2016) 285–291.
[193] S. Barik, S.K. Kisku, L. Behera, S.K. Swain, Enhancement of thermal properties of polyacrylonitrile by reinforcement of Mg-Al layered double hydroxide, Poylm. Compos 36 (2015) 2140–2144.
[194] Y.S. Gao, Q. Wang, L. Qiu, J.W. Wu, X.R. Yan, A. Umar, J. Guo, X. Zhang, J.Y. Wang, Z.H. Guo, Ethylene-vinyl acetate/LDH nanocomposites with enhanced thermal stability, flame retardancy, and rheological property, Polym. Compos. 37 (2016) 3449–3459.
[195] M. Messori, M. Toselli, F. Pilati, E. Fabbri, P. Fabbri, S. Busoli, L. Pasquali, S. Nannarone, Flame retarding poly(methyl methacrylate) with nanostructured organic–inorganic hybrids coatings, Polymer 44 (2003) 4463–4470.
[196] C.L. Chiang, C.C. Ma, Synthesis, characterization, thermal properties and flame retardance of novel phenolic resin/silica nanocomposites, Polym. Degrad. Stabil. 83 (2004) 207–214.
[197] T. Lan, P.D. Kaviratna, T.J. Pinnavaia, On the nature of polyimide-clay hybrid composites, Chem. Mater. 6 (1994) 573–575.
[198] C. Lu, Y.W. Mai, Influence of aspect ratio on barrier properties of polymer-clay nanocomposites, Phys. Rev. Lett. 95 (2005), 088303.
[199] D. Gomes, S.P. Nunes, K.V. Peinemann, Membranes for gas separation based on poly(1-trimethylsilyl-1-propyne)–silica nanocomposites, J. Membr. Sci. 246 (2005) 13–25.
[200] S.R. Ahmed, P. Kofinas, Magnetic properties and morphology of block copolymer-cobalt oxide nanocomposites, J. Magn. Magn. Mater. 288 (2005) 219–223.
[201] H. Nathani, R. Misra, Surface effects on the magnetic behavior of nanocrystalline nickel ferrites and nickel ferrite-polymer nanocomposites, Mater. Sci. Eng., B 113 (2004) 228–235.
[202] Z.M. Liang, C.Y. Wan, Y. Zhang, P. Wei, J. Yin, PVC/montmorillonite nanocomposites based on a thermally stable, rigid-rod aromatic amine modifier, Polymer 92 (2010) 567–575.
[203] Y. Yang, W.N. Li, Y.S. Luo, H.M. Xiao, S.Y. Fu, Y.W. Mai, Novel ultraviolet-opaque, visible-transparent and light-emitting ZnO-QD/silicone composites with tunable luminescence colors, Polymer 51 (2010) 2755–2762.
[204] Y.Q. Li, S.Y. Fu, Y.W. Mai, Preparation and characterization of transparent ZnO/epoxy nanocomposites with high-UV shielding efficiency, Polymer 47 (2006) 2127–2132.
[205] Y.S. Song, J.R. Youn, Influence of dispersion states of carbon nanotubes on physical properties of epoxy nanocomposites, Carbon 43 (2005) 1378–1385.
[206] A. Moisala, Q. Li, I.A. Kinloch, A.H. Windle, Thermal and electrical conductivity of single- and multi-walled carbon nanotube-epoxy composites, Compos. Sci. Technol. 66 (2006) 1285–1288.
[207] M. Shtein, R. Nadiv, M. Buzaglo, K. Kahil, O. Regev, Thermally conductive graphene-polymer composites: size, percolation, and synergy effects, Chem. Mater. 27 (2015), 150310150057001.
[208] Y. Su, J.J. Li, G.J. Weng, Theory of thermal conductivity of graphene-polymer nanocomposites with interfacial Kapitza resistance and graphene-graphene contact resistance, Carbon 137 (2018) 222–233.
[209] S.H. Yang, T. Nguyen, P.L. Rendu, C.S. Hsu, Optical and electrical investigations of poly(p -phenylene vinylene)/silicon oxide and poly(p -phenylene vinylene)/titanium oxide nanocomposites, Thin Solid Films 471 (2005) 230–235.
[210] W.K. Ji, S.G. Kim, H.J. Choi, M.S. Jhon, Synthesis and electrorheological properties of polyaniline-Na+-montmorillonite suspensions, Macromol, Rapid Commun 20 (1999) 450–452.
[211] M. Kawasumi, N. Hasegawa, A. Usuki, A. Okada, Nematic liquid crystal/clay mineral composites, Mater. Sci. Eng. C 6 (1999) 135–143.
[212] R.A. Vaia, S. Vasudevan, W. Krawiec, L.G. Scanlon, E.P. Giannelis, New polymer electrolyte nanocomposites: melt intercalation of poly(ethylene oxide) in mica-type silicates, Adv. Mater. 7 (1995) 154–156.
[213] S. Ahmad, S. Ahmad, S.A. Agnihotry, Nanocomposite electrolytes with fumed silica in poly(methyl methacrylate): thermal, rheological and conductivity studies, J. Power Sources 140 (2005) 151–156.
[214] J. Dalal, S. Lather, A. Gupta, S. Dahiya, A.S. Maan, K. Singh, S.K. Dhawan, A. Ohlan, EMI shielding properties of laminated graphene and $PbTiO_3$ reinforced poly(3,4-ethylenedioxythiophene) nanocomposites, Compos. Sci. Technol. 165 (2018) 222–230.